Structural Behavior of a 2nd Generation Ultra-High Performance Concrete Pi-Girder

U.S. Department of Transportation
Federal Highway Administration

FOREWORD

With the ever increasing congestion and deterioration of our nation's highway system, a need exists to develop highly durable and rapidly constructed infrastructure systems. Durable bridge structures that would require less intrusive maintenance and would exhibit longer life spans thus maximizing the use of the facility are highly desirable. Expediting bridge construction can minimize traffic flow disruptions. Ultra-high performance concrete (UHPC) is an advanced construction material which affords new opportunities to envision the future of the high infrastructure. The Federal Highway Administration has been engaged in research into the optimal uses of UHPC in the highway bridge infrastructure since 2001 through its Bridge of the Future initiative. This report presents results of a study aimed at refining a bridge superstructure system which facilitates rapid construction and long service life through the use of UHPC. The decked prestressed concrete girder which was developed and tested is expected to provide bridge owners with a new solution that meets many of their demands.

This report corresponds to the TechBrief titled, "Structural Behavior of a 2nd Generation UHPC Pi-Girder" (FHWA-HRT-09-069). This report is being distributed through the National Technical Information Service for informational purposes. The content in this report is being distributed "as is" and may contain editorial or grammatical errors.

TECHNICAL REPORT DOCUMENTATION PAGE

1. Report No. FHWA-HRT-10-026	2. Government Accession No. PB2009-115496	3. Recipient's Catalog No.	
4. Title and Subtitle Structural Behavior of a 2nd Generation Ultra-High Performance Concrete Pi-Girder		5. Report Date November 2009	
		6. Performing Organization Code:	
7. Author(s) Benjamin A. Graybeal		8. Performing Organization Report No.	
9. Performing Organization Name and Address Office of Infrastructure Research & Development Federal Highway Administration 6300 Georgetown Pike McLean, VA 22101-2296		10. Work Unit No.	
		11. Contract or Grant No.	
12. Sponsoring Agency Name and Address Office of Infrastructure Research & Development Federal Highway Administration 6300 Georgetown Pike McLean, VA 22101-2296		13. Type of Report and Period Covered Final Report: 2007-2009	
		14. Sponsoring Agency Code HRDI-06	
15. Supplementary Notes			

16. Abstract

Ultra-high performance concrete (UHPC) is an advanced cementitious composite material which has been developed in recent decades. When compared to more conventional cement-based concrete materials, UHPC tends to exhibit superior properties such as increased durability, strength, and long-term stability. This experimental investigation focused on the further development and structural testing of a newly developed highway bridge girder cross section, namely the pi-girder. This girder was developed and optimized specifically to exploit the advanced mechanical and durability properties of UHPC. Structural testing was completed on full-scale girders to investigate the transverse flexural response and the longitudinal joint structural behavior. The 2nd generation pi-girder system surpassed the AASHTO LRFD Bridge Design Specification demands for which it was designed.

17. Key Words Ultra-high performance concrete, UHPC, fiber-reinforced concrete, bridges, precast concrete, prestressed concrete, bridge design, accelerated construction, durable infrastructure systems.		18. Distribution Statement No restrictions. This document is available through the National Technical Information Service, Springfield, VA 22161.		
19. Security Classif. (of this report) Unclassified		20. Security Classif. (of this page) Unclassified	21. No. of Pages 114	22. Price A07

Form DOT F 1700.7 (8-72)   Reproduction of completed page authorized

SI* (MODERN METRIC) CONVERSION FACTORS

APPROXIMATE CONVERSIONS TO SI UNITS

Symbol	When You Know	Multiply By	To Find	Symbol
LENGTH				
in	inches	25.4	millimeters	mm
ft	feet	0.305	meters	m
yd	yards	0.914	meters	m
mi	miles	1.61	kilometers	km
AREA				
in^2	square inches	645.2	square millimeters	mm^2
ft^2	square feet	0.093	square meters	m^2
yd^2	square yard	0.836	square meters	m^2
ac	acres	0.405	hectares	ha
mi^2	square miles	2.59	square kilometers	km^2
VOLUME				
fl oz	fluid ounces	29.57	milliliters	mL
gal	gallons	3.785	liters	L
ft^3	cubic feet	0.028	cubic meters	m^3
yd^3	cubic yards	0.765	cubic meters	m^3
NOTE: volumes greater than 1000 L shall be shown in m^3				
MASS				
oz	ounces	28.35	grams	g
lb	pounds	0.454	kilograms	kg
T	short tons (2000 lb)	0.907	megagrams (or "metric ton")	Mg (or "t")
TEMPERATURE (exact degrees)				
^oF	Fahrenheit	5 (F-32)/9 or (F-32)/1.8	Celsius	^oC
ILLUMINATION				
fc	foot-candles	10.76	lux	lx
fl	foot-Lamberts	3.426	$candela/m^2$	cd/m^2
FORCE and PRESSURE or STRESS				
lbf	poundforce	4.45	newtons	N
lbf/in^2	poundforce per square inch	6.89	kilopascals	kPa

APPROXIMATE CONVERSIONS FROM SI UNITS

Symbol	When You Know	Multiply By	To Find	Symbol
LENGTH				
mm	millimeters	0.039	inches	in
m	meters	3.28	feet	ft
m	meters	1.09	yards	yd
km	kilometers	0.621	miles	mi
AREA				
mm^2	square millimeters	0.0016	square inches	in^2
m^2	square meters	10.764	square feet	ft^2
m^2	square meters	1.195	square yards	yd^2
ha	hectares	2.47	acres	ac
km^2	square kilometers	0.386	square miles	mi^2
VOLUME				
mL	milliliters	0.034	fluid ounces	fl oz
L	liters	0.264	gallons	gal
m^3	cubic meters	35.314	cubic feet	ft^3
m^3	cubic meters	1.307	cubic yards	yd^3
MASS				
g	grams	0.035	ounces	oz
kg	kilograms	2.202	pounds	lb
Mg (or "t")	megagrams (or "metric ton")	1.103	short tons (2000 lb)	T
TEMPERATURE (exact degrees)				
^oC	Celsius	1.8C+32	Fahrenheit	^oF
ILLUMINATION				
lx	lux	0.0929	foot-candles	fc
cd/m^2	$candela/m^2$	0.2919	foot-Lamberts	fl
FORCE and PRESSURE or STRESS				
N	newtons	0.225	poundforce	lbf
kPa	kilopascals	0.145	poundforce per square inch	lbf/in^2

*SI is the symbol for the International System of Units. Appropriate rounding should be made to comply with Section 4 of ASTM E380.
(Revised March 2003)

TABLE OF CONTENTS

LIST OF FIGURES

LIST OF TABLES

NTIS DISCLAIMER

CHAPTER 1. INTRODUCTION

INTRODUCTION

Ultra-high performance concrete (UHPC) is an advanced cementitious composite material. When compared to more conventional cement-based concrete materials, UHPC tends to exhibit superior properties such as exceptional durability, increased strength, and long-term stability.

This experimental investigation focused on the structural behavior of a newly developed highway bridge girder cross section, namely the pi-girder. This girder was developed and optimized specifically to exploit the advanced mechanical and durability properties of UHPC. The prototype version of the pi-girder was developed and tested through previous efforts within the present research program. A 2nd generation UHPC pi-girder was then developed. The fabrication and structural testing of this 2nd generation UHPC pi-girder is discussed herein.

OBJECTIVE

The objective of this research program is to evaluate the structural performance of a second generation UHPC pi-girder cross section intended for use in short-to-medium span highway bridge applications.

SUMMARY OF APPROACH

The research discussed herein includes two phases. The first phase focused on the fabrication of two UHPC pi-girders. These 0.91-m (33-inch) deep, 2.54-m (8.33-foot) wide, 7.6-m (25-foot) long prestressed girders were fabricated at a conventional precast bridge girder production plant. The second phase of the research focused on the physical testing of these full-scale girders through the application of structural loads. The girders were tested to failure, the results of the tests were then analyzed, and these results are presented herein.

OUTLINE OF REPORT

This report is divided into seven chapters. Chapters 1 and 2 provide an introduction to the study and relate relevant background information necessary in understanding the study's results. Chapter 3 presents the relevant mechanical properties of the UHPC pi-girders, the joint fill materials, and the mild reinforcing steel used in the joint. Information regarding the fabrication of and the experimental methods associated with the girders tested in this study is presented in Chapter 4. The results of the structural tests are presented in Chapter 5. Chapter 6 discusses and expands on the results presented in Chapter 5. Finally, Chapter 7 presents the conclusions of this research program.

CHAPTER 2.   BACKGROUND

INTRODUCTION

This chapter provides background information relevant to the focus of the research effort. A general discussion of UHPC constituent materials and material properties is presented first. The development of the concept for the UHPC pi-girder cross section studied in this research effort is presented next. Finally, results of prior full-scale structural testing focused on UHPC bridge components are presented.

UHPC CONSTITUENT MATERIALS

The specific UHPC investigated in this study is a product of a major worldwide construction materials manufacturer and supplier. It is currently the only product of this type that is widely available in the U.S. in the quantities necessary for large scale infrastructure applications. Table 1 provides a typical UHPC composition[1].

As reported in reference (1), the constituent material proportions were determined, in part, based on an optimization of the granular mixture. This method allows for a finely graded and highly homogeneous concrete matrix. Fine sand, generally between 150 and 600 µm (0.006 and 0.024 inch), is dimensionally the largest granular material. The next largest particle is cement with an average diameter of approximately 15 µm (0.0006 inch). Of similar size is the crushed quartz with an average diameter of 10 µm (0.004 inch). The smallest particle, the silica fume, has a diameter small enough to fill the interstitial voids between the cement and the crushed quartz particles. Dimensionally, the largest constituent in the mix is the steel fiber reinforcement. In this study, the fibers in the mix had a diameter of 0.2 mm (0.008 inch), a length of 12.7 mm (0.5 inch), and a minimum tensile strength of 2000 MPa (290 ksi). The fibers were included in the mix at two percent by volume. Given the relative sizes of the sand and the fibers, the steel fibers are able to reinforce the concrete matrix on the micro level.

Table 1. Typical UHPC composition.

Material	Amount (kg/m^3 (lb/yd^3))	Percent by Weight
Portland Cement	712 (1,200)	28.5
Fine Sand	1,020 (1,720)	40.8
Silica Fume	231 (390)	9.3
Ground Quartz	211 (355)	8.4
Superplasticizer	30.7 (51.8)	1.2
Accelerator	30.0 (50.5)	1.2
Steel Fibers	156 (263)	6.2
Water	109 (184)	4.4

UHPC MATERIAL PROPERTIES

The research program associated with reference (1) addressed the materials properties of the UHPC investigated in this study. A brief summary of the relevant results from the prior study is presented in Table 2.

Table 2. Typical UHPC material properties.

Material Characteristic	Average Result
Compressive Strength (ASTM C39; 28-day strength)	193 MPa
Modulus of Elasticity (ASTM C469; 28-day modulus)	52.4 GPa
Split Cylinder Cracking Strength (ASTM C496)	11.7 MPa
Prism Flexure Cracking Strength (ASTM C1018; 305-mm span; corrected)	9.0 MPa
Mortar Briquette Cracking Strength (AASHTO T132)	8.3 MPa
Direct Tension Cracking Strength (Axial tensile load)	9.7–11.0 MPa
Prism Flexural Tensile Toughness (ASTM C1018; 305-mm span)	$I_{30} = 53$
Long-Term Creep Coefficient (ASTM C512; 77 MPa sustained load)	0.29
Long-Term Shrinkage (ASTM C157; initial reading after set)	766 microstrain
Total Shrinkage (Embedded vibrating wire gage)	850 microstrain
Coefficient of Thermal Expansion (AASHTO TP60–00)	15.6×10^{-6}
Chloride Ion Penetrability (ASTM C1202; 28-day test)	18 coulombs
Chloride Ion Permeability (AASHTO T259; 12.7-mm depth)	$< 0.06 \, \text{kg/m}^3$
Scaling Resistance (ASTM C672)	No Scaling
Abrasion Resistance (ASTM C944 2x weight; ground surface)	0.17 grams lost
Freeze-Thaw Resistance (ASTM C666A; 600 cycles)	RDM = 96%
Alkali-Silica Reaction (ASTM C1260; tested for 28 days)	Innocuous

1 MPa = 145 psi
$1 \, \text{kg/m}^3 = 1.69 \, \text{lb/yd}^3$
1 g = 0.035 ounce

DEVELOPMENT OF THE UHPC PI-GIRDER

Prototype Pi-Girder Development

The concept of using decked-girder members for bridge applications in transportation and infrastructure is not new. The deck-bulb-Tee pretensioned concrete girder has been frequently implemented in various parts of the U.S., most notably in the Pacific Northwest. The double-Tee pretensioned concrete beam is widely used around the world in parking structures. In New England, governmental and industry partners are working to develop a pretensioned double-Tee suitable for short to medium span highway bridges. It is also the case that bridge designs are inherently a function of the mechanical and durability properties of the materials from which the bridge is to be constructed. In the case of reinforced or prestressed concrete bridges, these properties and the related design specifications have resulted in bridge component geometries which make efficient use of the material properties.

The development of new materials or the significant modification of the properties of existing materials results in the need for the development of new structural forms. The use of existing

geometries for materials with advanced properties, although simple to implement, results in inefficient designs and less cost effective solutions. Advanced material properties bring about the possibility of new design solutions which heretofore may not have been possible. The advanced properties of UHPC provide opportunities for the development of new structural forms focused on addressing any number of important focus areas. Straightforward topics such as creating longer-life bridges through enhanced durability or allowing for the spanning of longer distances with shallower superstructures can be addressed through the use of UHPC. In a systematic sense, UHPC also presents the opportunity to create new structural forms which facilitate accelerated construction and rapid renewal of the highway infrastructure.

The development of a prototype decked girder member which utilized UHPC as the primary structural component was initiated during the early stages of the FHWA UHPC research program, results of which are presented in references (1) and (2). It was evident that UHPC's mechanical and durability properties would allow for beneficial modifications to conventional concrete bridge component solutions as well as development of heretofore not feasible components. Given the exceptional durability properties of UHPC along with its comparatively high compressive and tensile strengths, the development of a decked pretensioned girder with slender cross sectional dimensions was an appropriate choice.

The geometric concept for the pi-girder also draws on construction of the Peace Footbridge in Seoul, Korea[3]. This arch bridge uses post-tensioned construction and the pi-girder cross sectional shape to span 120 meters (394 feet). Although significantly different than conventional highway bridges in the U.S. both in terms of bridge type and loading, this footbridge clearly demonstrated the opportunities that UHPC presents for slender, decked members.

The cross sectional dimensions of the prototype UHPC pi-girder were set through an analytical study completed at the Massachusetts Institute of Technology[4,5,6]. This research group was selected for this effort as they had completed prior work developing analytical models for the mechanical response of UHPC[7]. The models implemented in the design included one, two, and three dimensional analyses of the predicted response of the girder to the loadings prescribed in the AASHTO LRFD Bridge Design Specification[8].

Figure 1 presents the prototype pi-girder cross section. The cross section was designed to span between 21.3 and 30.5 m (70 to 100 feet). The girder is 0.84 m (33 inches) deep, 2.44 m (8 feet) wide, and can contain up to 15 prestressing strands in each bulb. The integral deck of the girder is 76 mm (3 inches) thick, and the webs range from 64 to 84 mm (2.5 to 3.3 inches) thick. A 156 mm (6.1 inch) deep shear key runs the length of each flange tip to allow for connection of adjacent modular components. Basic properties of the girder include an area of 0.392 m^2 (609 in^2), strong axis moment of inertia of 37.07×10^9 mm^4 (89,060 in^4), and a self-weight of 978 kg/m (657 lb/ft).
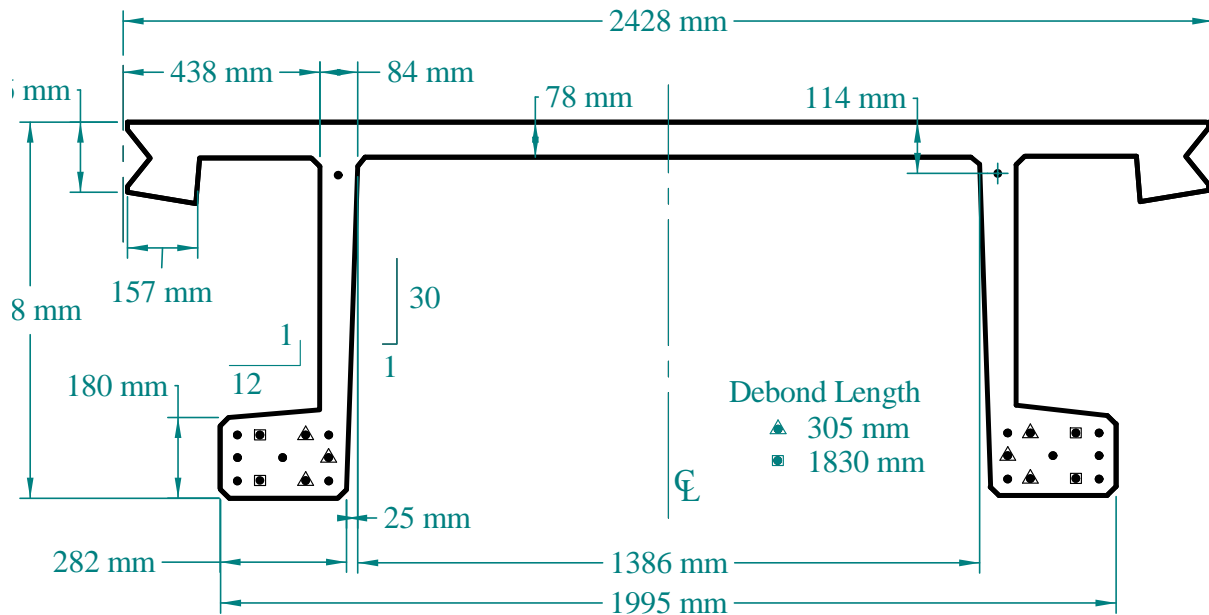
Figure 1. Illustration. Prototype pi-girder cross section and strand pattern.

2nd Generation Pi-Girder Development

An extensive test program was completed which focused on the fabrication and structural performance of the prototype pi-girder. The results of the study are presented in reference (9) and are summarized later in this chapter.   Briefly, the study demonstrated that the pi-girder concept was feasible; however, minor modifications were necessary in order to simplify girder fabrication and to address some specific structural performance concerns. Figure 2 illustrates the prototype and 2nd generation pi-girder cross sections. The significant modifications which were implemented included: 1) thickening the deck, 2) widening the deck, 3) shifting the legs inward, 4) eliminating the overhang blockouts, 5) thickening the webs, 6) rounding all reentrant corners, and 7) including intermediate diaphragms. Given these modifications to the cross section, basic engineering principles indicate that subjecting the 2nd generation pi-girder to the same battery of structural tests presented in reference (9) would result in increased elastic stiffnesses and ultimate capacities in primary flexure, primary shear, and transverse flexure.
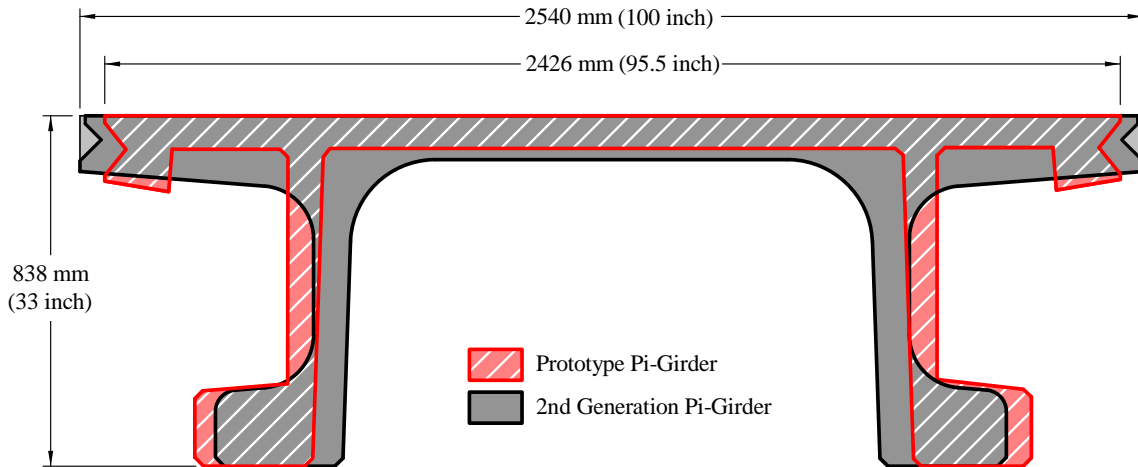
Figure 2. Illustration. Prototype and 2nd generation pi-girder cross sections.

FHWA FULL-SCALE UHPC I-GIRDER TESTING

As detailed in reference (2), full-scale structural behavior testing of UHPC I-girders was completed between 2001 and 2003. In the test program, AASHTO Type II pretensioned concrete bridge girders were cast using the same UHPC investigated in the current study. Other than the twenty-four 12.7 mm (0.5 inch), 1860 MPa (270 ksi) prestressing strands in their bottom bulb and the two additional strands in their top flange, these girders did not contain any mild steel reinforcement.

A flexure test was completed wherein a girder was subjected to four-point loading over a 23.9 m (78.5 foot) span. The ultimate dead plus live load capacity of the girder was 4800 kN-m (42480 kip-inches).

Three shear tests were completed wherein a girder was subjected to three-point bending with shear span-to-depth ratios ranging from 2.0 to 2.5. These test setups had varying levels of restraint provided to strands near the reaction location so as to consider the effect of strand slip on shear capacity results. The lowest ultimate dead plus live load shear capacity recorded was 1710 kN (384 kips) while the highest was 2230 kN (502 kips). This lower load was observed to occur concurrent with significant strand slip, while the higher load represented a true shear failure wherein no strand slip was observed.

FHWA FULL-SCALE PROTOTYPE UHPC PI-GIRDER TESTING

As detailed in reference (9), an earlier phase of the present research program focused on the development of the prototype UHPC pi-girder and the testing of this girder's response to structural loading. Four 21.3-m (70 foot) long prestressed pi-girders with the cross-sectional dimensions shown in Figure 1 were fabricated for testing by FHWA. The testing on these girders included foci on primary flexural response, primary shear response, and transverse flexural response. A summary of the results of these tests is provided herein.

Flexural Response of a Prototype UHPC Pi-Girder

Three tests were completed which provided results directly relevant to the flexural response of the prototype UHPC pi-girder. In each of these tests the prestressed girder contained 11 strands in each bulb, with the strands being initially stressed to 1316 MPa (190.8 ksi). Two of the relevant tests were conducted on girders loaded in four point bending with span lengths of 13.7 and 21 m (45 and 69 feet) and 1.8 m (6 foot) constant moment region at midspan. The third test was setup as a shear test which was loaded in three-point bending with a 1.8 m (6 foot) shear span between the point load and the closer reaction point.

A summary of the flexural response of the pi-girder is as follows. Considering the prestressing moment in the girders, the applied moment beyond decompression at first cracking was approximately 735 kN-m (6,500 kip-inches). An elastic analysis indicated that the stress in the tensile face of the UHPC girder was approximately 10.3 MPa (1.5 ksi) at first cracking. The average ultimate flexural capacity was 4,235 kN-m (37,500 kip-inches), with the lowest flexural capacity of 4,150 kN-m (36,720 kip-inches) resulting from the third test wherein slippage of strands may have reduced the capacity.

A capacity analysis of this girder was completed according to the requirements of the AASHTO LRFD Bridge Design Specifications[14]. A 21.3 m (70 foot) simple span was considered since this is the span for which the included quantity of prestressing strand was initially designed. Due to the limited capability of the prototype pi-girder to distribute loads laterally between girders, the demand on the girder was calculated by considering the critical load cases on half of a girder. The lever rule was used to distribute loads. The girder's own self weight load was supplemented by an additional 122 kg/m^2 (25 lb/ft^2) applied load to account for a thin wearing surface. Multiplying the demands by two allows for easy comparison to the test results which pertain to the symmetric loading of the as-fabricated prototype pi-girder. The Service III and Strength I demands for an as-fabricated girder are 2250 kN-m (19940 kip-inches) and 4470 kN-m (39600 kip-inches), respectively. The experimentally observed flexural cracking in Tests P2-70F and P4-45F was approximately equal to the Service III demand. The experimentally observed ultimate flexural capacity of this girder is approximately 5 percent less than the demand, indicating that additional prestressing force is necessary in order to meet the flexural requirement.

A deflection analysis was also completed using the optional deflection provisions of the AASHTO LRFD Bridge Design Specifications. The considered loading included the design truck with impact factor on the 21.3 m (70 foot) simple span. The resulting applied moment on an as-fabricated girder is 1,740 kN-m (15,440 kip-inches). The recommended deflection limit obtained by dividing the span length by 800 is 26.7 mm (1.05 inch). At this applied moment in the test of the 21.3 m (70 foot) span girder, the average observed midspan deflection of the girder bulbs was 34.3 mm (1.35 inch). Clearly, the prototype pi-girder does not meet the recommended deflection provisions. Recognize, however, that this analysis involves conservatively applying an entire truck load to the 2.4 m (8 ft) wide girder, whereas there is inevitably some level of load distribution transversely across the bridge.

Shear Response of a Prototype UHPC Pi-Girder

Three tests were completed which provided results directly relevant to the shear response of the prototype UHPC pi-girder. In each of these tests the prestressed girder contained 11 strands in each bulb, with the strands being initially stressed to 1316 MPa (190.8 ksi). Note that in one of the tests, three of the strands in each bulb were harped into the web. Loads in all three tests were applied in a three-point bending configuration; shear span-to-depth ratios ranged from 2.17 to 2.53 in the shorter shear span.

The least shear capacity observed in the three tests was a total dead plus live load shear of 1,630 kN (366 kips). Two of these tests resulted in diagonal tensile failures of the web, while the third resulted in a flexural failure as discussed previously. The shear capacity of this girder was assessed using a similar methodology to the flexural capacity analysis discussed above. The Service III demand from the dead loads and the HL-93 loading is 493 kN (110.8 kips), while the Strength I demand is 961 kN (216 kips). All experimentally observed shear capacities are at least 69 percent greater than the Strength I demand.

The ultimate shear capacity of this girder was also analyzed using basic engineering principles as presented in Graybeal[2]. Note that this method of analysis is a modified version of the design provisions presented in the Association Française de Génie Civil *Interim Recommendations for Ultra High Performance Fiber-Reinforced Concretes* [16]. The analysis assumes that the girder webs carry all of the shear forces and that the diagonal tensile force, which can be resolved from the shear force, acts uniformly over the relevant cross-sectional area of the webs. At peak shear load, the angles of the web shear cracks in the three girder tests were approximately 35 degrees from the horizontal. This angle pertained to the failure plane in two of the tests, while it pertained to the average crack angle in the third. The entire depth of web and the average web width were assumed to be uniformly effective in resisting the diagonal tensile force. From these values, the average direct tensile force carried across the critical shear crack at failure was determined to range from 14.6 MPa (2.1 ksi) to 20.3 MPa (2.9 ksi) in the three specimens.

Transverse Flexural Response of a Prototype UHPC Pi-Girder

A final pair of tests were completed wherein the transverse flexural response of the prototype UHPC pi-girder was investigated. In both tests, a pair of wheel patch loads was applied along the midline of the girder near midspan in a configuration consistent with the design tandem detailed in the AASHTO LRFD Bridge Design Specifications[8]. In the first test, P4-24T, the only supplemental restraint provided to the bulbs to resist transverse displacement was the shearing resistance provided by the elastomeric bearing pads at the support points. In the second test, P4-24D, additional passive restraint was provided through blocking installed outside of the bulbs at the support points and through steel straps installed between the bottom faces of the bulbs near midspan.

In test P4-24T, the girder exhibited first cracking of the deck at total applied loads of 53 kN (12 kips) per loading patch (i.e., 106 kN (24 kips) total applied load). A slightly higher load of 58 kN (13 kips) per loading patch (i.e., 116 kN (26 kips) total applied load) caused first cracking in test P4-24D. This load capacity at first cracking is approximately equivalent to the design

tandem wheel patch live loads defined in the AASHTO LRFD[8]; however, the capacity is insufficient to account for impact factors or lane loads prior to cracking.

The midspan middeck vertical deflection response of the two test girders is shown in Figure 3. The figure shows that the responses were similar until first cracking, after which P4-24T shows significantly increased vertical deflection per load increment applied. The peak load carried by P4-24D is 60 percent greater than the peak load carried by P4-24T with both girders undergoing similar magnitude deflections prior to failure.

Visual observations and data recorded during and after failure indicate that the responses of the two girders differed significantly. In P4-24T, the girder seemed to exhibit behaviors consistent with one-way bending of a deck which was simply supported at the girder legs. In P4-24D, the girder seemed to exhibit behaviors consistent with one-way bending of a deck which was restrained at the leg-to-deck interface. These different responses were most clearly depicted in the bulb spreading response of the two girders, through the flexural cracking above the legs in P4-24D, and in the steel strap forces observed in P4-24D.
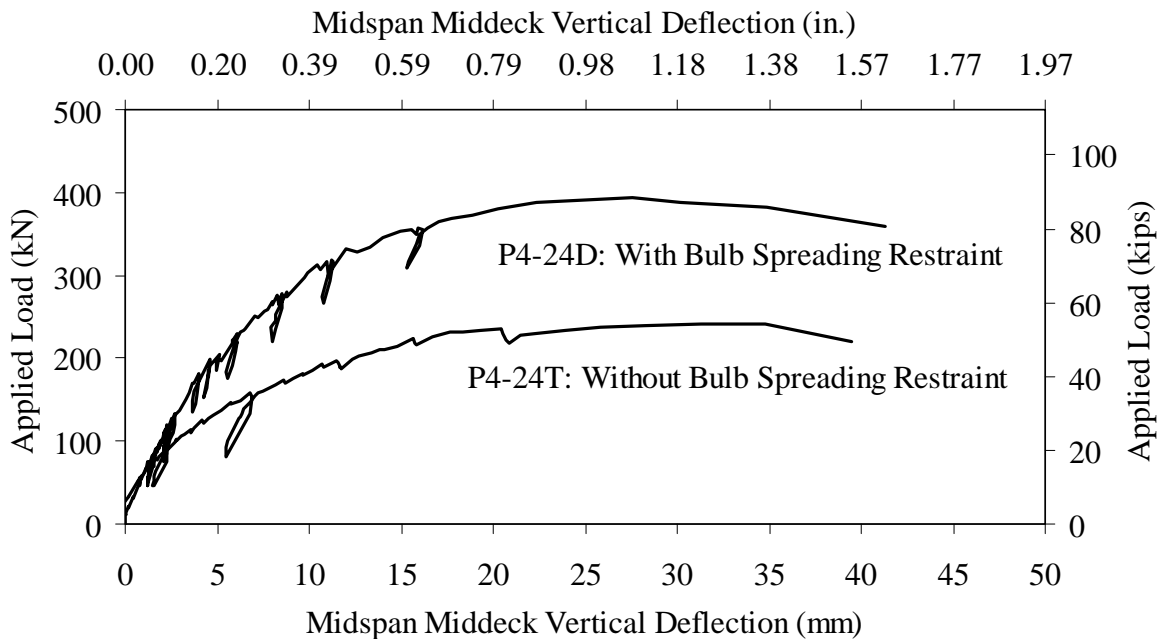
Figure 3. Graph. Midspan middeck vertical deflection results from two transverse flexural response tests.

CHAPTER 3. MATERIAL PROPERTIES

INTRODUCTION

The material properties of the UHPC in the pi-girder specimens were obtained through the testing of cylinders cast with the girder specimens. The properties of the UHPC and the high performance grout used in the joint detail were similarly tested. Finally, tension tests of the steel rebar installed transversely in the joint detail were completed. These material property results are reported herein.

PI-GIRDER CONCRETE MATERIAL PROPERTIES

During the casting of the pi-girder specimens, 76-mm (3-inch) and 102-mm (4-inch) diameter cylinder specimens were cast in order to allow for material property characterization. These cylinders were cast in the field alongside the girders using UHPC obtained from the trucks which were casting the girders. As the concrete for each leg of the girders came from an individual truck which held a specific batch of UHPC, cylinders were made from each truck's concrete. After casting, the cylinders were stored with the girders during curing and heat treatment.

The cylinders were prepared for testing by grinding both ends to create parallel surfaces through the use of an end grinder. After preparation, the cylinders exhibited length to diameter ratios of approximately 1.9. Three tests were carried out on the cylinders, namely density, compressive strength, and split cylinder tensile strength. Density measurements were obtained through conventional means by measuring weight of each cylinder and dividing by the volume. The average density of the UHPC was 2560 kg/m^3 (160 lb/ft^3).

The compressive strength tests were completed on 76-mm (3-inch) diameter cylinders. The tests were completed according to ASTM C39[10], except that the load rate was increased to 1.0 MPa/sec (150 psi/sec). The compressive strength results are presented in 0. The tests were completed during the timeframe when the girders were being tested. In general, the cylinders were 3 to 4 months old. Overall, the compressive strength of the UHPC used in the girders was 258 MPa (37.5 ksi) with a standard deviation of 6.2 MPa (0.9 ksi).

Table 3. UHPC pi-girder compressive strength results.

Ready Mix Truck	No.	Compressive Strength	
		Average, MPa (ksi)	Standard Deviation, MPa (ksi)
Truck #1	6	256 (37.1)	7.6 (1.1)
Truck #2	6	261 (37.8)	3.5 (0.5)

The split cylinder tensile strength tests were completed on 102-mm (4-inch) diameter cylinders. The tests were completed according to the procedure described briefly in reference (1) and more fully in reference (12). The procedure is the same as that described in ASTM C496[13] with the

exception of an increased load rate (3.45 MPa/min (500 psi/min)) and extra data collection allowing for determination of lateral specimen expansion throughout the test. Three 102-mm (4-inch) diameter cylinders were tested from the concrete in each truck. Results from these tests are presented in Table 4. The resulting overall cracking tensile strength was 13.5 MPa (2.0 ksi) with a standard deviation of 1.93 MPa (0.28 ksi).

Table 4. UHPC pi-girder split cylinder tensile test results.

Ready Mix Truck	No.	Cracking Strength, MPa (ksi)		Peak Strength, MPa (ksi)	
		Average	Standard Dev.	Average	Standard Dev.
Truck #1	3	12.5 (1.81)	0.62 (0.09)	22.1 (3.20)	1.45 (0.21)
Truck #2	3	14.5 (2.11)	2.41 (0.35)	23.6 (3.43)	2.07 (0.30)

JOINT DETAIL MATERIAL PROPERTIES

The joint detail implemented in Tests T1J and T2J included two different types of grout, as well #8 reinforcing bars which were inserted in pockets and spanned across the grouted joint. The grout and rebar test results are as follows.

Transverse Reinforcing Bars

Standard #8 reinforcing bars, 0.66 m (26 inch) in length, were installed in pockets spanning across the grouted joints. Two samples of these bars were tested in uniaxial tension according to ASTM A370[14]. The yield strengths of the steel were determined to be 503 and 505 MPa (72.9 and 73.3 ksi) for the two bars based on the 0.2% offset method. The ultimate strengths were 769 and 771 MPa (111.6 and 111.8 ksi). At failure, the elongations over an initial gage length of 200 mm (7.88 inch) were 14.9% and 15.3%. Figure 4 shows the stress-strain response from one of the two tests. Note that the stress is based on the nominal cross section of the bar and thus represents engineering stress. Additionally, note that the strain was calculated through readings captured by an extensometer placed on the bar until the initiation of strain hardening, after which the extensometer was removed and the machine cross-head displacement readings were used.
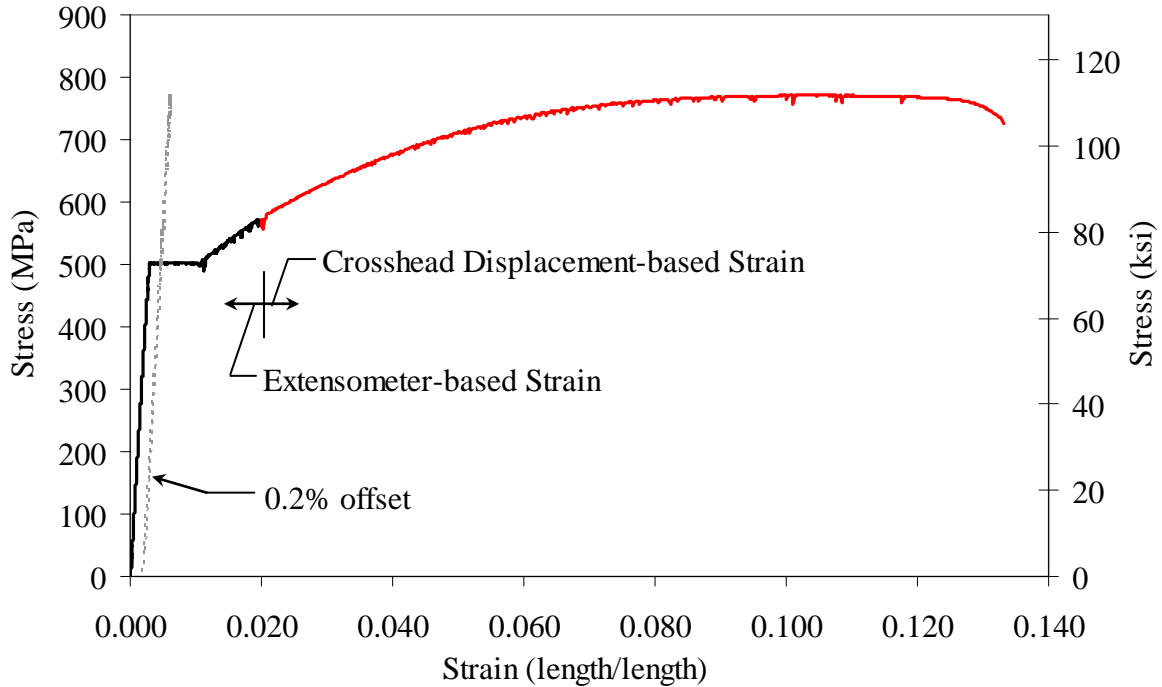
Figure 4. Graph. Uniaxial stress-strain response of a #8 rebar.

Test T1J Joint Fill Grout

The same UHPC formulation used in the fabrication of the UHPC pi-girders was used in the construction of the grouted joint in Test T1J. A total of 0.23 m³ (8.0 cubic feet) of UHPC was mixed in a Lancaster Model K-4 pan mixer. During the casting of the joint, 76-mm (3-inch) and 102-mm (4-inch) diameter cylinder specimens were cast in order to allow for material property characterization. After casting, the cylinders were stored alongside the girder so as to endure similar curing conditions.

The 76-mm (3-inch) diameter cylinders were tested for compressive strength following the same procedure as previously discussed for the pi-girder cylinders. Six cylinders were tested. The average compressive strength was 200 MPa (29.0 ksi), with a standard deviation of 2.8 MPa (0.4 ksi).

The 102-mm (4-inch) diameter cylinders were tested for splitting cylinder tensile strength following the same procedure previously discussed for the pi-girder cylinders. The results are presented in Table 5. The average tensile cracking strength was 4.8 MPa (0.70 ksi).

Table 5. UHPC joint fill split cylinder tensile test results.

No.	Cracking Strength, MPa (ksi)		Peak Strength, MPa (ksi)	
	Average	Standard Dev.	Average	Standard Dev.
4	4.83 (0.70)	0.97 (0.14)	21.7 (3.15)	0.55 (0.08)

13

T2J Joint Fill Grout

A magnesium phosphate grout, Eucospeed MP, was used as the joint fill material for Test T2J. This prebagged grout was extended with pea gravel at 240 kg/m^3 (15 lb/ft^3). The grout was mixed according to manufacturers instructions in 6.5 liter (0.23 ft^3) batches. In total, 29 batches were mixed with the first 26 being poured into the joint and the final three being used to fabricate 102-mm (4-inch) diameter cylinders. Ten cylinders were fabricated.

Ten compressive strength tests were completed according to ASTM C39[10], with three cylinders first being tested for modulus of elasticity tests according to ASTM C469[11]. After the conclusion of the three modulus of elasticity tests, the compressometer was removed and the cylinders were subsequently tested to failure according to ASTM C39. The average modulus of elasticity result was 40.5 GPa (5880 ksi) with a standard deviation of 1.7 GPa (250 ksi). The average compressive strength result from all 10 cylinders was 44.7 MPa (6.5 ksi) with a standard deviation of 3.2 MPa (0.5 ksi).

CHAPTER 4. GIRDER DESIGN, FABRICATION, AND TESTING METHODS

INTRODUCTION

The experimental program is described in this chapter. The girder design is described first. The girder fabrication process is then presented, followed by a discussion of the test matrix and the test setups. The specific details of each girder specimen and the instrumentation plan for each girder test are then presented.

GIRDER DESIGN

The pi-girder was developed to efficiently utilize the advanced material properties of UHPC. Its design is based on resisting the loadings prescribed in the AASHTO LRFD Bridge Design Specification[8]. The concept for the design was described previously in Chapter 2. Analytical calculations completed as part of the design effort were primarily conducted through the use of 1D, 2D, and 3D computer analyses. Additionally, experience gained through the development and testing of the prototype pi-girder significantly informed the development of the 2nd generation pi-girder.

The cross section investigated in this study is a modification of the prototype pi-girder cross section designed to span between 21.3 and 30.5 m (70 to 100 feet). The 2nd generation cross section is shown in Figure 5. The girder is 0.84 m (33 inches) deep, 2.54 m (8.33 feet) wide, and can contain up to 16 prestressing strands in each bulb. The integral deck of the girder is 105 mm (4.13 inches) thick, and the webs range from 81 to 89 mm (3.2 to 3.5 inches) thick. A 133 mm (5.25 inch) deep shear key runs the length of each flange tip to allow for connection of the modular components. Basic properties of the girder include an area of 0.555 m^2 (861 in^2), strong axis moment of inertia of approximately 44×10^9 mm^4 (106,000 in^4), and a self-weight of 1,390 kg/m (932 lb/ft). As compared to the prototype pi-girder, this girder weighs 42% more per unit length and has a 19% greater moment of inertia.

The 2nd generation pi-girder was also designed to include intermediate diaphragms. These diaphragms are included so as to assist in maintaining the integrity of the cross section during erection and under structural loading. For the testing completed herein, two diaphragms were installed for each test with each diaphragm being located 1.83 m (6 feet) from midspan. Figure 6 and Figure 7 show the details of the diaphragms. Figure 6 shows the two different diaphragms configurations with one designed for the space between the legs of an individual girder and the other designed to be installed between two adjacent girders. Figure 7 shows the details of the end plates welded onto the end of the steel tubes that comprise the length of the diaphragms. Note that the dimensions shown in these two figures are in inches.

During the installation of the diaphragms for Tests T1D and T2D it was recognized that the diaphragms were overlength and thus could not be installed without imparting stresses into the pi-girder. As such, these two diaphragms were modified so as to allow proper fit-up. Each end plate of each of these girders was milled such that the thickness of the plate was reduced from 13 mm (0.5 inch) to a thickness between 8 and 9 mm (0.31 and 0.35 inch). This reduction in overall diaphragm length allowed the diaphragms to slide into place.

Figure 5. Illustration. Girder cross section and strand pattern.

Figure 6. Illustration. Elevation view of diaphragms.

Figure 7. Illustration. End view of diaphragm end plate.

The design of the 2nd generation pi-girder also allowed for the development of a novel longitudinal joint detail. This joint detail, which is shown in Figure 8, is a combination of a longitudinal shear key and periodic mild-steel reinforced grout pockets. The diamond-shaped shear key is 90-mm (3.5-inch) tall and has a 25-mm (1-inch) opening along the top to allow for insertion of the grout. The periodic grout pockets extend 356 mm (14 inch) into each adjacent

16

girder and are 102 mm (4 inch) wide and deep. Each pocket is intersected by two #5 reinforcing bars. A 660- mm (26-inch) long #8 reinforcing bar is to be installed in each pocket with the pockets being spaced at 457 mm (18 inch) along the length of the girder.
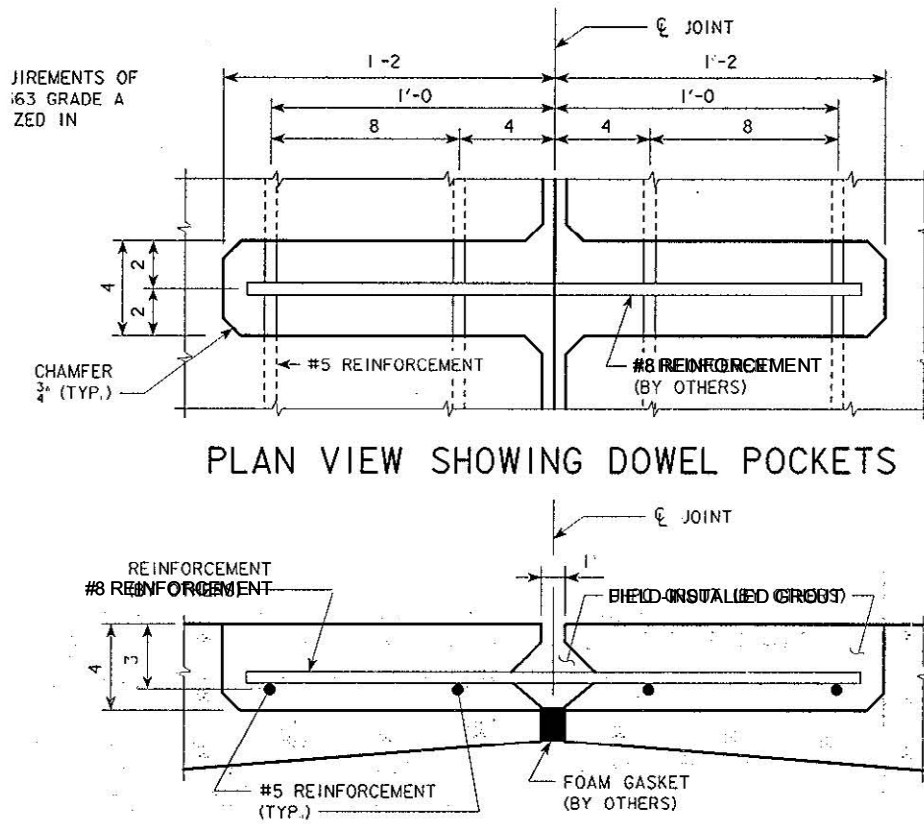
Figure 8. Illustration. Longitudinal grouted joint detail.

GIRDER FABRICATION

Two UHPC pi-girders were fabricated at the Lafarge Precast facility in Winnipeg, Manitoba. The two girders were fabricated together on the same casting bed in September 2008. The formwork used for the fabrication of the girders was fabricated by Helser Industries, Inc. of Tualatin, Oregon. A pair of approximately 11-m (36-ft) long forms were fabricated and installed end-to-end on the girder casting bed. This casting bed was wide enough to allow for the entire girder width to be supported as well as to allow for the exterior side forms to be slid back from the girder during assembly and disassembly. Figure 9 shows the formwork during assembly on the bed. As can be observed in the figure, the left and right form pieces which support the underside of the concrete deck adjacent to the form's center post can articulate down and toward the middle so as to allow for unrestrained transverse dimensional changes in the girder during setting and hydration. The mechanism for transverse restraint release is shown specifically in Figure 10. An overhead photograph of the forms for girders T1 and T2 is shown in Figure 11.

17

Figure 9. Photo. Girder formwork.

Figure 10. Photo. Girder formwork mechanism for releasing transverse restraint.

Figure 11. Photo. Girder formwork for T2 (near) and T1 (far).

The process of preparing the form for casting included: 1) assembling and locking in place the center portion of the form, 2) installing the bulkheads at the ends of the girders, 3) pulling the prestressing strands through the form, 4) sealing gaps in the form using silicone caulk, 5) installing the side forms, 6) installing rebar in the deck at designated locations, and 7) installing Styrofoam blockouts in the deck to create the grout pockets for the dowel bars. Extra care was taken to ensure that, to the greatest extent possible, the forms were securely bolted to the prestressing bed and any gaps in the formwork were sealed.

The girders were prestressed through the use of 15.2-mm (0.6-inch) diameter, 1860 MPa (270 ksi) low-relaxation prestressing strands. The girders contained 22 strands, with 9 in each of the two bulbs and two in the deck above each web. The strands in the bulbs were all stressed to 189 kN (42.5 kips). The strands in the deck were each pulled to 22 kN (5 kips). Figure 5 shows the girder cross section along with the strand pattern. Six of the strands were debonded for 0.91 m (36 inch) from each end of each girder.

Ductal BS1000, a UHPC premix manufactured by Lafarge, was mixed according to the proportions shown in Table 6. Each girder had a volume of 4.2 m^3 (5.5 yd^3), thus 4.96 m^3 (6.5 yd^3) was mixed to allow for 18% wasteage. This precise volume was chosen as it required twelve full bags of premix per girder. The premix was blended approximately 5 months prior to mixing. Discontinuous, dispersed steel fibers are included in the mix at 2 percent by volume. These steel fibers were 13 mm (0.5 inch) long and had a diameter of 0.2 mm (0.008 inch). They were manufactured by Baumbach-Metall and had a specified minimum tensile strength of 2000 MPa (290 ksi).

19

Table 6. UHPC mix design.

Constituent	Quantity
Premix	2195 kg/m^3 (3700 lb/yd^3)
Chryso Premia 150 Superplasticizer	30 kg/m^3 (50.5 lb/yd^3)
H$_2$O (Ice)	130 kg/m^3 (219 lb/yd^3)
Steel Fibers	156 kg/m^3 (262.5 lb/yd^3)

The volume of UHPC necessary for the casting of the two girders was mixed simultaneously in two conventional ready mix concrete trucks. The trucks were sized so as to ensure that they remained at or below 60% volumetric capacity during the mixing. All constituents were placed directly into each drum through the charge/discharge opening.

The mixing process began with the insertion of the total volume of premix into each drum, after which the premix was mixed to ensure homogenization. The cubed ice was then added into the drum, followed by the superplasticizer. This process, which took approximately 20 minutes, was completed while the drum was rotating at approximately 6 revolutions per minute (rpm). The drum was then rotated at 12 rpm until the ice had melted and the UHPC had mixed to form a thick slurry. This mixing, which lasted approximately 15 minutes, was halted as soon as the slurry formed so as to minimize the heat buildup in the UHPC. The steel fiber reinforcement was then added to the mix with the drum slowly rotating at 6 rpm. Finally, once all constituents were added, the drum was rotated at 12 rpm for approximately 15 minutes to finalize mixing and at 2 rpm for at least 2 minutes to eliminate trapped air. Figure 12 shows a photograph of the premix being added to one of the ready-mix trucks.
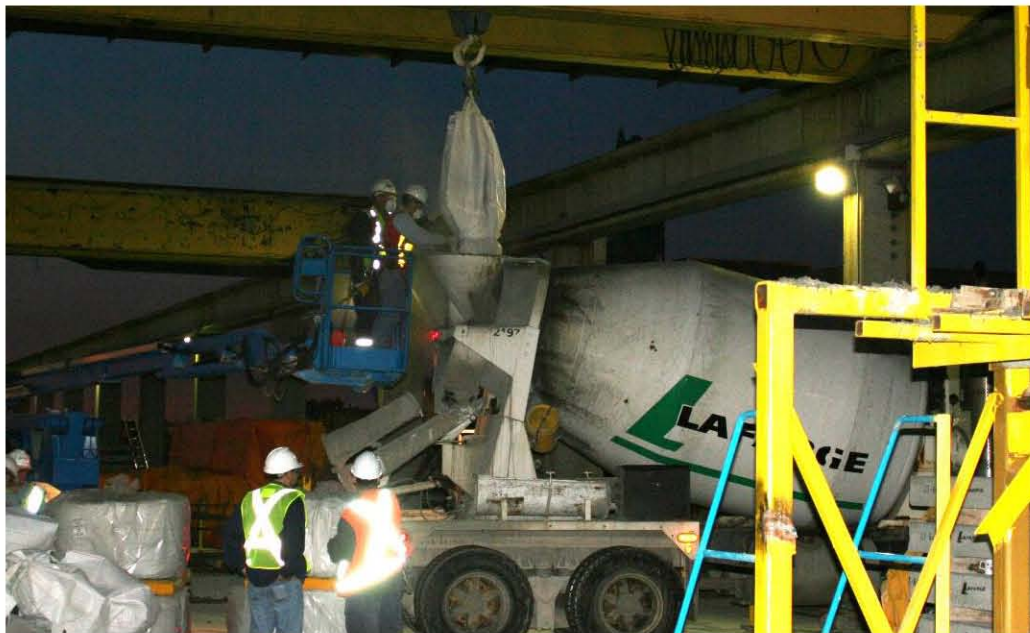
Figure 12. Photo. UHPC premix being added to mixer.

After the mixing was complete, the trucks transported the concrete to the form. The first girder was completely cast using concrete from both trucks prior to the start of the filling of the second girder's form. In each case, the bulbs and webs were filled first with one truck on each side of the formwork discharging concrete into the top of the web opening. As the concrete is self-consolidating, the concrete was discharged beginning at one end of the girder and allowed to flow toward the other end. The discharge point moved along the girder length as the form began to fill up, but always remained behind the leading edge of the flowing concrete. Figure 13 shows the concrete being placed in one of the girder legs. Once both webs of the form were full to approximately two-thirds of their height, a trough was inserted in the placement stream to allow for uniform dispersion of the concrete across the deck width.   Again, the concrete was always allowed to flow along the length of the girder with deposition of new concrete occurring behind the leading edge. Figure 14 presents a photograph of the placing of the concrete for the deck through the trough which is shown sitting above the form. Short duration bursts of external form vibration were used infrequently during the placing process. This vibration was intended to facilitate the expulsion of air trapped in the concrete during the placing process. As soon as the girder form was full, a thin layer of curing compound was sprayed onto the surface of the deck and then plastic sheeting was placed over the concrete. The plastic was placed directly in contact with the concrete, as is shown in Figure 15.

In total, the placing of the concrete into the two girder forms lasted for approximately 2 hours. Aside from the time required to repeatedly fill the trough and then reposition it over the form, the placing went quickly. Minimal dehydration of the exposed UHPC on the deck surface was observed during casting; likely this was assisted by the favorable weather conditions inside the enclosed precast facility.

Figure 13. Photo. Concrete placement for girder legs.

Figure 14. Photo. Concrete placement for girder deck.

Figure 15. Photo. Plastic tarp installed immediately after concrete placement.

The environment in the indoor precast facility had an ambient temperature of between 15 and 22 ℃ (59 and 72 ℉) for days following girder casting. No supplemental heat or steam was provided to the girders during their initial curing. The interior and exterior forms were released when match-cured cylinders indicated that the compressive strength of the concrete was 35 MPa (5.1 ksi). This occurred approximately 33 hours after first water (ice) addition during UHPC mixing.

After form release, the concrete was allowed to continue to cure until match-cast cylinders demonstrated that the compressive strength of the concrete was at least 100 MPa (14.5 ksi). Once this strength was reached, the prestressing strands were detensioned by flame-cutting individual strands.

After stressing, the two girders were moved to a casting bed which had been arranged for application of a steam treatment. The steam treatment consisted of releasing live steam under the girders which were insulated by multiple layers of insulating tarps. The volume of steam released was ramped up and down over 6 hours so as not to thermally shock the girders. The environment surrounding the girders was maintained at a temperature of at least 90 ℃ (194 ℉) and not more than 96 ℃ (205 ℉) for more than 48 hours. After the application of the steam treatment, the girders were transported to the FHWA's Turner-Fairbank Highway Research Center.

GIRDER TEST PROCEDURE

Upon delivery to TFHRC, the two girders were brought into the Structural Testing Laboratory. Four full-scale destructive investigations of structural behavior were completed through the use of these two girders. All structural tests focused on the ability of this 2nd generation UHPC pi-girder cross section to transversely transmit locally applied wheel loads from the deck into adjacent girder legs. Table 7 provides details on these tests, with the tests being completed in the order shown in the table. In all four tests, the loads were applied by hydraulic jacks pushing vertically downward on the top of the deck.

As fabricated, Girders T1 and T2 differed only in that Girder T1 did not contain any mild steel reinforcement in the deck while Girder T2 included 1.68-m (66-inch) long #5 reinforcing bars in the deck at a spacing of 0.30 m (12 inch). The mild steel reinforcement spanned between the Girder T2 legs with 25-mm (1-inch) clear cover to the bottom of the deck. The test setup for Tests T1J and T2J induced another difference between the specimens; namely, that UHPC joint fill was used in Test T1J while Eucospeed MP was used in Test T2J.

Table 7. Girder tests.

Test Identifier	Girder	Description
T1D	T1	Transverse flexural behavior w/ no rebar in deck
T2D	T2	Transverse flexural behavior w/ rebar in deck
T1J	T1	Joint behavior w/ UHPC joint fill
T2J	T2	Joint behavior w/ Eucospeed MP joint fill

TEST SETUP AND INSTRUMENTATION

Tests T1D and T2D

Tests T1D and T2D were nearly identical tests applied to Girders T1 and T2, respectively. These tests focused on the transverse flexural behavior of the 2nd generation pi-girder cross section when subjected to loads applied between an individual girder's legs. The loading setup for these tests is illustrated in Figure 16. Figure 17 and Figure 18 provide photographs of the setup as applied for Test T2D. Loads were applied vertically downward by hydraulic jacks situated near midspan. Loads were transmitted to the deck through 0.25 m by 0.51 m (10 inch by 20 inch) elastomeric pads located along the centerline of the girder and situated 0.61 m (2 ft) on either side of midspan. These 25 mm (1 inch) thick elastomeric pads were backed by 25 mm (1 inch) thick steel plates. Loads were reacted through 0.15 m by 0.30 m (6 inch by 12 inch) elastomeric pads placed under the girder bulbs at the abutment locations. These elastomeric pads were also 25 mm (1 inch) thick.

Figure 16. Illustration. Loading setup and instrumentation lines for Tests T1D, T2D, T1J, and T2J.

Figure 17. Photo. Setup for Test T2D.

Figure 18. Photo. West end of Test T2D.

Strain gages, potentiometers, and LVDTs were used to capture the behavior of the girder throughout the application of loads in these tests. The instrumentation was applied to cross sections at midspan, at the quarter point, and at the abutment toward the west end of each test setup. Figure 19 and Figure 20 show the locations of strain gages applied to the surface of the girder. Figure 21 and Figure 22 show the locations of the linear potentiometers. Figure 23 shows the locations of the LVDTs. Note that the two LVDTs measured displacement of the girder relative to the abutment at the northwest support elastomeric pad.

Figure 19. Illustration. Midspan strain gage locations for Test T1D and Test T2D.

Figure 20. Illustration. Quarter point strain gage locations for Test T1D and Test T2D.

Figure 21. Illustration. Midspan potentiometer locations for Test T1D and Test T2D.

Figure 22. Illustration. Quarter point potentiometer locations for Test T1D and Test T2D.
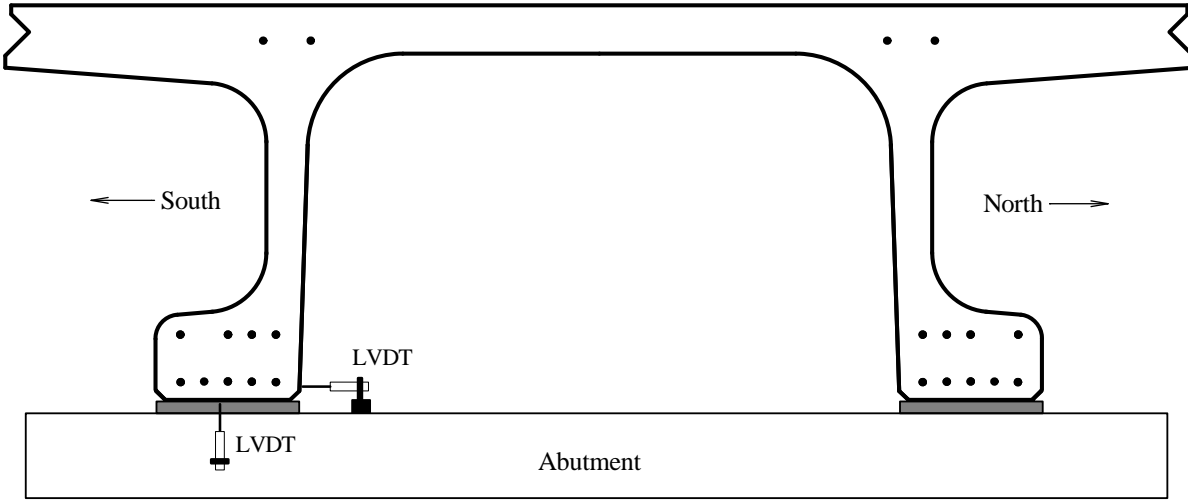
Figure 23. Illustration. Abutment LVDT locations for Test T1D and Test T2D.

Tests T1J and T2J

Tests T1J and T2J were nearly identical tests applied to Girders T1 and T2, respectively. These tests focused on the transverse flexural and shear behaviors of the 2nd generation pi-girder cross section when subjected to loads applied between an individual girder's legs. The elevation view of the loading setup for these tests is identical to that implemented for Tests T1D and T2D and is illustrated in Figure 16. Figure 24 and Figure 25 provide photographs of the setup. Loads were

applied vertically downward by hydraulic jacks situated near midspan. Loads were transmitted to the deck through 0.25 m by 0.25 m (10 inch by 10 inch) elastomeric pads situated 0.61 m (2 ft) on either side of midspan. The pads were aligned such that their south edges coincided with the centerline of the grouted joint. A photograph of the location of the loading pads is provided in Figure 26. These 25 mm (1 inch) thick elastomeric pads were backed by 25 mm (1 inch) thick steel plates. Loads were reacted through 0.15 m by 0.30 m (6 inch by 12 inch) elastomeric pads placed under the girder bulbs at the abutment locations. These elastomeric pads were also 25 mm (1 inch) thick.
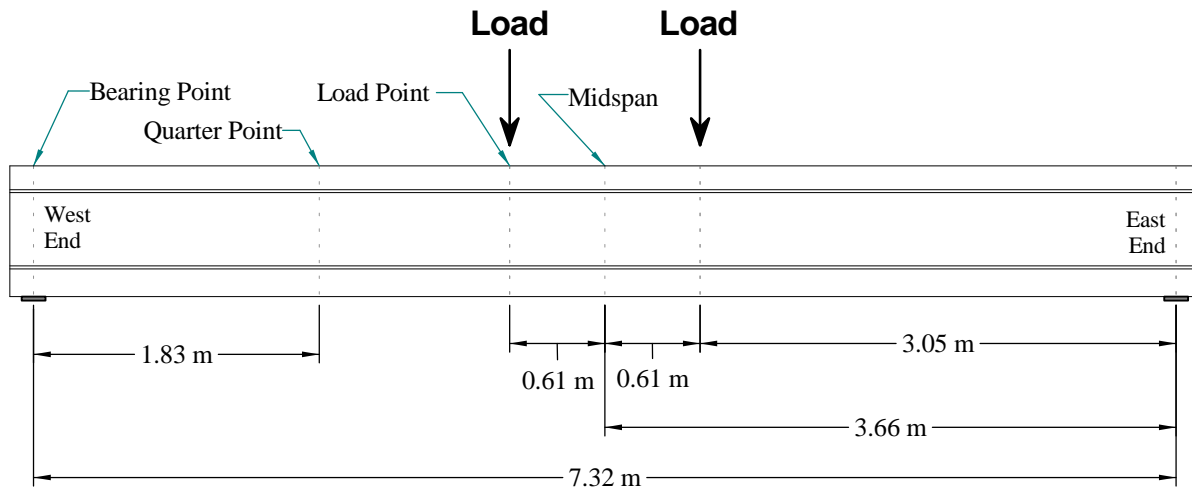

Figure 24. Photo. Setup for Test T2J.

Figure 25. Photo. East end of Test T1J.
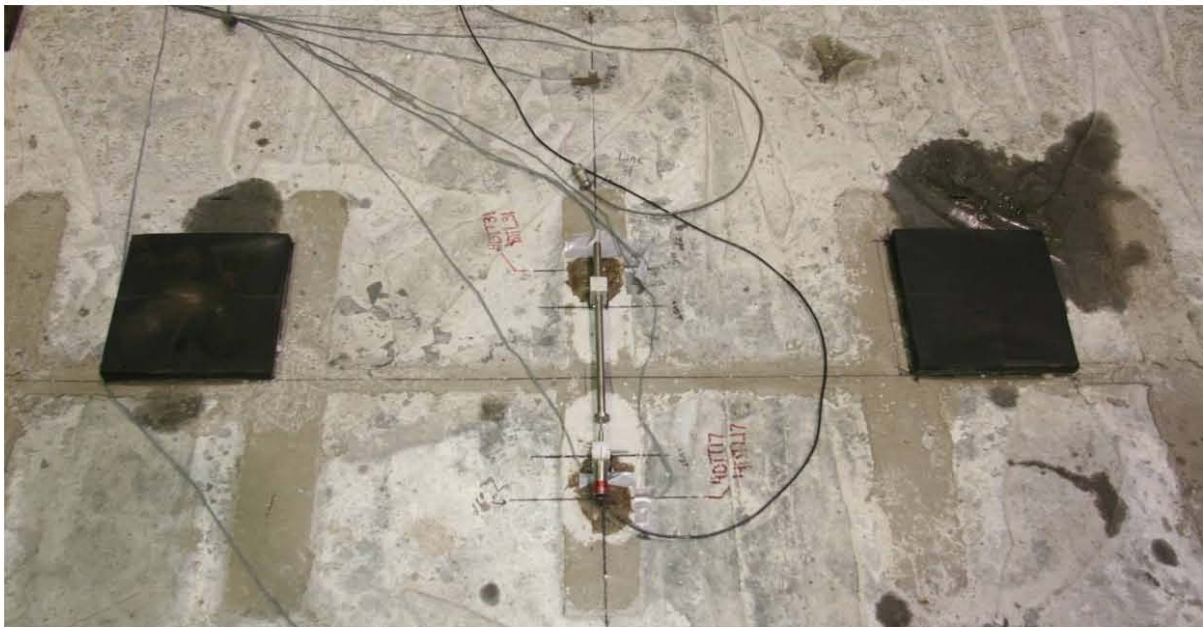
Figure 26. Photo. Elastomeric loading pads abutting the centerline of the grouted joint in Test T2J.

Strain gages, potentiometers, and LVDTs were used to capture the behavior of the girder throughout the application of loads in these tests. The instrumentation was applied to cross sections at midspan, at the quarter point, and at the abutment toward the west end of each test setup. Figure 27 and Figure 28 show the locations of strain gages applied to the surface of the girder. Figure 29 and Figure 30 show the locations of the linear potentiometers. Figure 31 and Figure 32 show the locations of the LVDTs. Note that the two LVDTs at the abutment measured displacement of the girder relative to the abutment at the northwest supporting elastomeric pad. The two LVDTs at midspan measured the transverse displacement of one girder flange tip relative to the other across the grouted joint.
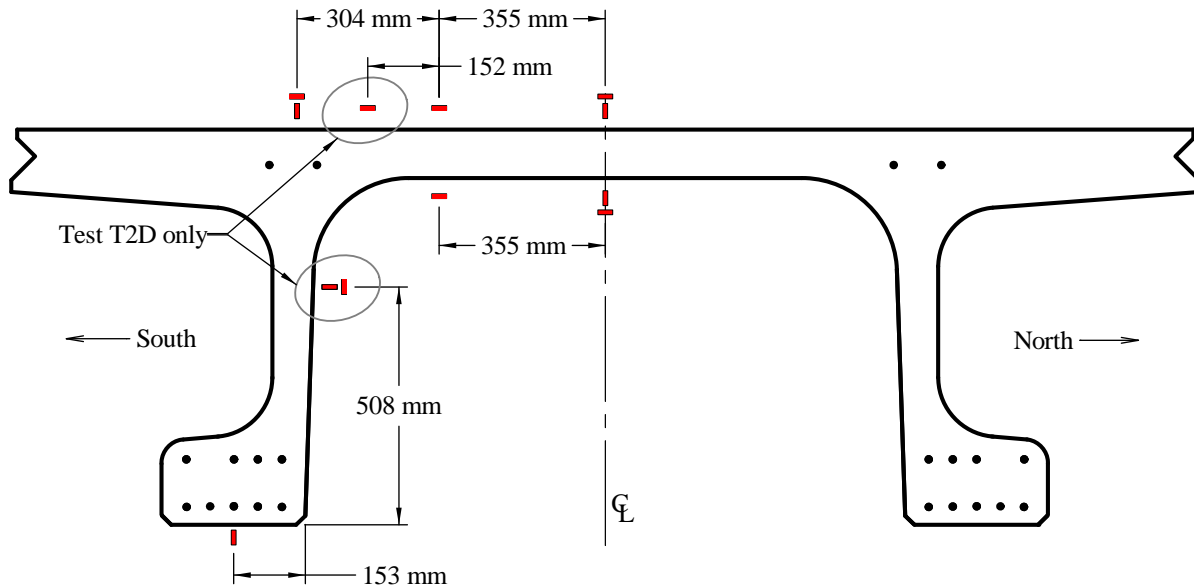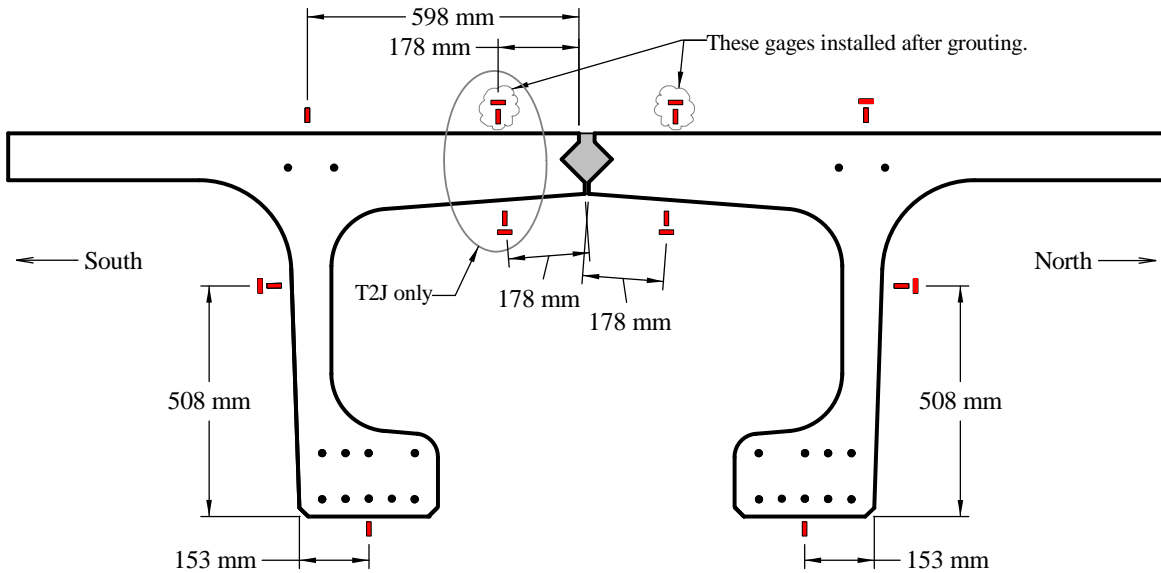

Figure 27. Illustration. Midspan strain gage locations for Test T1J and Test T2J.
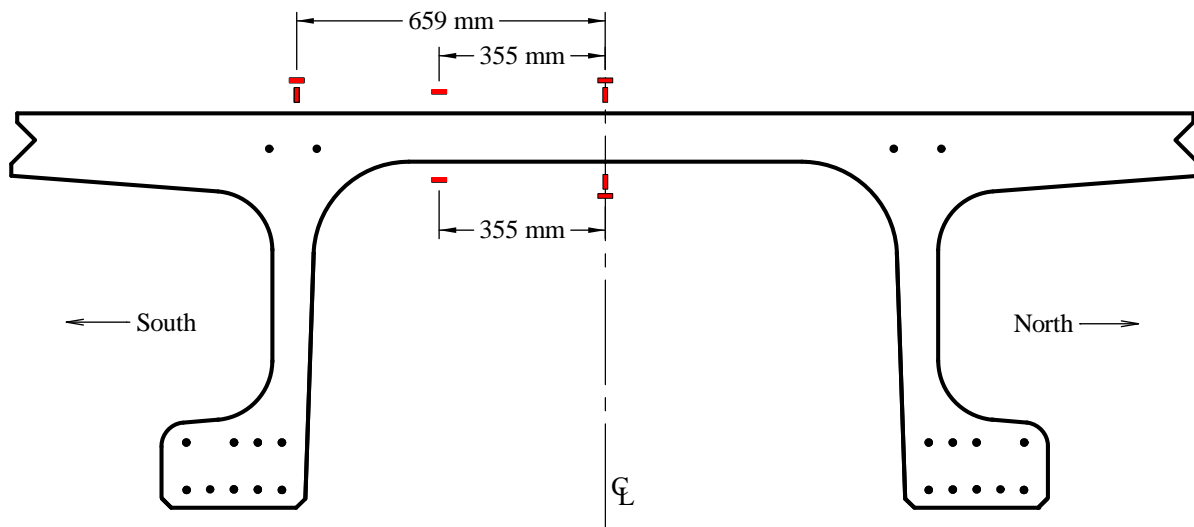
31
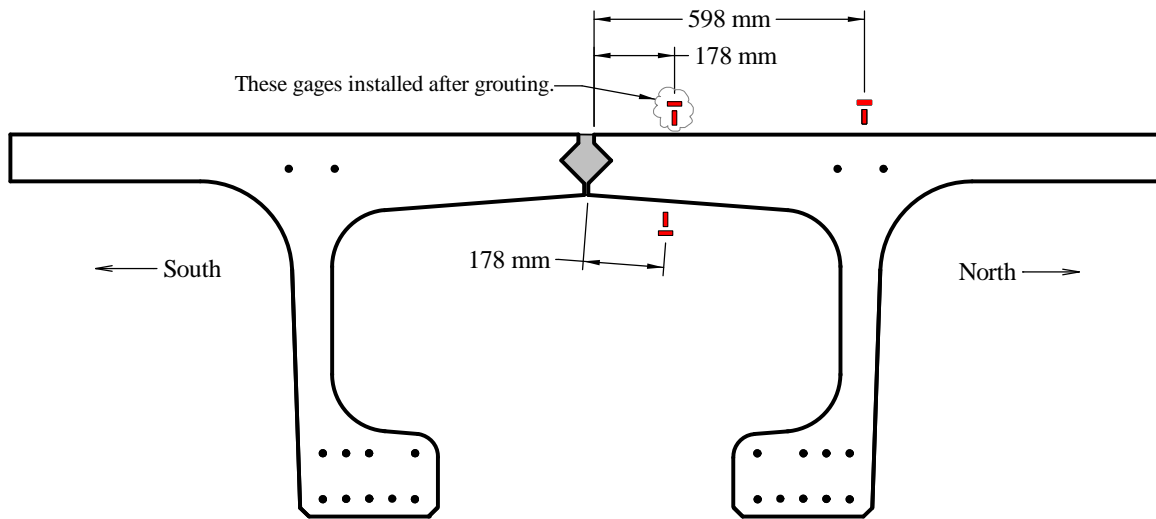
Figure 28. Illustration. Quarter point strain gage locations for Test T1J and Test T2J.
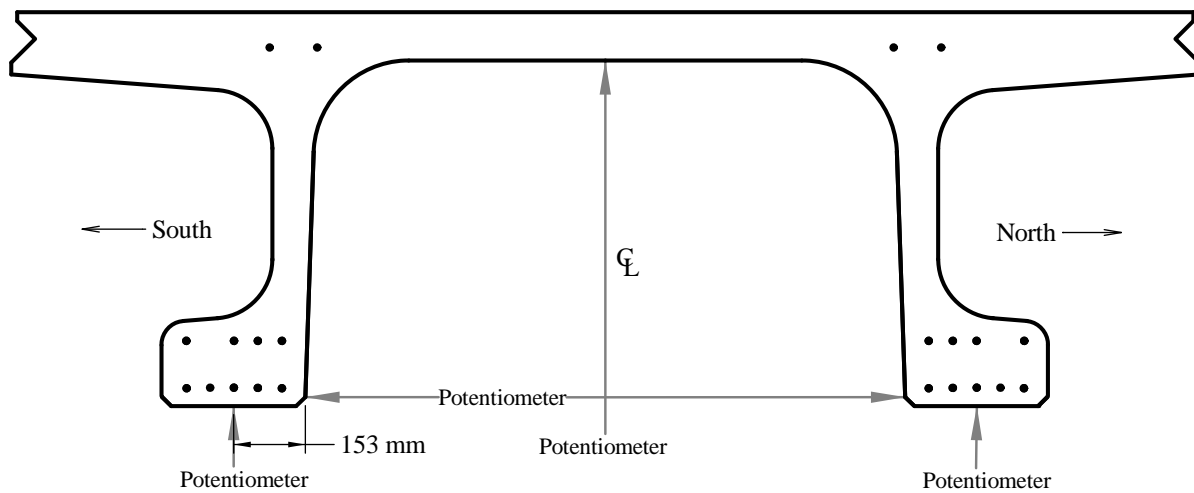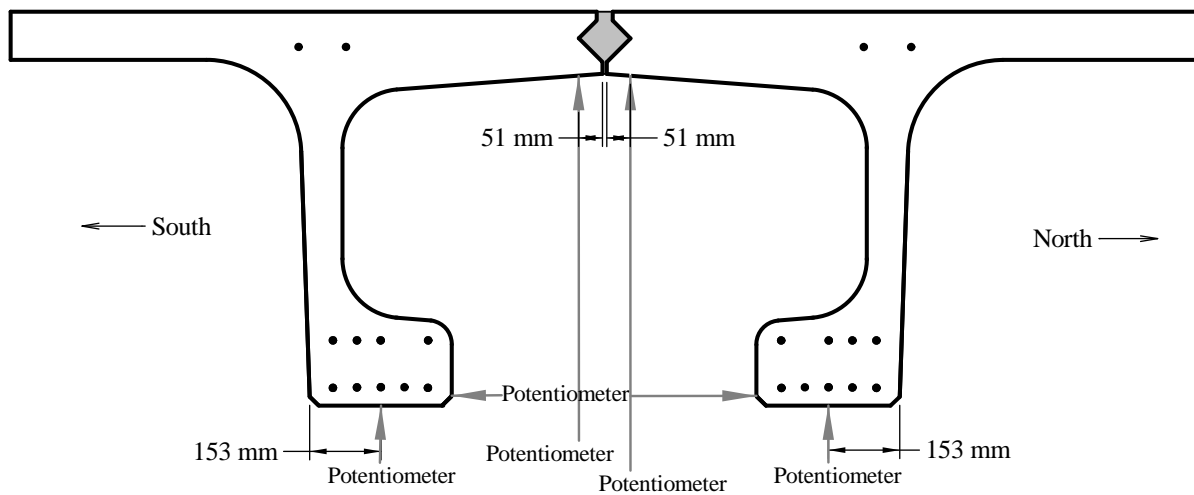

Figure 29. Illustration. Midspan potentiometer locations for Test T1J and Test T2J.
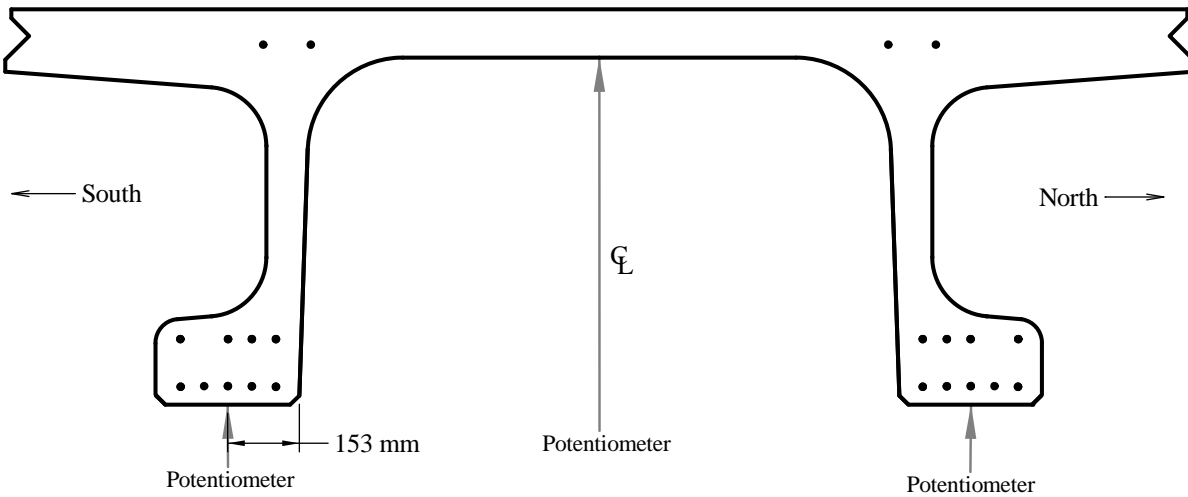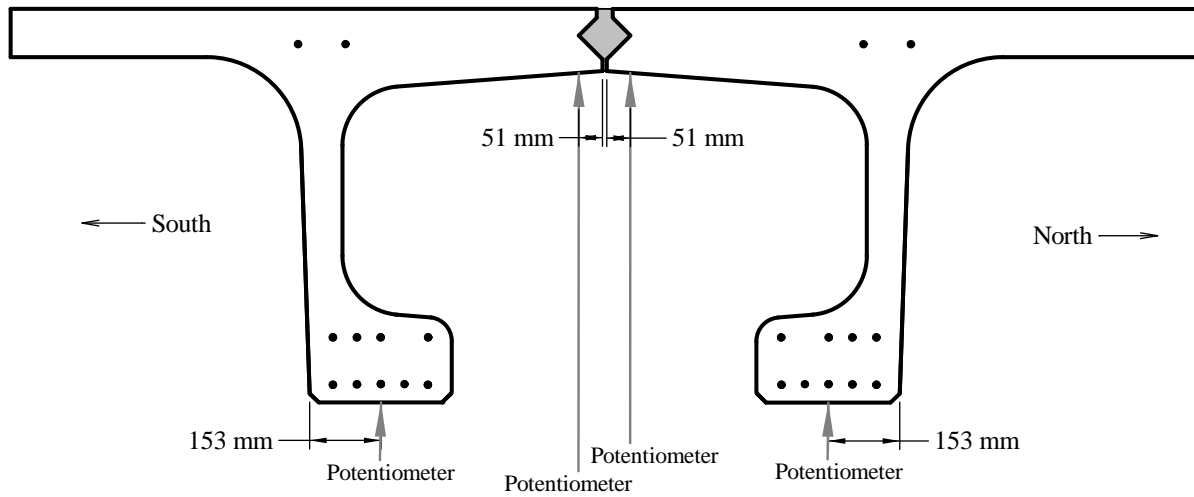
**Figure 30. Illustration. Quarter point potentiometer locations for Test T1J and Test T2J.**
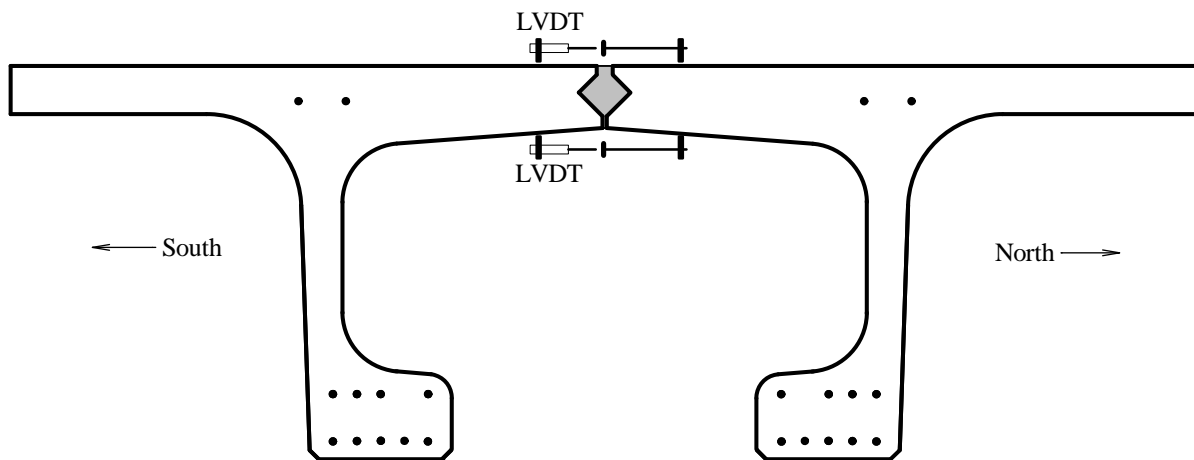
Figure 31. Illustration. Midspan LVDT locations for Test T1J and Test T2J.
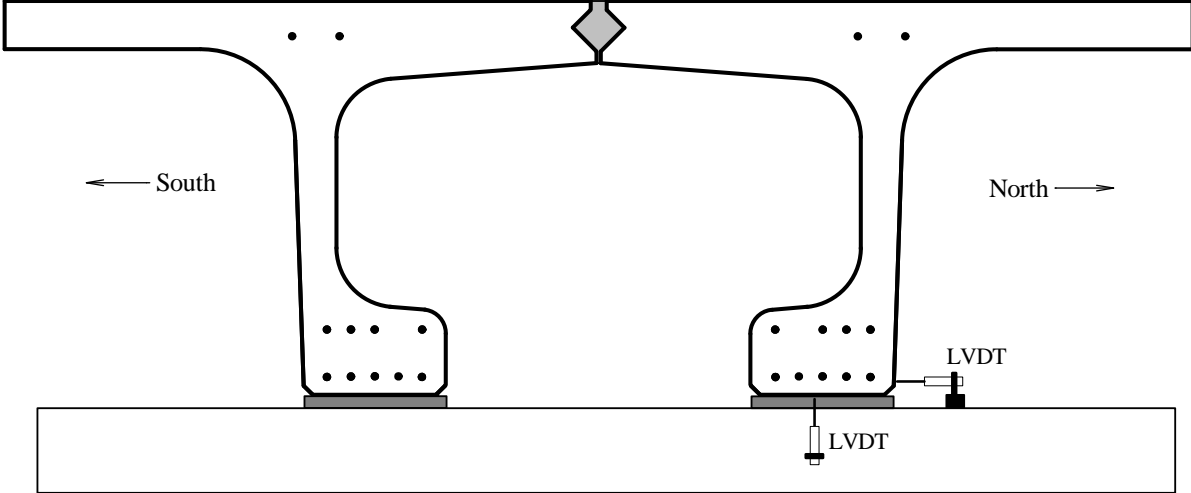
Figure 32. Illustration. Abutment LVDT locations for Test T1J and Test T2J.

CHAPTER 5. TEST RESULTS

INTRODUCTION

The results of the full-scale structural testing completed in this study are presented in this chapter. Results from the two transverse flexure tests completed on as-fabricated 2nd generation pi-girders are presented first. Results from the two transverse flexure tests which focused on the structural response of the longitudinal joint then follow.

STATIC TRANSVERSE FLEXURE TESTING

Four structural tests were completed with the aim of investigating the response of the girder cross-section to loads applied between girder webs. Tests T1D and T2D were completed on girders that had not previously been tested. These tests focused on the response of the girder cross section to loads applied between the two legs of an individual girder. Tests T1J and T2J were completed thereafter. These tests focused on the response of the girder cross section to loads applied near the longitudinal joint which connects two adjacent pi-girders.

T1D

Test T1D was intended to investigate the transverse flexural response of the 2nd generation pi-girder cross section. The test was completed using the previously untested, 7.6-m (25-foot) long Girder T1. The setup for the test included a 7.3 m (24 foot) span, two point loads applied in the middle of the deck with each being 0.61 m (2 feet) from midspan, and four reaction points centered under the bulbs. Recall that the loads were applied through two 25-mm (1-inch) thick elastomeric pads and were reacted through four 25-mm (1-inch) thick elastomeric pads. Loads were monitored through load cells mounted between the hydraulic jacks and the reaction frame.

Prior to the start of testing, the girder deck was checked for preexisting cracks. Alcohol was sprayed onto the top and bottom surfaces of the deck to facilitate identification of any cracks. No cracks were observed on the top of the deck between the girder webs. Preexisting cracks were visible on the underside of the deck. Near the east load point, a representative set of six cracks was observed to run parallel to the length of the girder. Investigation of these cracks with a microscope revealed that the did not have the sharp, distinct edges common to structural cracks in UHPC; as such, these cracks likely occurred during fabrication, possibly due to restrained transverse shrinkage of the deck. These preexisting cracks were marked in red in crack map photos from this beam, while additional cracks caused by the applied structural loadings were marked in black.

A precursor elastic load test was completed prior to the testing of this specimen to failure. In this test, loads were applied to the girder in the configuration described previously without the steel diaphragms being installed. The peak applied load was 62 kN (14 kips), and this loading was not observed to cause any inelastic distress in the girder. The girder was then unloaded, the diaphragms were slid into place, and the bolts attaching the diaphragms to the girder bulbs were tightened. The installation of the diaphragms was completed so as to minimize the forces induced into the diaphragms and the girders; however, in this case the girder legs were brought together slightly and a tensile force was induced in the diaphragms. Following the diaphragm

installation, the loading of the girder in the test to failure was initiated. Data was collected throughout this entire process without resetting any of the instrumentation; thus, data from the string potentiometers displays the hysteretic behavior to which these instruments are susceptible during displacement reversals.

Audible cracking of the underside of the deck was first observed at a total applied load of 214 kN (48 kips). The peak load applied to the girder was 983 kN (221 kips). At this applied load, the girder was unloaded to 156 kN (35 kips), reloaded to the peak load, then completely unloaded. The test was halted at this peak applied load due to concern with the tensile force being carried by the diaphragms. These two diaphragms were slated to be used in Test T2D, thus loading them beyond their elastic limit was to be avoided.

Figure 33 shows the applied load versus vertical deflection response of the midspan cross section of the girder. Observe the divergence between the deflection responses of the girder legs and the mid-deck, beginning at approximately 267 kN (60 kips). This behavior is also shown in Figure 34 where the results from the three potentiometers measuring vertical deflection of the midspan cross section are presented at ten discrete load steps from throughout the test. Figure 35 presents similar information from the three potentiometers measuring vertical deflection at the quarter point of the test span.

Additional observations related to the global deformation of the girder are presented in Figure 36 which shows the spreading of the girder bulbs at midspan. As described above, this plot shows the girder response from the initial elastic loading, the diaphragm installation, and final load application. Recognizing the hysteretic behavior inherent in the potentiometer, this plot shows that the midspan bulbs moved together approximately 0.6 mm (0.024 inch) during the diaphragm installation. In total, the bulbs at midspan spread less than 5 mm (0.2 inch) during the application of over 980 kN (220 kips) of applied load along the girder centerline.

Figure 37 presents the axial load observed in the west diaphragm as calculated from the axial strains measured on the structural tube at midlength. The plot shows that an initial tensile force of 40 kN (9.0 kips) was imparted into the diaphragm during installation, then an additional 76 kN (17.1 kips) was induced during loading to the peak load. During the unload/reload at peak load, the force in the diaphragm abruptly decreased, likely due to slip within the diaphragm to bulb connection. Otherwise, the applied load versus diaphragm force relationship was substantially linear.

Results from the strain gages which monitored the transverse strain on the top of the deck at midspan are presented in Figure 38. Results from three gages are presented at ten discrete load points throughout the test. The complete response from the gage installed at midspan and middeck on top of the girder is presented in Figure 39. These plots show that the transverse strain of top of the deck remained small until approximately 340 kN (76 kips) of applied load, after which the transverse strain at middeck began to progressively increase. This increase coincides with audible observations of increased cracking in the deck. The gages measuring transverse strain under the deck at midspan were intercepted by cracks early in the response and thus did not provide useful results.

The cracking response of the girder deck primarily consisted of longitudinal cracks visible both on the middle underside of the deck and just inside the webs on top of the deck. The cracks on the top of the deck became visible to the unaided eye at 800 kN (180 kips) of applied load. These cracks were visible both north and south of each load point, located between 710 and 790 mm (28 and 31 inches) in from the edge of the deck. Cracking in the middle underside of the deck was not quantitatively assessed until after the peak load had been reached. Figure 40 shows the cracking in the vicinity of the east load point as viewed from under the deck. Note that the primary cracking is longitudinal, but secondary transverse cracking also has occurred immediately under the load point. At the peak load, a longitudinal crack was observed to have extended from the east load point to the east end of the girder; this crack was not present along this entire span length at 800 kN (180 kips) of applied load.
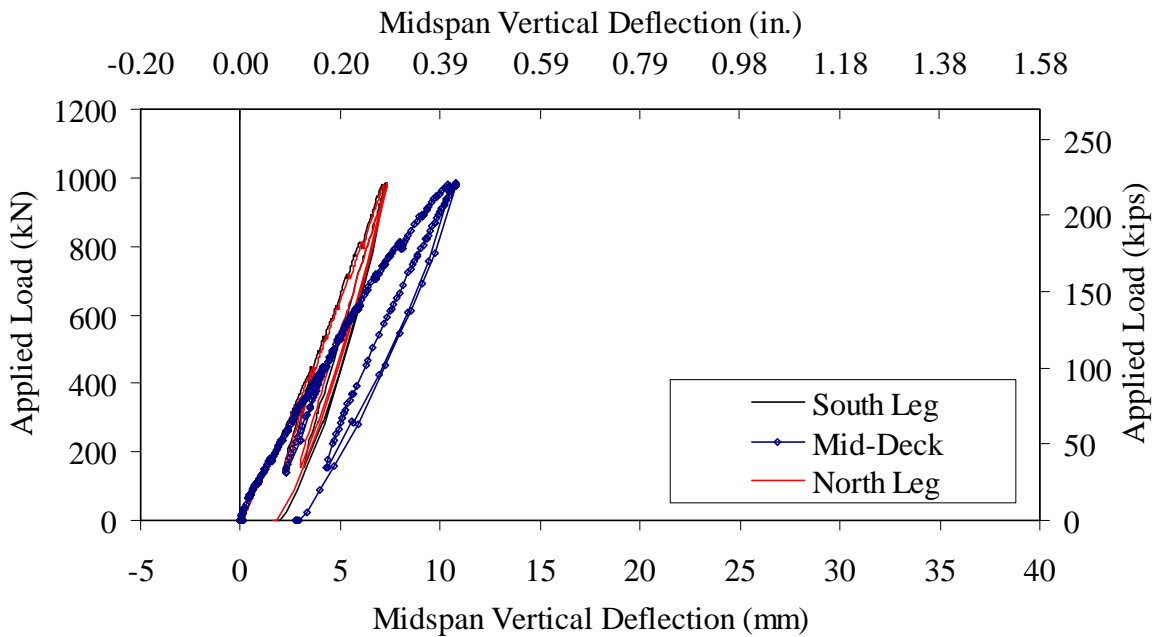
Figure 33. Graph. Load versus midspan deflection response of Test T1D.
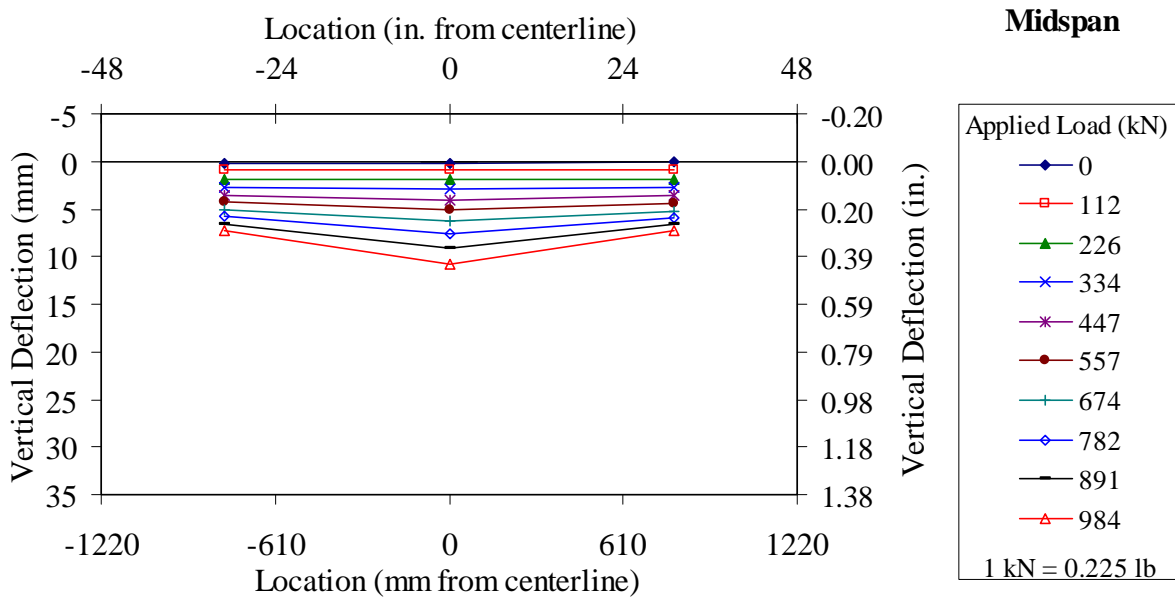
Figure 34. Graph. Load versus deflection response across T1D at midspan.
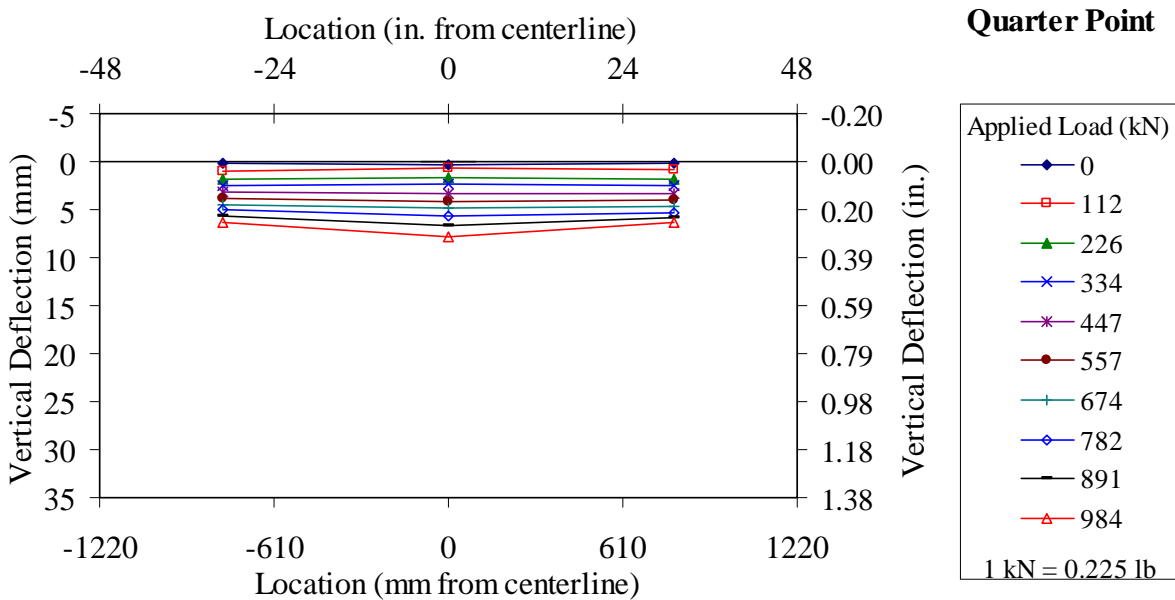
Figure 35. Graph. Load versus deflection response across T1D at quarter span.

Figure 36. Graph. Spreading between bulbs at midspan of Test T1D.
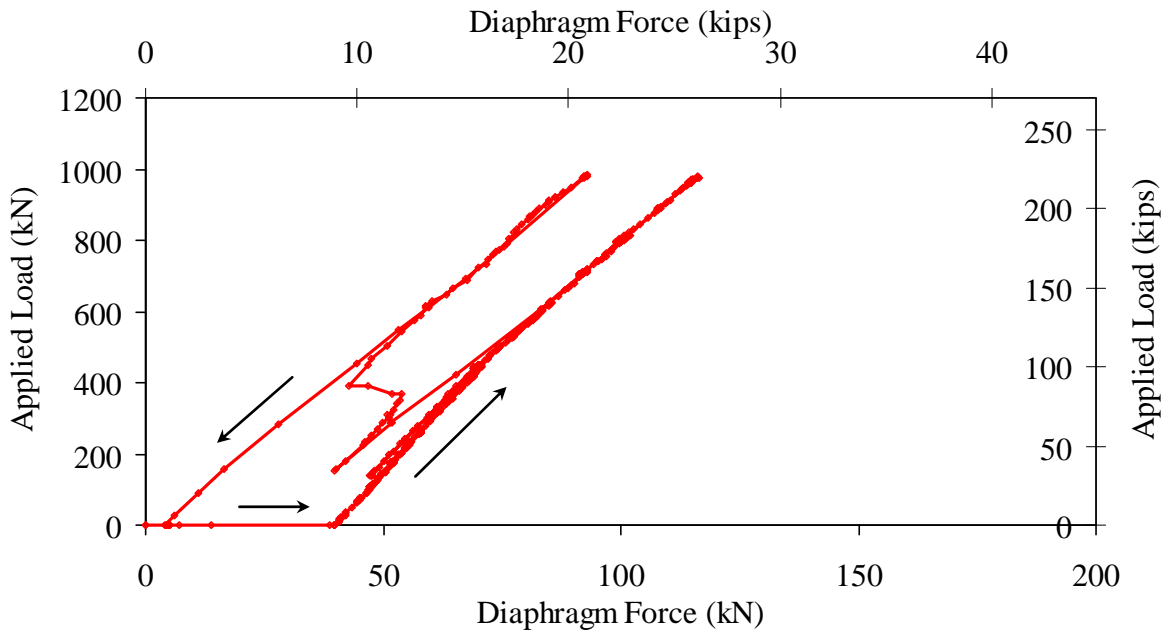
Figure 37. Graph. West diaphragm force in Test T1D.
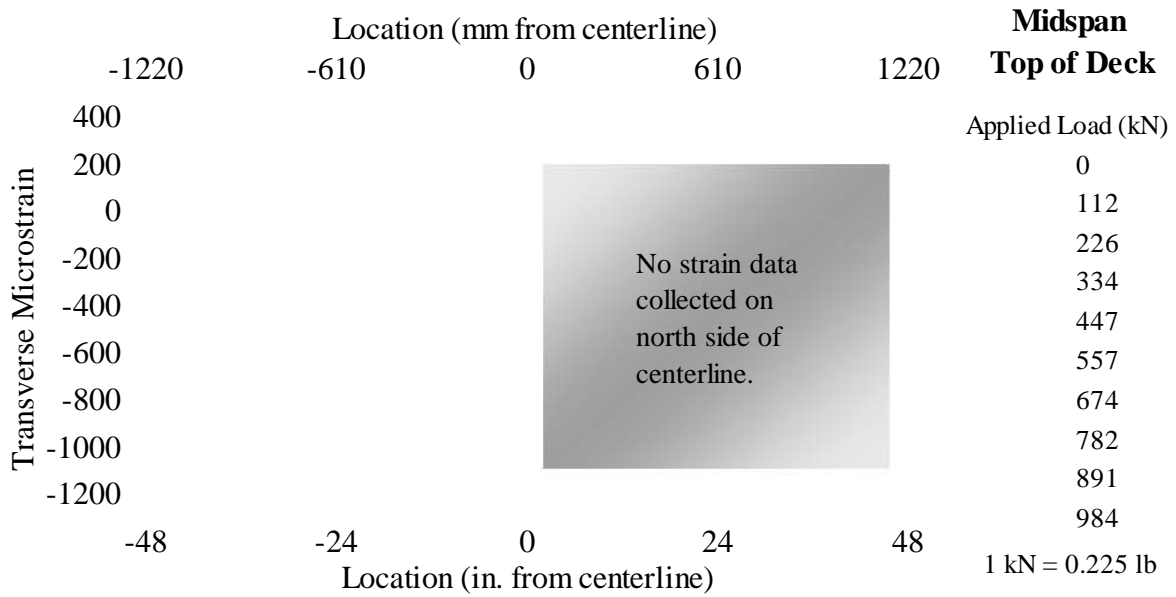
Figure 38. Graph. Transverse strain on top of deck across midspan of Test T1D.

The graph shows the following axes and labels:

Location (mm from centerline): -1220, -610, 0, 610, 1220

Transverse Microstrain: 400, 200, 0, -200, -400, -600, -800, -1000, -1200

Location (in. from centerline): -48, -24, 0, 24, 48

Midspan Top of Deck

Applied Load (kN): 0, 112, 226, 334, 447, 557, 674, 782, 891, 984

No strain data collected on north side of centerline.

1 kN = 0.225 lb
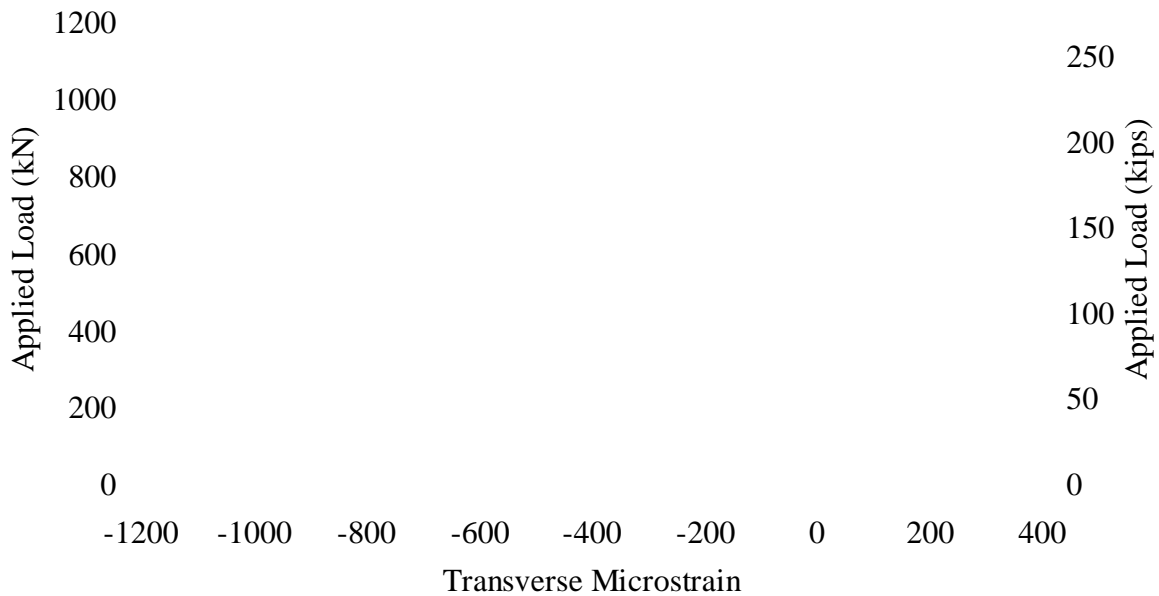
Figure 39. Graph. Transverse strain on top of deck at midspan and middeck Test T1D.

Applied Load (kN): 1200, 1000, 800, 600, 400, 200, 0

Applied Load (kips): 250, 200, 150, 100, 50, 0

Transverse Microstrain: -1200, -1000, -800, -600, -400, -200, 0, 200, 400

East
Load
Applied
Above
Here
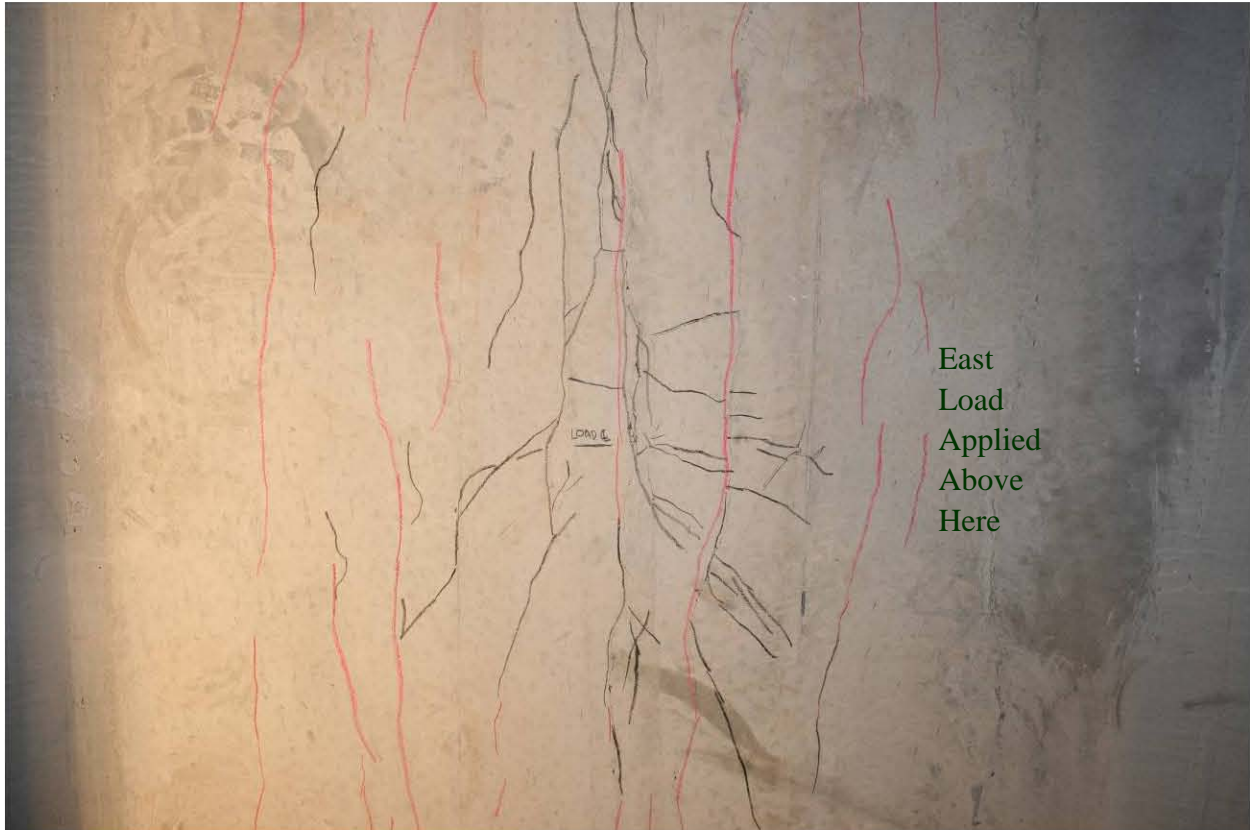
Figure 40. Photo. Under-deck cracking after conclusion of Test T1D.

T2D

Test T2D was also intended to investigate the transverse flexural response of the 2nd generation pi-girder cross section. The test was completed using the previously untested, 7.6-m (25-foot) long Girder T2. The setup for the test included a 7.3 m (24 foot) span, two point loads applied in the middle of the deck with each being 0.61 m (2 feet) from midspan, and four reaction points centered under the bulbs. Recall that the loads were applied through two 25-mm (1-inch) thick elastomeric pads and were reacted through four 25-mm (1-inch) thick elastomeric pads. Loads were monitored through load cells mounted between the hydraulic jacks and the reaction frame. The only difference between the design of the T1 and T2 girders was the mild steel reinforcement included in the deck of Girder T2. This transverse reinforcement consisted of #5 bars spaced at 305 mm (12 inches) with 25 mm (1 inch) clear cover to the bottom of the deck.

Prior to the start of testing, the girder deck was checked for preexisting cracks. Alcohol was sprayed onto the top and bottom surfaces of the deck to facilitate identification of any cracks. No cracks were observed on the top of the deck between the girder webs, but transverse cracks were observed to be emanating from the corners of the most deck joint block-outs and running for 305 to 610 mm (12 to 24 inches) generally across the girder. Aside from a single, 460-mm (18-inch) long longitudinal crack at middeck near the west support, no preexisting cracks were visible on the underside of the deck.

The diaphragms were installed following a similar procedure to that used in Test T1D. After the girder was seated on its supports and the strain gages were activated, the diaphragms were slid into place then the bolts were tightened. The tightening of the bolts resulted in a tensile load being induced in the diaphragms. The initial (baseline) values reported from the strain gages for Test T2D include strains induced by the diaphragm installation; however, the LVDTs and potentiometers were reset after the diaphragm installation so as to eliminate any hysteretic behavior inherent in these devices.

Audible cracking of the underside of the deck was first audibly and visually observed at a total applied load of 254 kN (57 kips). The peak load applied to the girder was 1512 kN (340 kips). The test was halted at this applied load due to concern regarding potential diaphragm failure.

Figure 41 shows the applied load versus vertical deflection response of the midspan cross section of the girder. Observe the divergence between the deflection responses of the girder legs and the mid-deck, beginning at approximately 267 kN (60 kips). This behavior is also shown in Figure 42 where the results from the three potentiometers measuring vertical deflection of the midspan cross section are presented at ten discrete load steps from throughout the test. Figure 43 presents similar information from the three potentiometers measuring vertical deflection at the quarter point of the test span.

Additional observations related to the global deformation of the girder are presented in Figure 44 which shows the spreading of the girder bulbs at midspan. In total, the bulbs at midspan had spread approximately 17 mm (0.67 inch) by the time the peak load was applied along the girder centerline.

Figure 41. Graph. Load versus midspan deflection response of Test T2D.

42
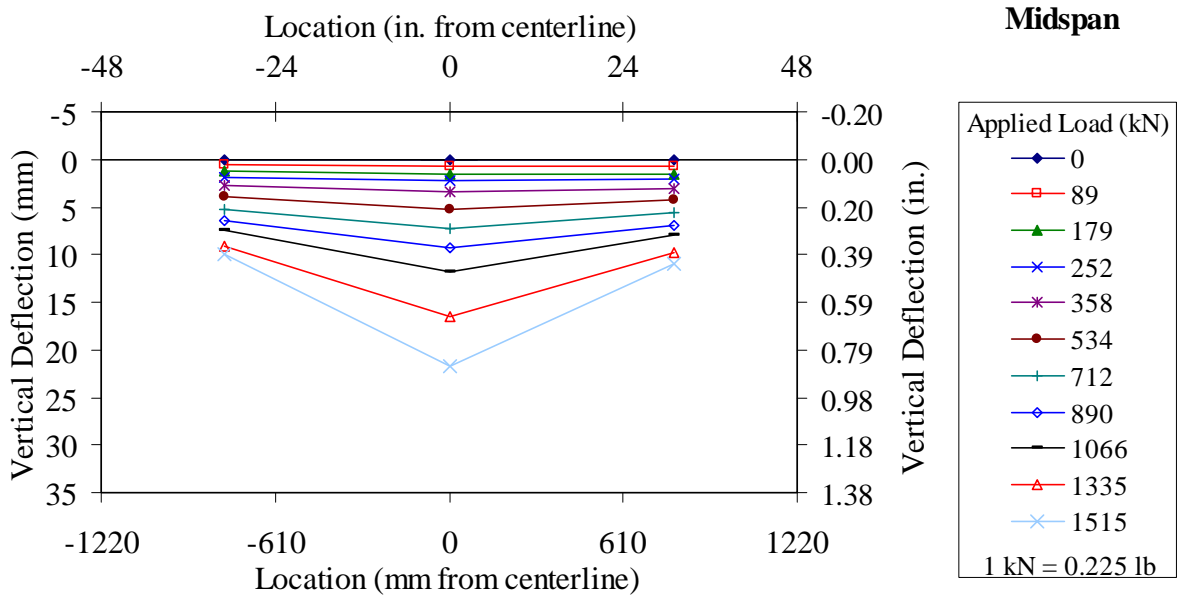
Figure 42. Graph. Load versus deflection response across T2D at midspan.
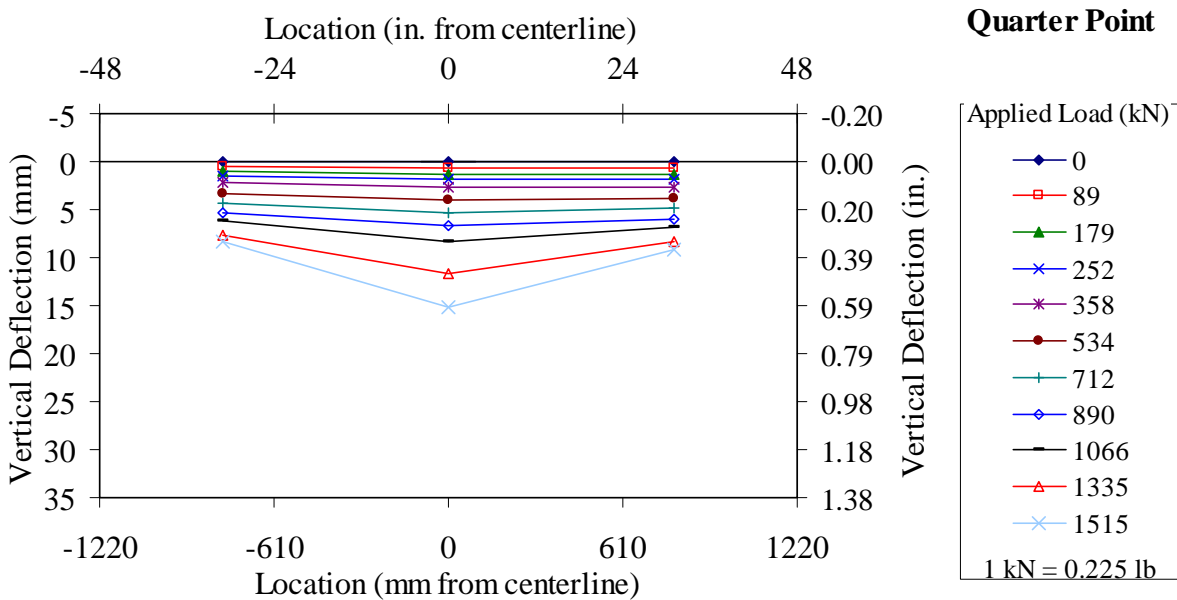
Figure 43. Graph. Load versus deflection response across T2D at quarter span.
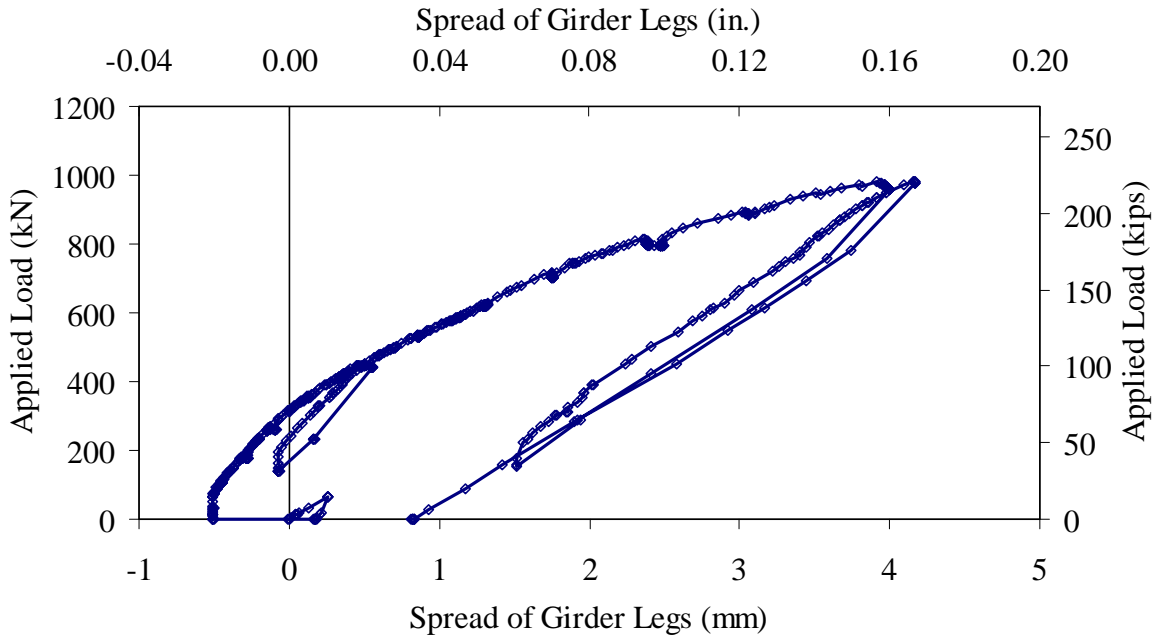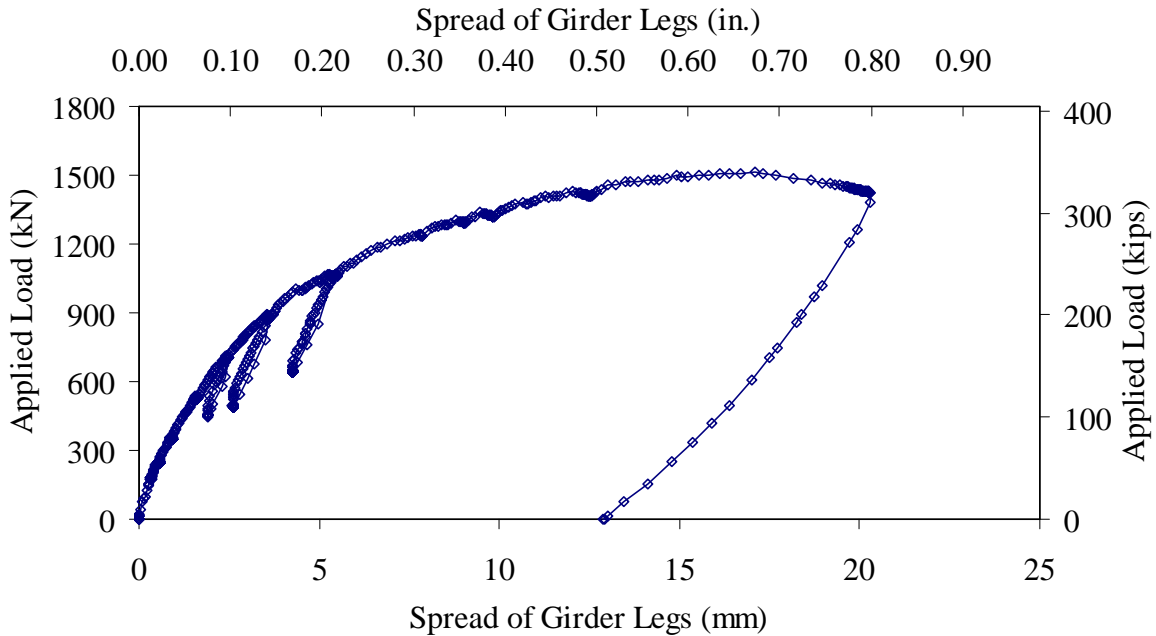
**Figure 44. Graph. Spreading between bulbs at midspan of Test T2D.**

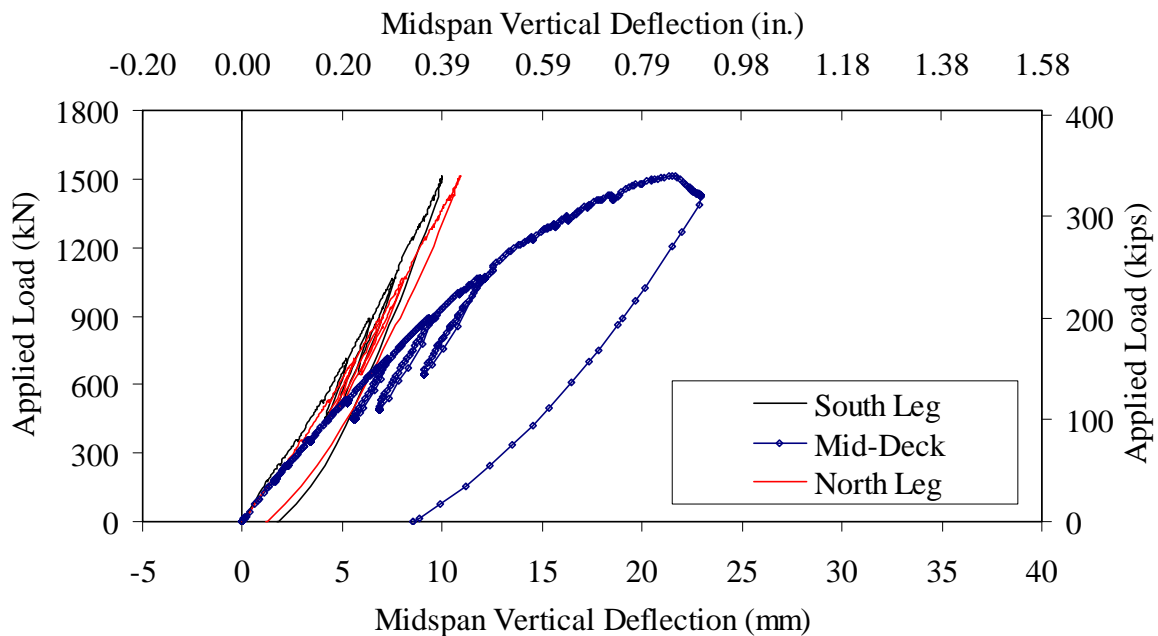Figure 45 presents the axial load observed in the west diaphragm as calculated from the axial strains measured on the structural tube at midlength. The plot shows that an initial tensile force of 24 kN (5.3 kips) was imparted into the diaphragm during installation, and a total maximum load of 142 kN (31.9 kips) was generated in the west diaphragm. The plot shows that the peak diaphragm force occurred at first at an applied load of 1330 kN (300 kips), then recurred at an applied load of 1470 kN (330 kips). Thereafter, the diaphragm force decreased as the applied load increased to the peak load of 1512 kN (340 kips). The relationship between the applied load and the diaphragm force was substantially linear until the maximum diaphragm force was reached.

Results from the strain gages which monitored the transverse strain on the top of the deck at midspan are presented in Figure 46. Results from three gages are presented at ten discrete load points throughout the test. The complete response from the gage installed at midspan and middeck on top of the girder is presented in Figure 47. These plots show that the transverse strain response on top of the deck was linear elastic until approximately 267 kN (60 kips) of applied load, after which the transverse strain at middeck began to increase more quickly. This increase coincides with audible observations of cracking in the deck. The gages measuring transverse strain under the deck at midspan were intercepted by cracks early in the response and thus did not provide useful results.

As can be inferred from the results presented above, the global response of the girder in Test T2D was significantly influenced by the behavior of the steel diaphragms. Figure 48 provides a photograph of the east end of the girder after the conclusion of the test. Figure 49 provides a photograph of the north end of the east diaphragm at the time when the peak load was applied to the girder. As the peak diaphragm force was reached, the end plates began to pry and the welds

44

connecting the end plates to the tubes began to crack. These behaviors resulted in a loss of transverse deformational restraint in the girder bulbs thus allowing increased bulb spreading.

As with Test T1D, the cracking response of this girder primarily consisted of longitudinal cracks visible both on the middle underside of the deck and just inside the webs on top of the deck. Figure 50 shows a photograph of the underside of the deck from midspan to the east end of the girder. The photograph is annotated to indicate key features of the test setup and the girder cross section. Similar photographs were generated to map the cracking apparent on the underside of the girder at six load sets throughout the loading as well as after the completion of the test. Note that cracks were located with the assistance of an alcohol spray and were marked with a black wax crayon.

Figure 51 through Figure 57 provide illustrations of the cracking visible on the underside of the deck. These figures demonstrate that between first cracking and an applied load of 534 kN (120 kips) the cracking is constrained to the area between the diaphragms and is primarily oriented longitudinally. By 890 kN (200 kips) of applied load, the cracks have extended out to near the end of the girder and additional transverse cracks have occurred immediately under the load point. At 1068 kN (240 kips), extensive cracking was apparent on the underside of the deck throughout the entire eastern half of the span. The cracks continued to distribute throughout the remainder of the test until the pattern observed at the conclusion of the test as shown in Figure 57 was captured.

The cracking on the top of the deck was also observed periodically. Figure 58 presents a photograph of the vicinity of the east load point at 1068 kN (240 kips) of applied load. The cracks occur between the centerlines of the two girder webs and tend to encircle the load points with greater longitudinal cracking than transverse cracking.
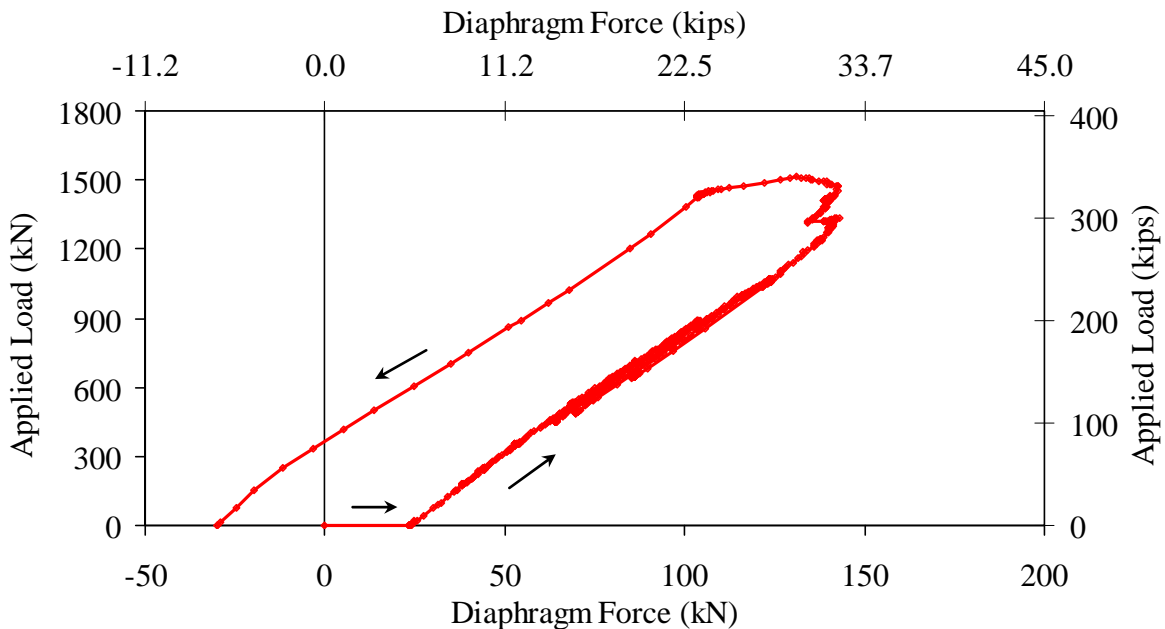
Figure 45. Graph. West Diaphragm force in Test T2D.

Location (mm from centerline)

| -1220 | -610 | 0 | 610 | 1220 | **Midspan Top of Deck** |

Transverse Microstrain

400
-100
-600
-1100
-1600
-2100
-2600
-3100
-3600

No strain data collected on north side of centerline.

Applied Load (kN)
0
89
179
252
358
534
712
890
1066
1335
1515

-48   -24   0   24   48

Location (in. from centerline)

1 kN = 0.225 lb
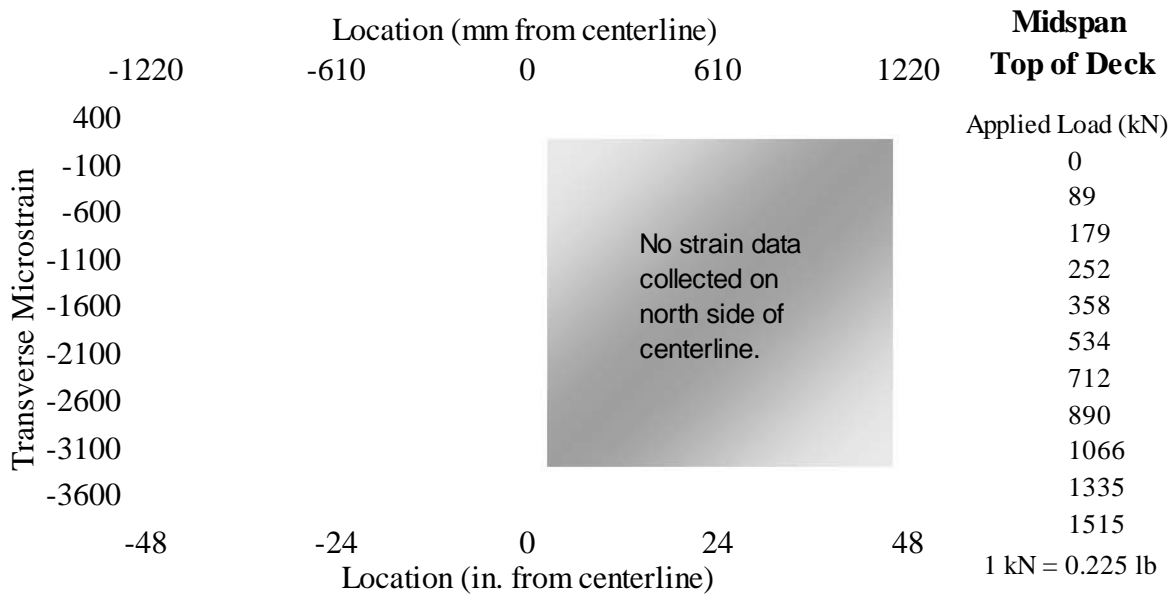
Figure 46. Graph. Transverse strain on top of deck across midspan of Test T2D.

Applied Load (kN)
1800
1600
1400
1200
1000
800
600
400
200
0

Applied Load (kips)
400
350
300
250
200
150
100
50
0

-4000 -3500 -3000 -2500 -2000 -1500 -1000 -500   0   500

Transverse Microstrain
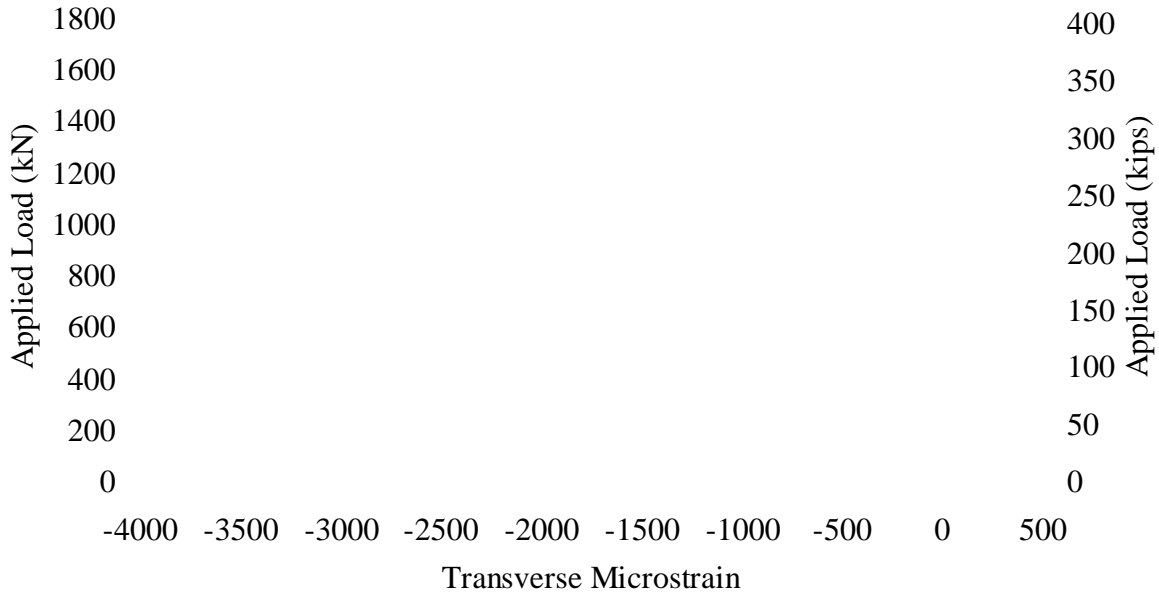
Figure 47. Graph. Transverse strain of top of deck at midspan and middeck of Test T2D.

Figure 48. Photo. View from east end after conclusion of Test T2D.
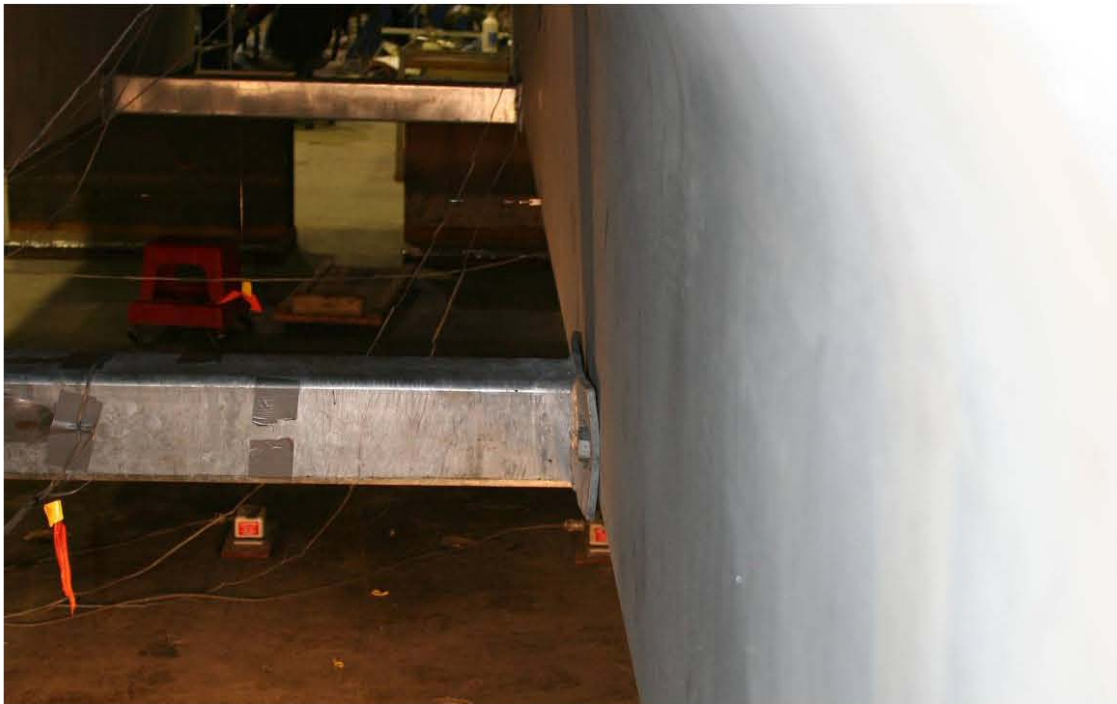
Figure 49. Photo. Prying at peak applied load in Test T2D east diaphragm.
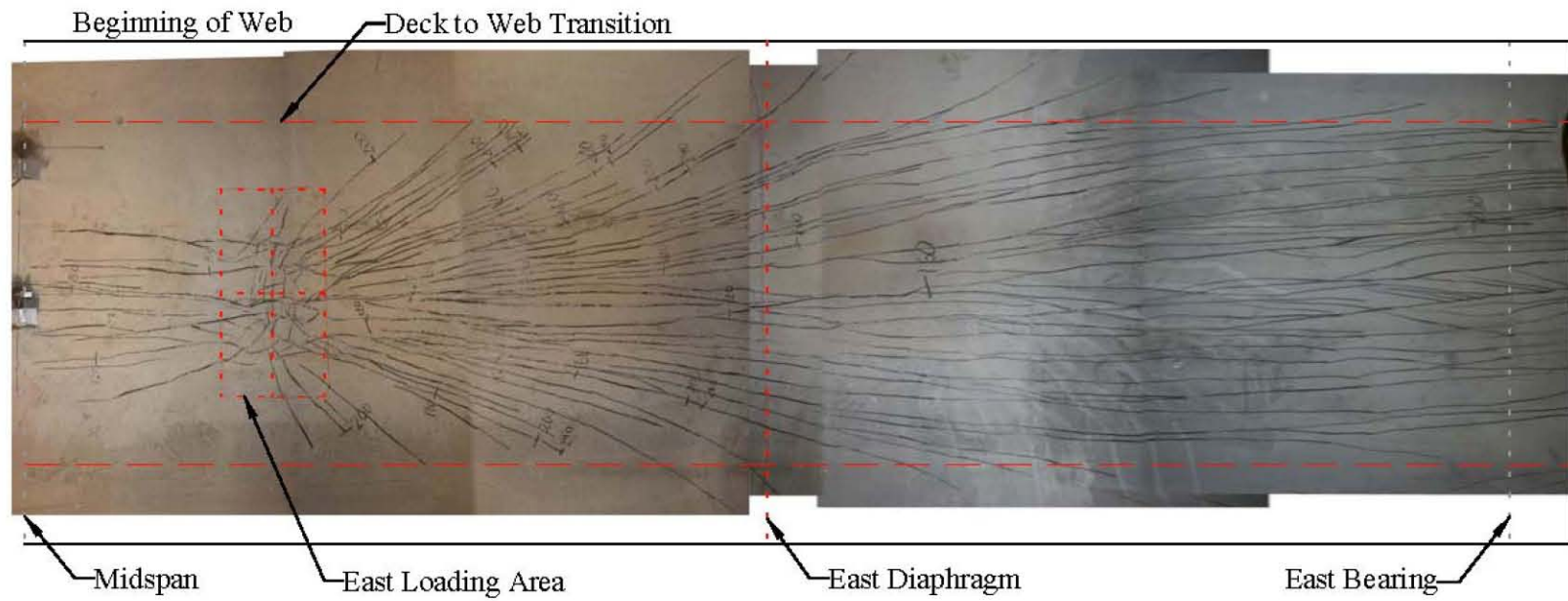
Figure 50. Photo. Underside deck cracking map of T2D after conclusion of test.
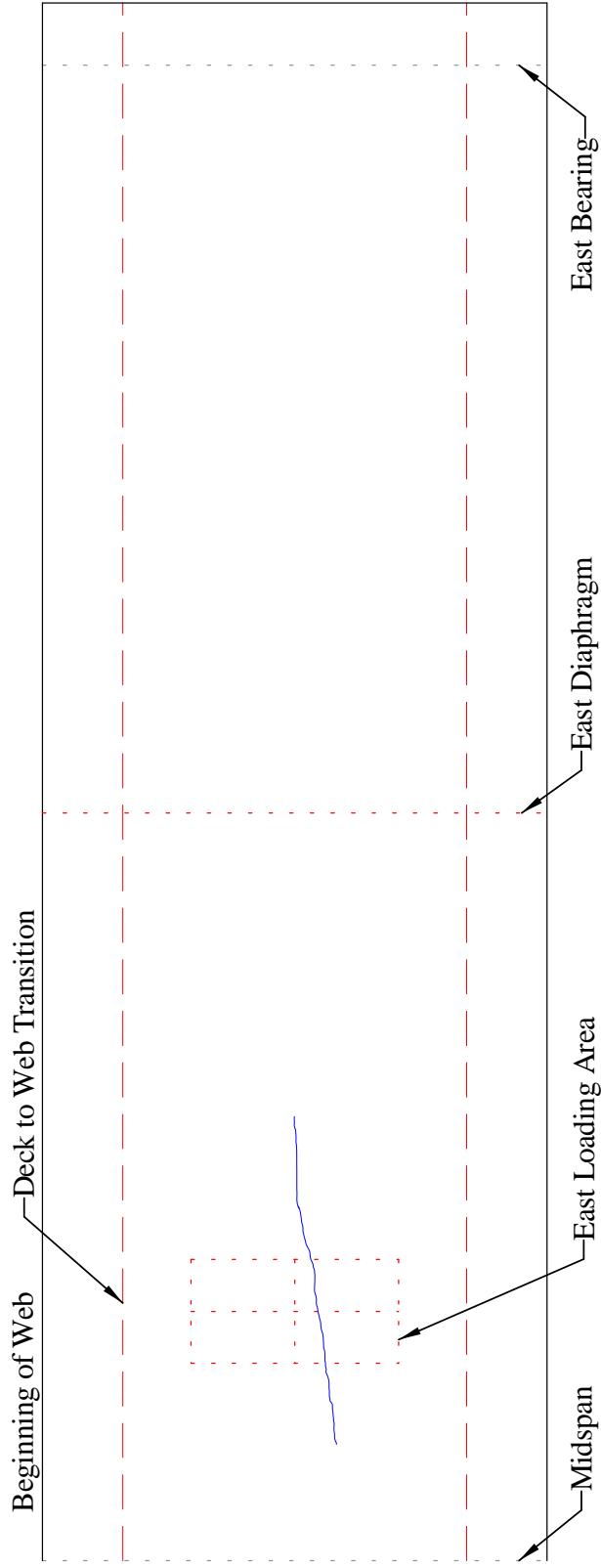
Figure 51. Illustration. Underside deck crack map of T2D at 249 kN (56 kips) of applied load.
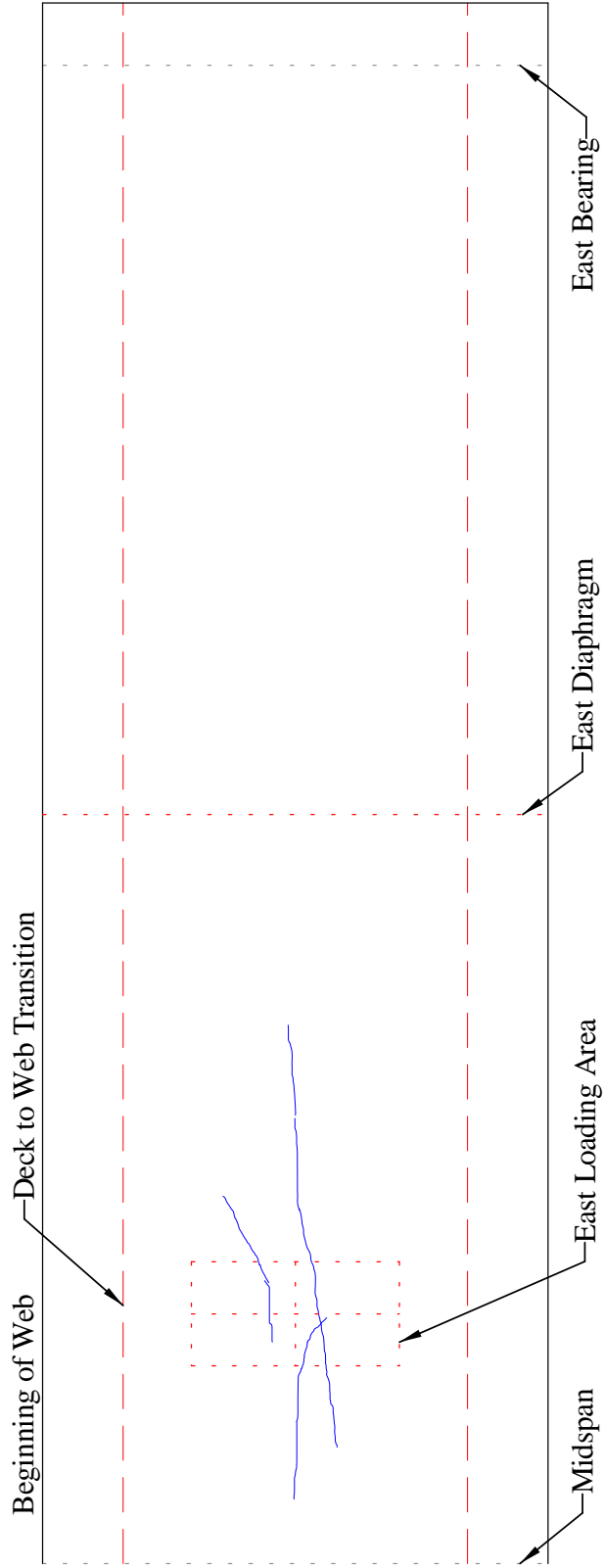
Figure 52. Illustration. Underside deck crack map of T2D at 356 kN (80 kips) of applied load.
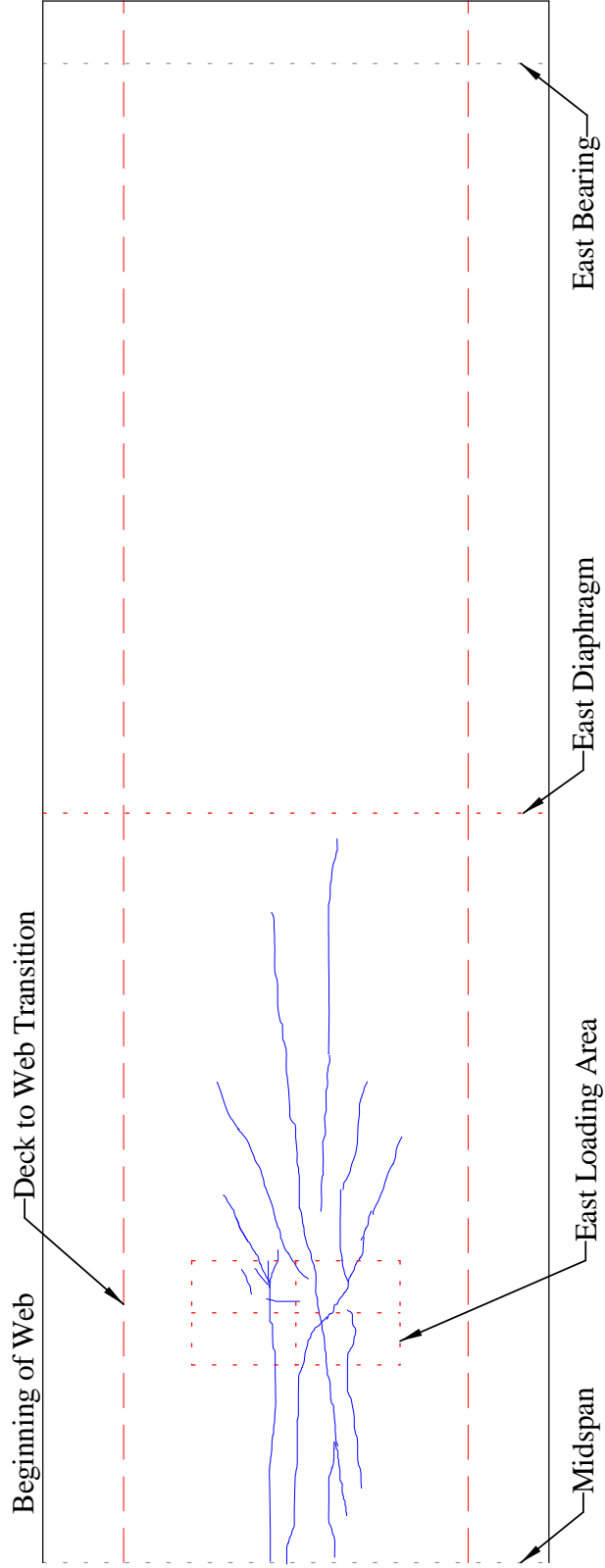
Figure 53. Illustration. Underside deck crack map of T2D at 534 kN (120 kips) of applied load.

Beginning of Web

Deck to Web Transition

East Bearing

East Diaphragm

East Loading Area

Midspan
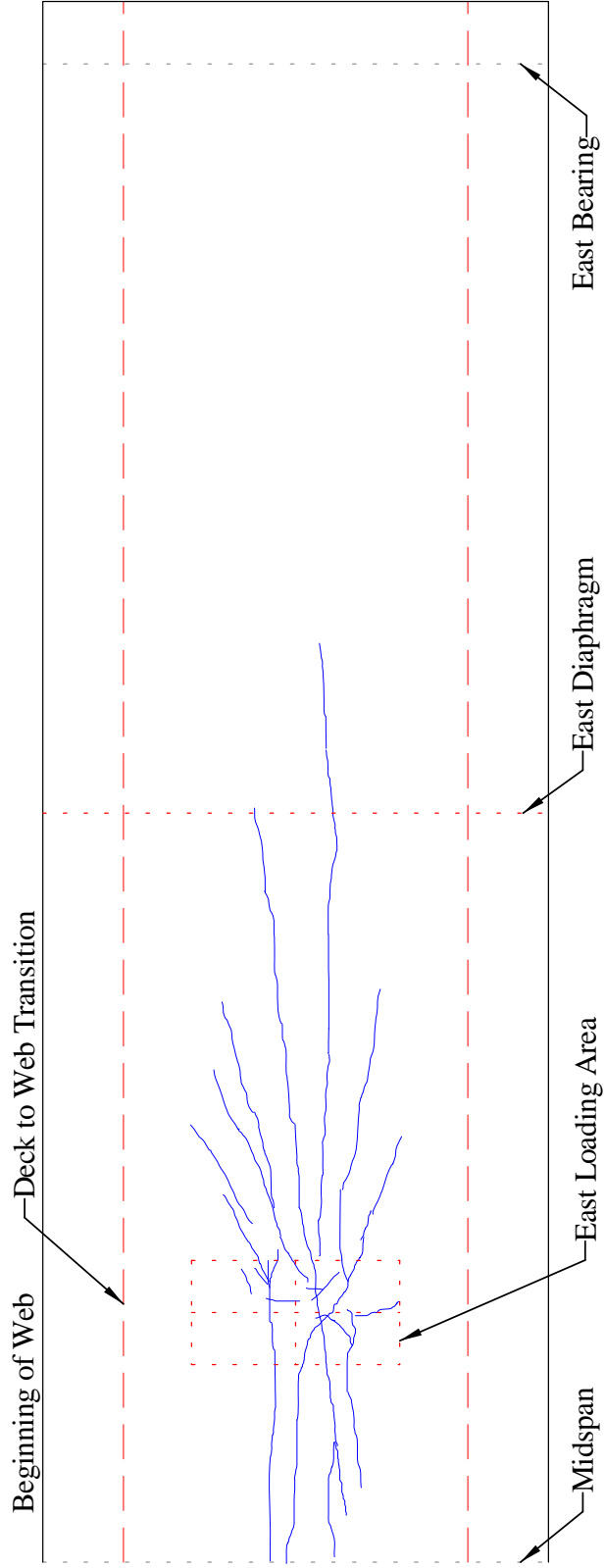
Figure 54. Illustration. Underside deck crack map of T2D at 712 kN (160 kips) of applied load.
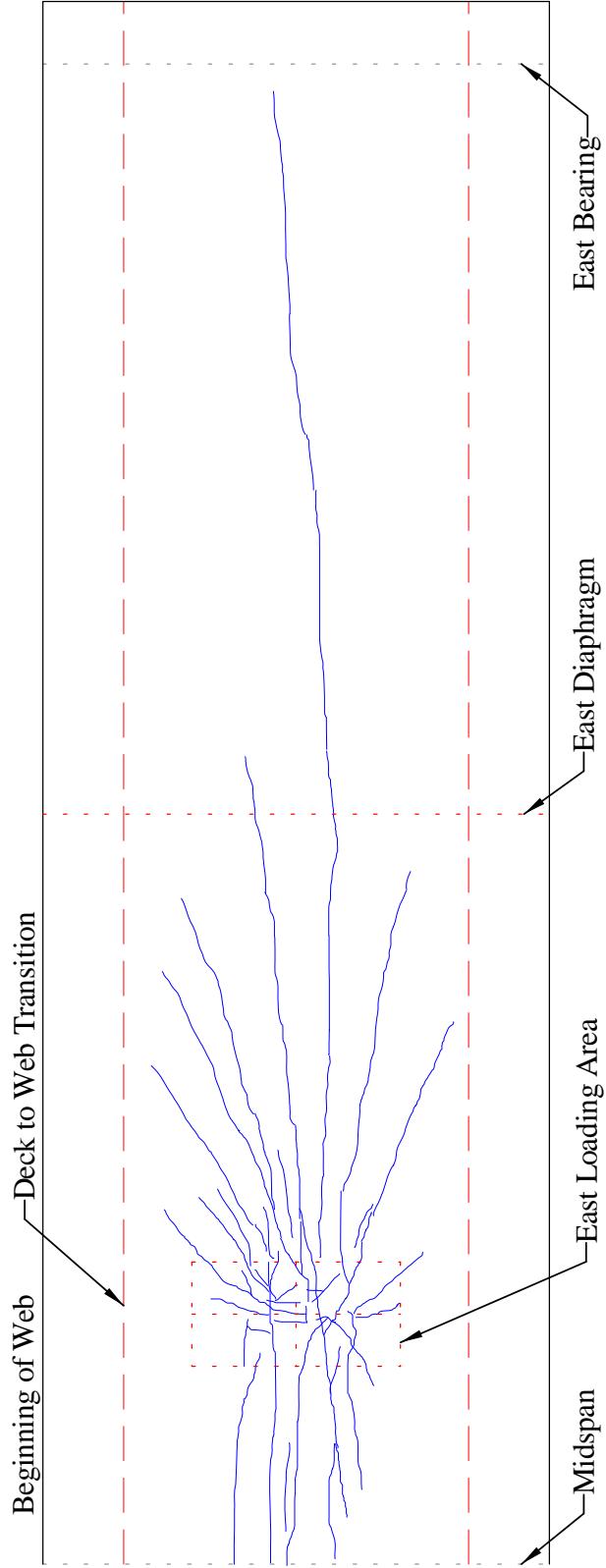
Figure 55. Illustration. Underside deck crack map of T2D at 890 kN (200 kips) of applied load.
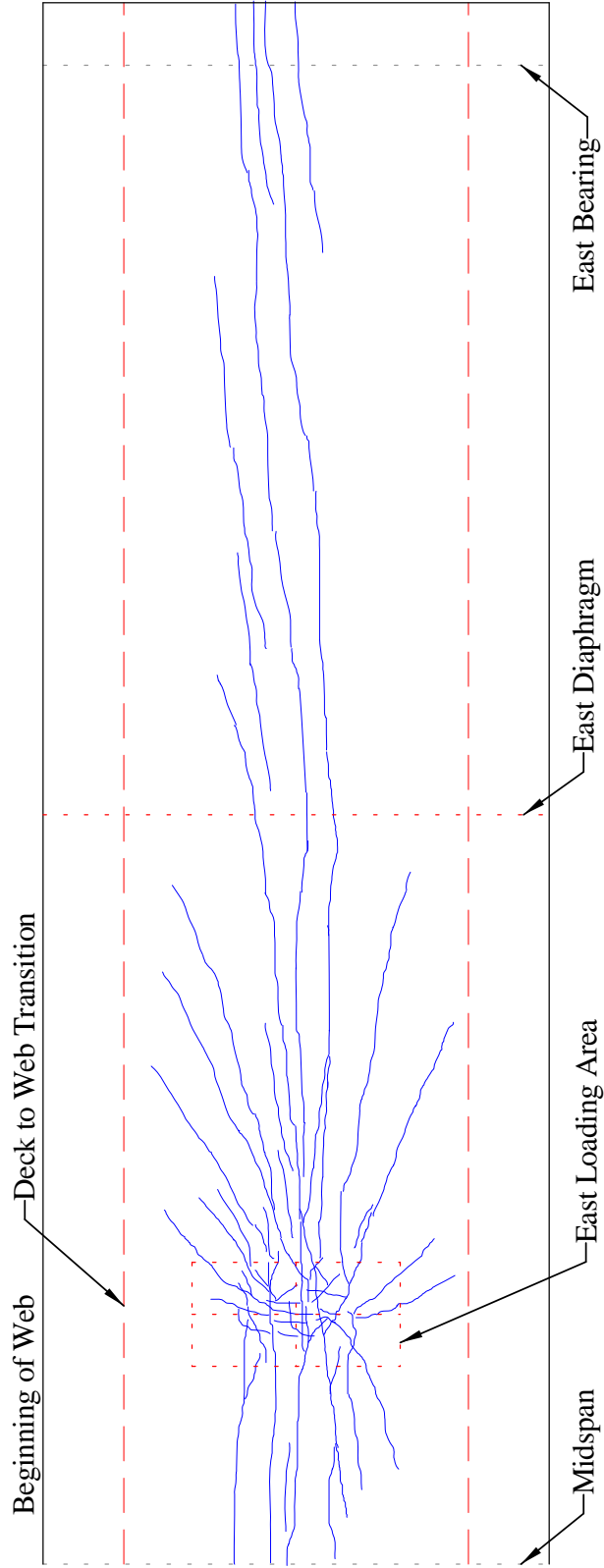
Figure 56. Illustration. Underside deck crack map of T2D at 1067 kN (240 kips) of applied load.
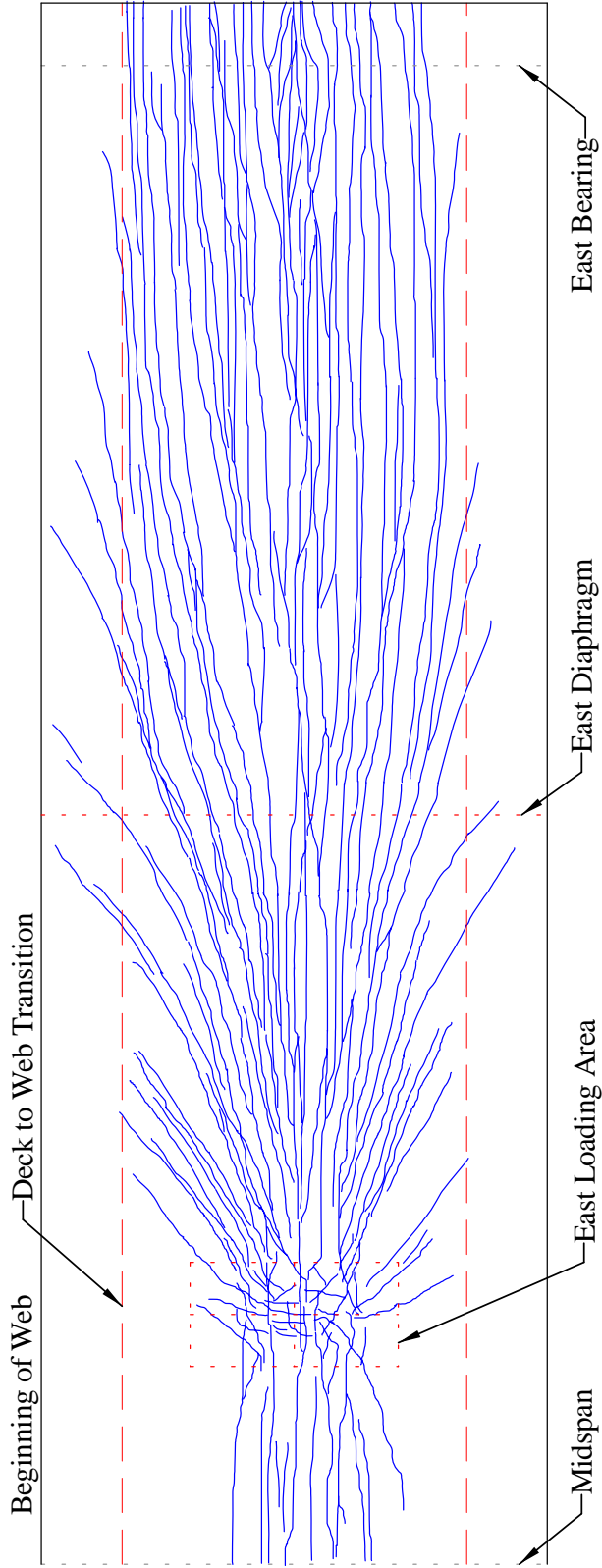
Figure 57. Illustration. Underside deck crack map of T2D after conclusion of test.
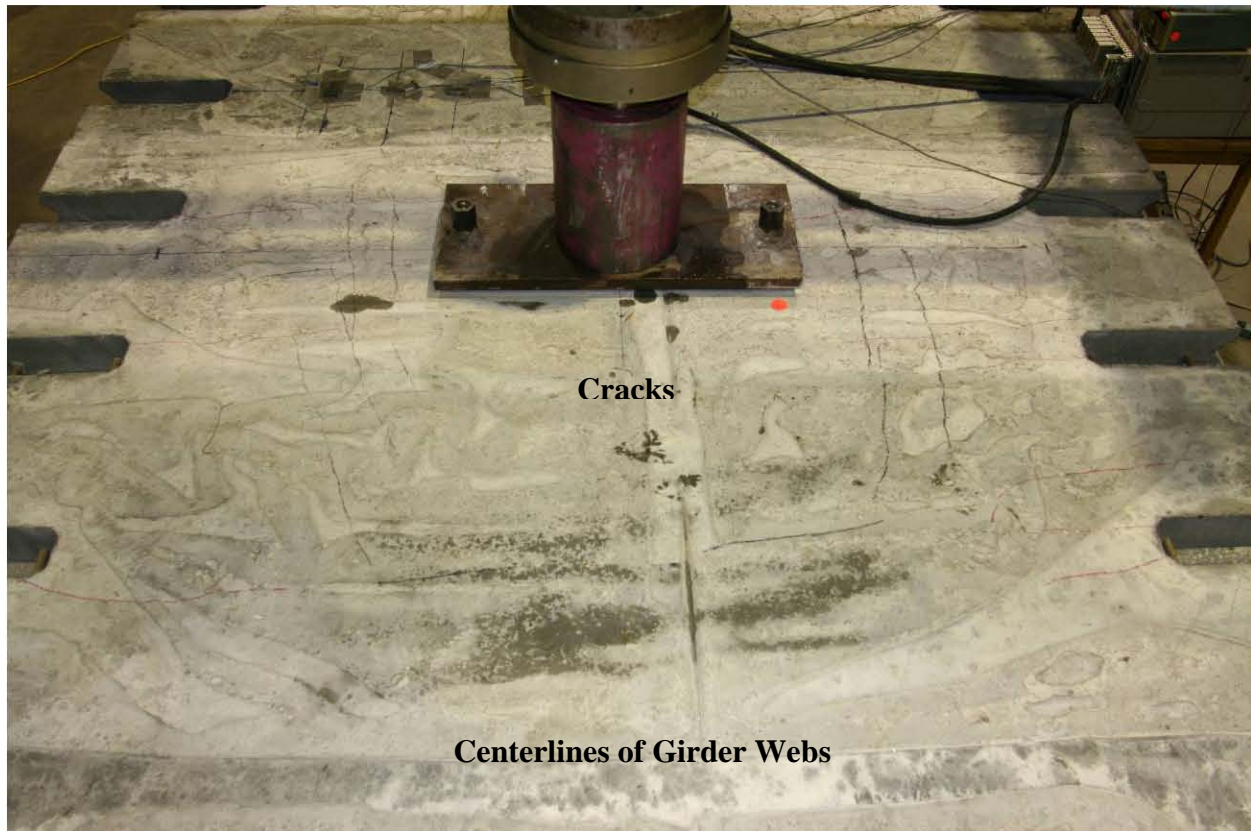
Figure 58. Photo. Topside deck cracking of T2D at 1067 kN (240 kips) of applied load.

T1J

Test T1J was intended to investigate the transverse flexural and shear responses of the 2nd generation pi-girder cross section. The test was completed using pieces of the previously tested, 7.6-m (25-foot) long Girder T1. After the completion of Test T1D, Girder T1 was cut along its midline to create two disconnected half-pi-girders. These two pieces were arranged such that their flange tips were adjacent, then the diaphragm members were bolted into place. Finally, the #8 mild steel reinforcement dowel bars were placed into the connection pockets and the joint was cast. The joint fill material implemented for this test was UHPC which had the same mix design as the UHPC in the girders. However, note that the joint did not receive any curing treatment aside from covering it with a plastic sheet. The girder was tested after the joint fill had been allowed to cure for 30 days.

The setup for the test included a 7.3-m (24-foot) span, two point loads offset 127-mm (5-inch) north of the joint centerline with each being 0.61 m (2 feet) from midspan, and four reaction points centered under the bulbs. Recall that the loads were applied and reacted through 25-mm (1-inch) thick elastomeric pads. Loads were monitored through load cells mounted between the hydraulic jacks and the reaction frame.

Prior to the start of testing, the girder deck and joint were checked for preexisting cracks. Alcohol was sprayed onto the top and bottom surfaces of the deck to facilitate identification of any cracks. No cracks were noted on either side of the joint from centerline of web to centerline

56

of web. Additionally, no cracks were noted within the surface of the joint fill, and the interface bond between the joint fill and the girder deck appeared intact.

Prior to the start of the test, all gages were reset and all potentiometers were set so as to minimize hysteretic behavior.

First cracking of the girder was not noted in this test. The peak load applied to the girder was 1880 kN (422 kips). The test was halted at this applied load due to concern regarding the high tensile load being carried by the diaphragms and the need to reuse these diaphragms in the Test T2J.

Figure 59 shows the applied load versus vertical deflection response of the midspan cross section of the test specimen. The responses can be observed to be primarily linear until the applied load surpasses 534 kN (120 kips). From this load level until 1330 kN (300 kips), a slight increase in deck deformation relative to leg deformation can be observed. After approximately 1330 kN (300 kips) nonlinear behavior can be observed in the north leg, and after approximately 1600 kN (360 kips) nonlinear behavior can be observed in the south leg. These behaviors are also shown in Figure 60 where the results from the four potentiometers measuring vertical deflection of the midspan cross section are presented at ten discrete load steps from throughout the test. Figure 61 presents similar information from the four potentiometers measuring vertical deflection at the quarter point of the test span.

Additional observations related to the global deformation of the girder are presented in Figure 62 which shows the spreading of the girder bulbs at midspan. In total, the bulbs at midspan had spread approximately 15 mm (0.59 inch) by the time the peak load was applied.

Figure 63 presents the axial load observed in the west diaphragm as calculated from the axial strains measured on the structural tube at midlength. The plot shows that a total maximum load of 135 kN (30.4 kips) was generated in the west diaphragm, and that this peak diaphragm force occurred at the peak applied load. The relationship between the applied load and the diaphragm force was substantially linear throughout the loading.

Transverse displacement results from the LVDTs which were mounted above and below the joint at midspan are presented in Figure 64. The LVDTs were centered over the joints, were installed with 279-mm (11-inch) center-to-center gage lengths, and were placed 25 mm (1 inch) above and below the exterior surfaces of the joint.

The axial strain results recorded from two of the #8 reinforcing bar dowels embedded in the grouted joint are presented in Figure 65. One of these reinforcing bars was located in the pocket at midspan, while the other was located above the east diaphragm at the east quarter span point. Electrical resistance strain gages were affixed to the surface of the bars, with their orientation parallel to the length of the bar. The bars were then placed at the centerline of the joint prior to the casting of the joint fill material. This plot shows that significantly greater strain was experienced in the midspan grouted pocket. Additionally, note that the slope of the curves change abruptly at a strain level similar to the rebar yield strain as reported in Chapter 3.

Further analysis of the dowel strain results was completed by applying the uniaxial stress-strain response in Figure 4 to the results in Figure 65. The outcome is shown in Figure 66. Note that unloading/reloading strain cycles were assumed to occur with a stiffness concurrent with the initial elastic stiffness. Also, the plotted results do not include the final unloading of the specimen at the conclusion of the test. This plot shows that the reinforcing bars in both pockets yielded prior to the application of maximum load to the specimen.

Recall that the specimen was asymmetrically loaded, thus leading to different load proportions being carried by each leg. The proportion of the flexural load carried by each leg can be estimated based on the strain observed on the bottom face of the bulbs at midspan. Figure 67 presents the strain results captured from the two gages affixed to the bottom faces of the north and south bulbs at this location. The results from these gages are only plotted up through approximately 400 microstrain due to inconsistent readings resulting from cracking of the underlying concrete. Linear interpolation was completed to determine the slope of these responses relative to the applied loadings. These slopes indicate that approximately 41% of the flexural loading was carried by the south leg of the specimen, while 59% was carried by the north leg. These proportions are consistent with the transverse location of load application relative to the specimen centerline.

The cracking response of the specimen was monitored qualitatively from north and south of the specimen during the test, and more thoroughly after the completion of the test. During the test, the only distress visually observed was horizontal cracking occurring on the outside of the north and south webs. These cracks emanated symmetrically from midspan toward the ends of the specimen. The cracking was more prevalent on the north side than on the south side. Figure 68 shows the north face of the north web near midspan at an applied load of 1800 kN (400 kips). The large crack visible in the photo is indicative of the initiation of fiber pullout in this face of this leg. Figure 69 shows the entire east end of the north face of the north leg after the conclusion of the test. In this photo, all of the cracks in the web have been located either with the naked eye or through the use of an alcohol spray and indicated on the surface of the girder with red wax crayon. Similar but less extensive cracking was observed in the south face of the south web. Four generally horizontal cracks were noted here at 900 kN (200 kips) of applied load, and nine were noted at 1330 kN (300 kips). The photo in Figure 70 shows the crack map of the south face of the south web after the conclusion of the test.

After the conclusion of the test, the cracking on the top of and the underside of the deck was assessed. Figure 71 provides a photograph of the underside of the deck showing red markings indicating the location of cracks observed. This crack assessment covered the entire underside of the deck from midspan to the east end of the specimen. This figure shows that the cracking to the north of the joint was generally more concentrated in the vicinity of the load point, and the cracking to the south of the joint was more dispersed.

Aside from a single 2.0-m (79 inch) long crack in the grouted joint symmetrically centered about midspan, no other cracks were visible to the naked eye on the top of the deck. This small width crack, was located in the UHPC grout (i.e., not at the grout to precast member interface). Additional structural cracking visible only with the aid of an alcohol spray was observed between the line denoting the extents of the grout pockets and the legs of the girder halves. Identification of these cracks was made difficult by the irregular surface of the deck. These

cracks tended to parallel the length of the girder between the load points then turn at a shallow angle toward the joint as they progressed beyond the load points. There were approximately three to five of these cracks on both the north and south sides of the joint. A photo of the top of the deck after the conclusion of the test is shown in Figure 72.
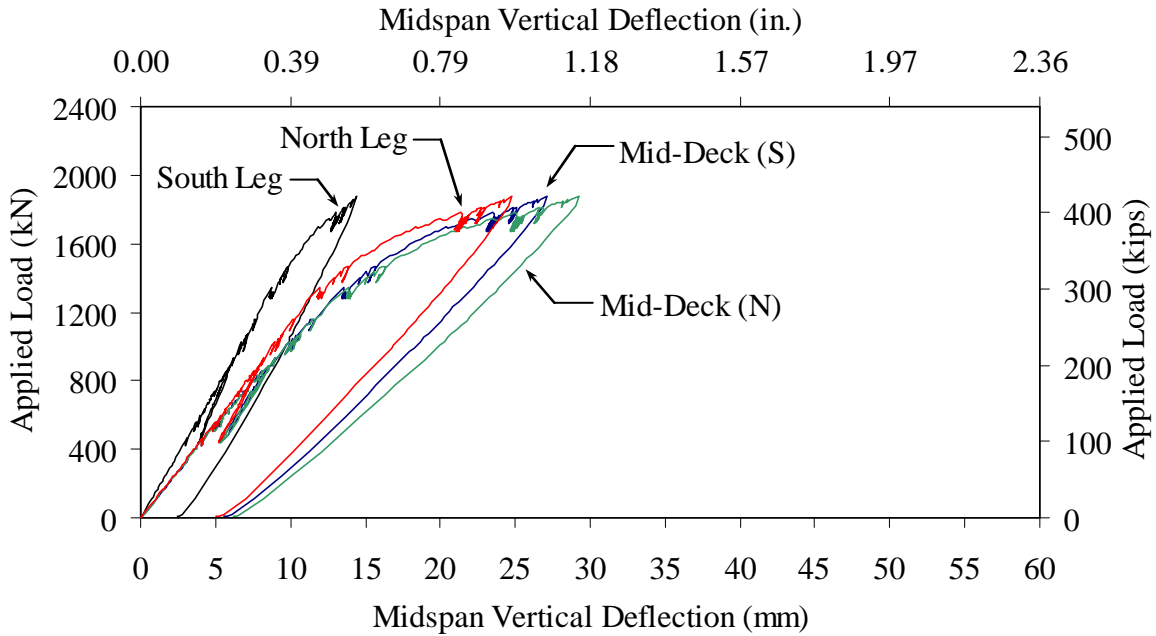
Figure 59. Graph. Load versus midspan deflection response from Test T1J.
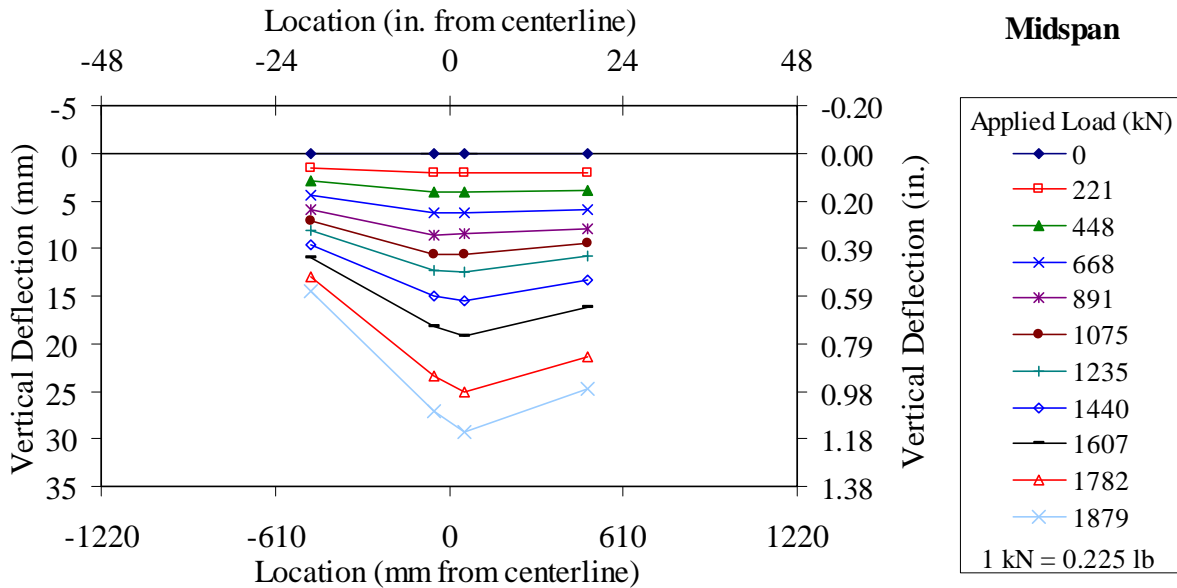
Figure 60. Graph. Load versus deflection response across T1J at midspan.
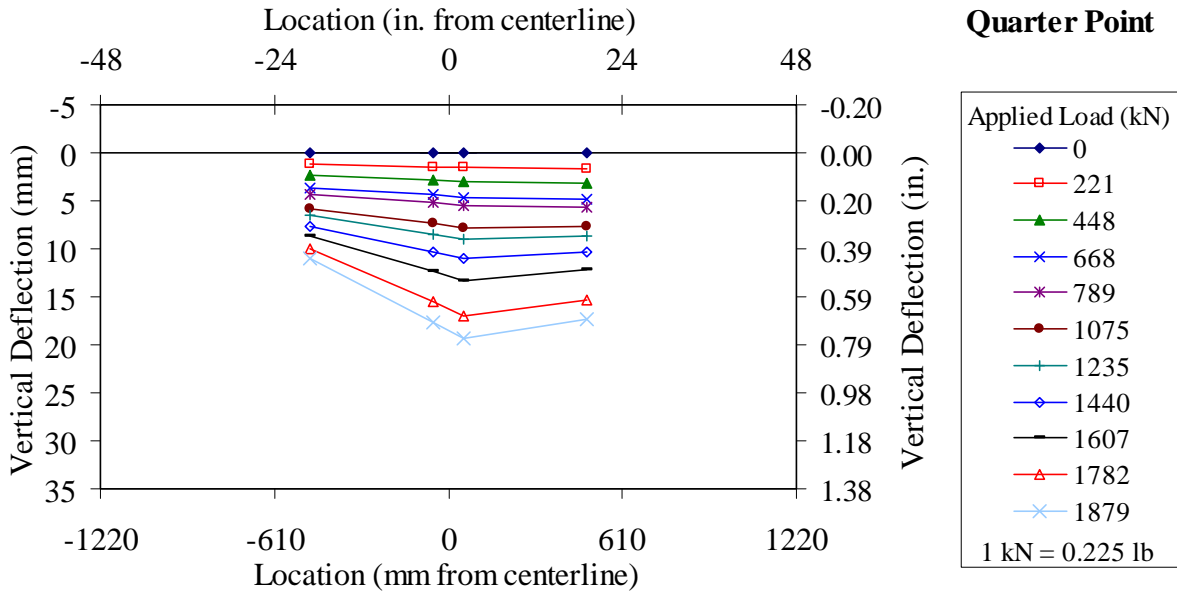
Figure 61. Graph. Load versus deflection response across T1J at quarter span.
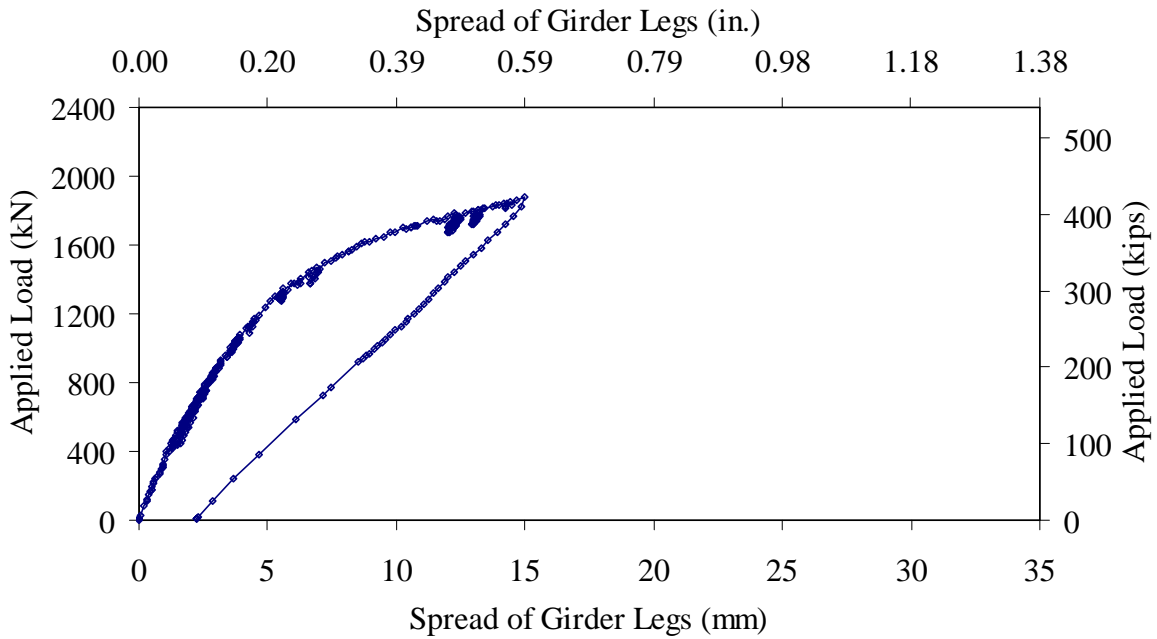
Figure 62. Graph. Spreading between bulbs at midspan of Test T1J.
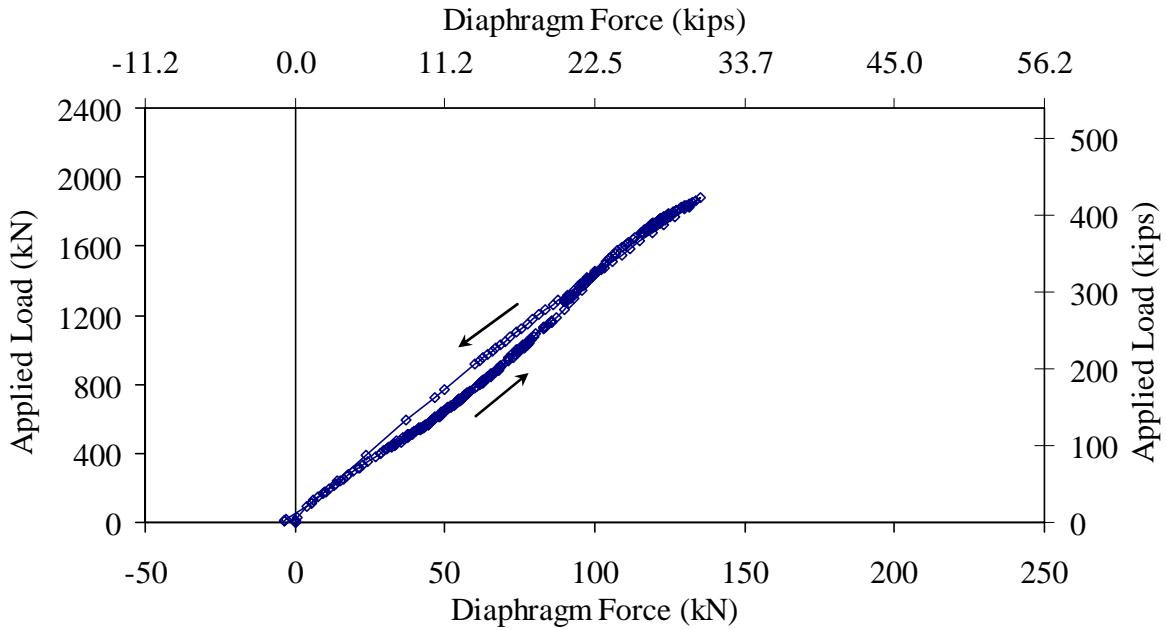
Figure 63. Graph. West Diaphragm force in Test T1J.
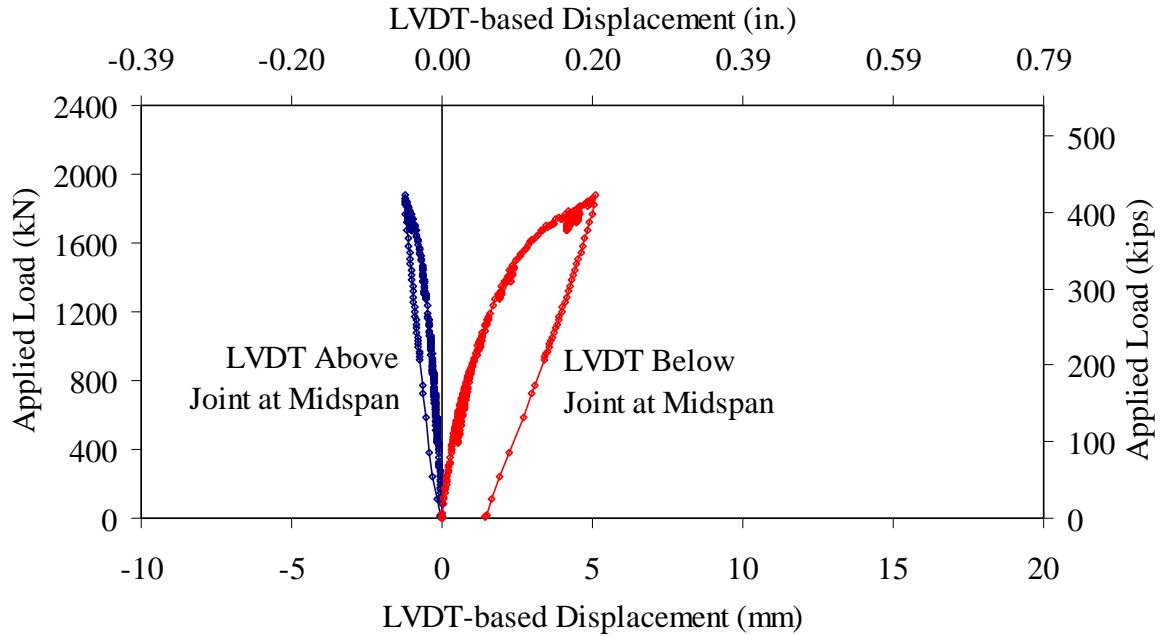
Figure 64. Graph. LVDT-based displacement across joint at midspan in Test T1J.

61
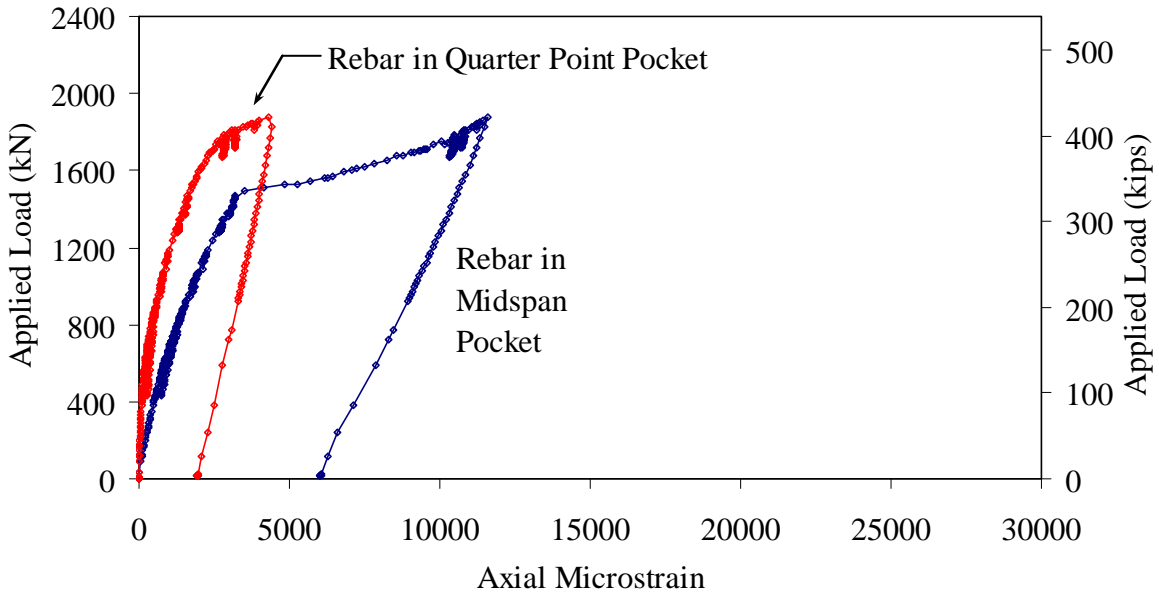
Figure 65. Graph. Axial strain in dowel rebars in Test T1J.
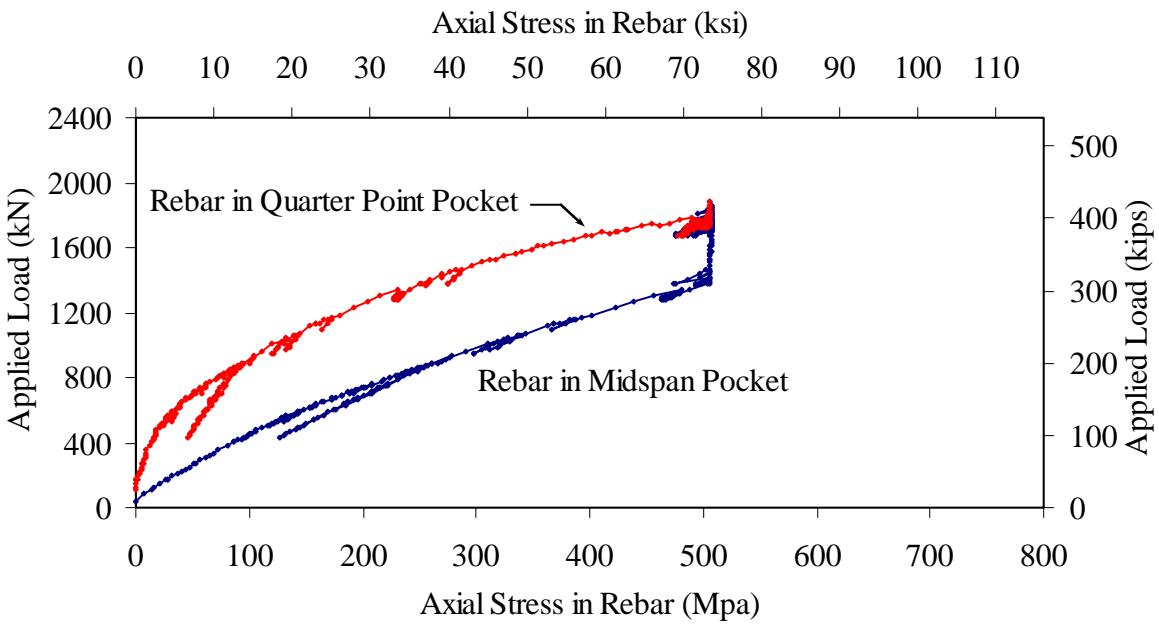
Figure 66. Graph. Axial stress in dowel rebars in Test T1J.
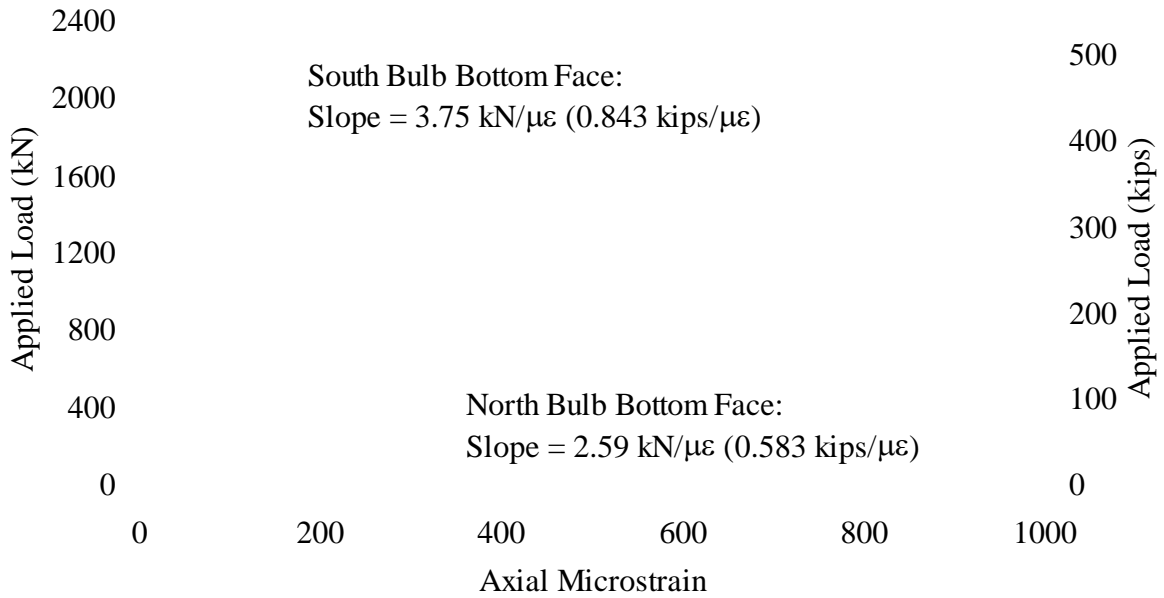
Figure 67. Graph. Bottom bulb tensile strains in Test T1J.

South Bulb Bottom Face:
Slope = 3.75 kN/με (0.843 kips/με)

North Bulb Bottom Face:
Slope = 2.59 kN/με (0.583 kips/με)

Crack on north face of north web.

Figure 68. Photo. North face of north web at 1780 kN (400 kips) applied load in Test T1J.

Figure 69. Photo. North face of north web after conclusion of Test T1J.

Figure 70. Photo. South face of south web after conclusion of Test T1J.
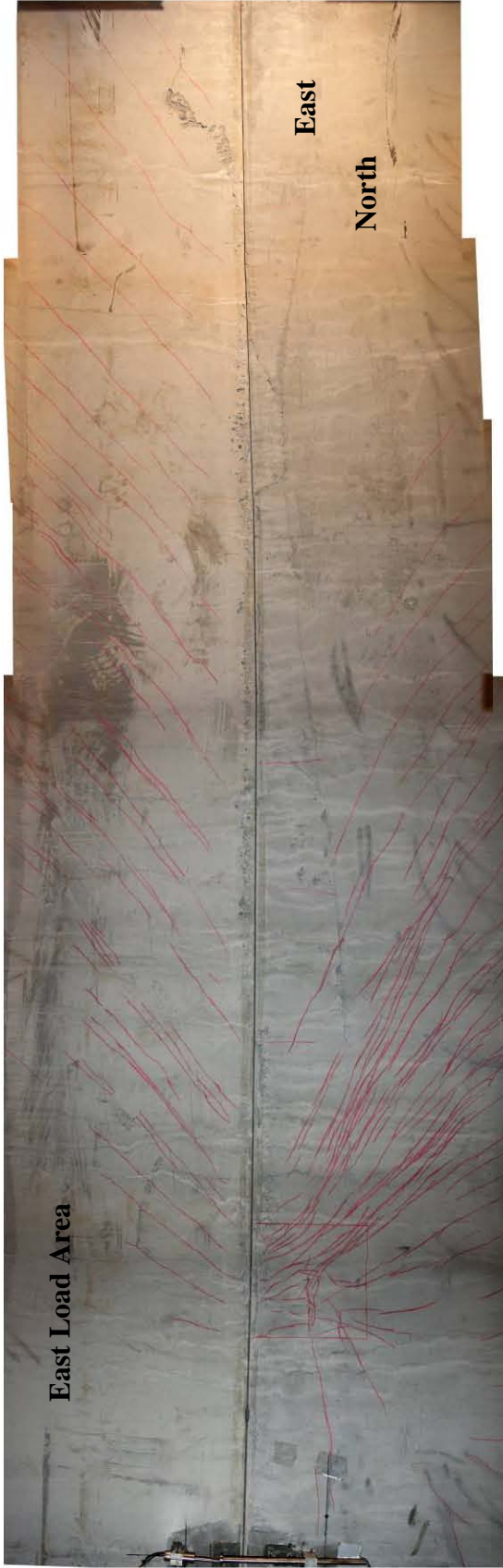
Figure 71. Photo. Underside of deck from midspan to east end after the conclusion of Test T1J.
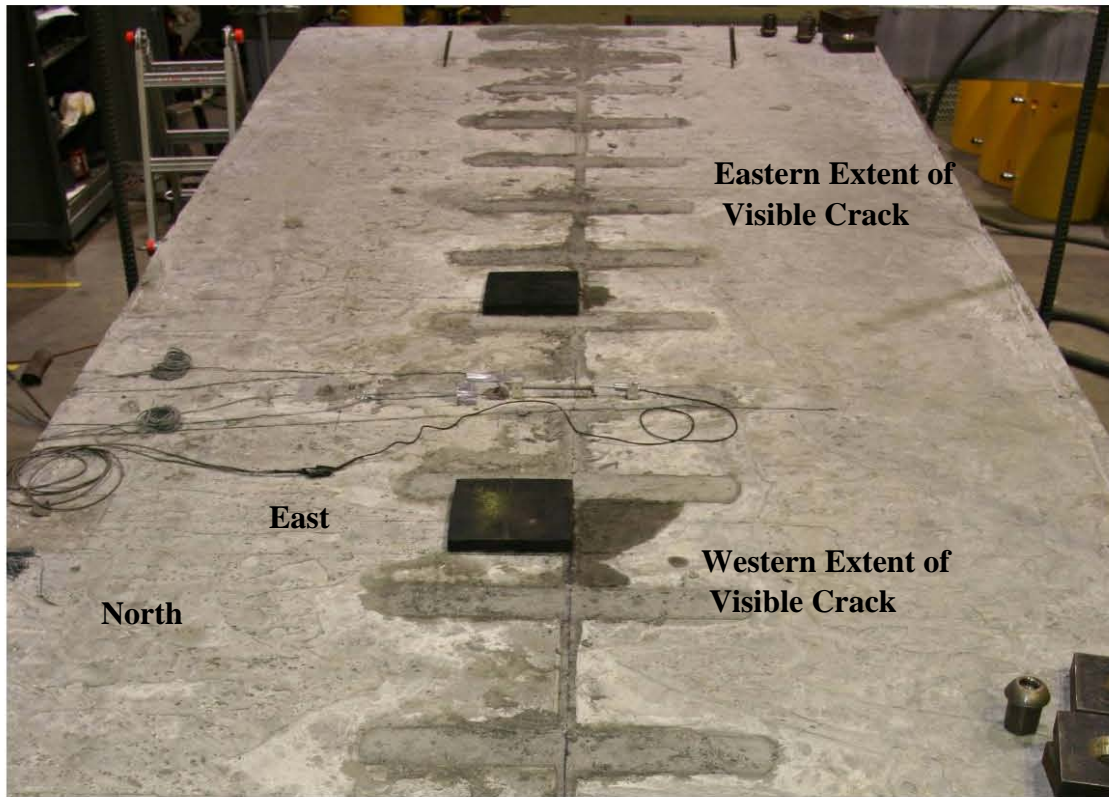
Figure 72. Photo. Top of deck after the conclusion of Test T1J.

T2J

Similar to Test T1J, Test T2J was intended to investigate the transverse flexural and shear responses of the 2nd generation pi-girder cross section. The test was completed using pieces of the previously tested, 7.6-m (25-foot) long Girder T2. After the completion of Test T2D, Girder T2 was cut along its midline to create two disconnected half-pi-girders. These two pieces were arranged such that their flange tips were adjacent, then the diaphragm members were bolted into place. Finally, the #8 mild steel reinforcement dowel bars were placed into the connection pockets and the joint was cast. The joint fill material implemented for this test was Eucospeed MP. The girder was tested after the joint fill had been allowed to cure for 21 days.

The setup for the test included a 7.3-m (24-foot) span, two point loads offset 127-mm (5-inch) north of the joint centerline with each being 0.61 m (2 feet) from midspan, and four reaction points centered under the bulbs. Recall that the loads were applied and reacted through 25-mm (1-inch) thick elastomeric pads. Loads were monitored through load cells mounted between the hydraulic jacks and the reaction frame.

Prior to the start of testing, the girder deck, joint, and webs were checked for preexisting cracks. Alcohol was sprayed onto the surfaces to facilitate identification of any cracks. No cracks were noted on the north face of the north web or on the south face of the south web. Additionally, no cracks were noted within the surface of the joint fill, and the interface bond between the joint fill and the girder deck appeared intact. A small number of cracks visible only through the use of a volatile alcohol spray were observed on the underside of the deck. These cracks tended to be

transverse or nearly transverse to the length of the specimen. As mentioned previously with regard to Test T2D, cracks, some visible with alcohol and some with the naked eye, were also observed on the top of the deck, primarily emanating from the corners of the grout pockets and running transverse to the length of the specimen.

Prior to the start of the test, all gages were reset and all potentiometers were set so as to minimize hysteretic behavior.

First audible cracking of the girder was heard at an applied load of 458 kN (103 kips). The emanation point of this cracking behavior could not be specifically located on the surface of the specimen. The peak load applied to the girder was 2015 kN (453 kips). Additional displacements of the loading pads were imparted into the specimen after this peak load so as to demonstrate that the specimen global behavior had entered a post-peak declining response phase. The test was halted at a post-peak applied load of 1877 kN (422 kips).

Figure 73 shows the applied load versus vertical deflection response of the midspan cross section of the test specimen. The responses can be observed to be primarily linear until the applied load surpasses approximately 622 kN (140 kips). From this load level until approximately 1330 kN (300 kips), a slight increase in deck deformation relative to leg deformation can be observed. After approximately 1330 kN (300 kips) nonlinear behavior can be observed in the north leg, and after approximately 1560 kN (350 kips) nonlinear behavior can be observed in the south leg. These behaviors are also shown in Figure 74 where the results from the four potentiometers measuring vertical deflection of the midspan cross section are presented at ten discrete load steps. Figure 75 presents similar information from the four potentiometers measuring vertical deflection at the quarter point of the test span.

Additional observations related to the global deformation of the girder are presented in Figure 76 which shows the spreading of the bulbs at midspan. This figure shows that the spreading of the bulbs progressed much more rapidly under applied loads above 1420 kN (320 kips), with the spread reaching approximately 25.4 mm (1.0 inch) at the peak applied load. The relative distance between the bulbs had increased by 27.7 mm (1.09 inch) by the time the test was halted.

Figure 77 presents the axial load observed in the west diaphragm as calculated from the axial strains measured on the structural tube at midlength. The plot shows that a total maximum load of 206 kN (46.2 kips) was generated in the west diaphragm, and that this peak diaphragm force occurred at the peak applied load. The relationship between the applied load and the diaphragm force was substantially linear throughout the loading and final unloading, with the induced force returning to zero.

Transverse displacement results from the LVDTs which were mounted above and below the joint at midspan are presented in Figure 78. The LVDTs were centered over the joints, were installed with 279-mm (11-inch) center-to-center gage lengths, and were placed 25 mm (1 inch) above and below the exterior surfaces of the joint.

The axial strain results recorded from two of the #8 reinforcing bar dowels embedded in the grouted joint are presented in Figure 79. One of these reinforcing bars was located in the pocket at midspan, while the other was located above the east diaphragm at the east quarter span point.

Electrical resistance strain gages were affixed to the surface of the bars, with their orientation parallel to the length of the bar. The bars were then placed at the centerline of the joint prior to the casting of the joint fill material. This plot shows that significantly greater strain was experienced in the midspan pocket. Additionally, note that the slope of the curves change abruptly at a strain level similar to the rebar yield strain as reported in Chapter 3.

Further analysis of the dowel strain results was completed by applying the uniaxial stress-strain response in Figure 4 to the results in Figure 79. The outcome is shown in Figure 80. Note that unloading/reloading strain cycles were assumed to occur with a stiffness concurrent with the initial elastic stiffness. Also, the plotted results do not include the final unloading of the specimen at the conclusion of the test. This plot shows that the reinforcing bars in both pockets yielded and the reinforcing bar at midspan began strain hardening prior to the application of the peak load to the specimen.

Recall that the specimen was asymmetrically loaded, thus leading to different load proportions being carried by each leg. The proportion of the flexural load carried by each leg can be estimated based on the strain observed on the bottom face of the bulbs at midspan. Figure 81 presents the strain results captured from the two gages affixed to the bottom faces of the north and south bulbs at this location. The results from these gages are only plotted up through approximately 400 microstrain due to inconsistent readings captured at higher strains as a result of cracking of the underlying concrete. Linear interpolation was completed to determine the slope of these responses relative to the applied loadings. These slopes indicate that approximately 43% of the flexural loading was carried by that south leg of the specimen, while 57% was carried by the north leg. These proportions are consistent with the transverse location of load application relative to the midline of the joint.

The cracking response of the specimen was monitored qualitatively from north, south, and above the specimen during the test, and more thoroughly from all sides after the completion of the test. The cracking observed on the top of the deck was similar to, but more extensive than, the cracking observed in Test T1J. A visual crack assessment was completed of the top of the deck at both 1330 kN (300 kips) and 1780 kN (400 kips) of applied load. Each time, the only crack visible with the naked eye was a single crack in the joint fill material traversing the midspan grout pocket just north of the joint midline. This crack is shown in Figure 82. As the loads increased beyond 1780 kN (400 kips), the cracking apparent on the top of the deck became much more prevalent. Figure 83 shows a photo of the top of the deck just after the peak applied load was reached. Note the grout crushing visible along the joint and the tensile crack visible to the south (left) of the hydraulic jacks. The photograph captured in Figure 84 shows the distress evident on the top of the deck after the conclusion of the test. For clarity, the hydraulic jacks have been removed and the elastomeric loading pad remains in place.

Following the completion of the test, the distress within the grouted joint was investigated further through coring the joint at eight locations near and west of midspan. The full depth, 152-mm (6-inch) diameter cores were obtained both at locations were dowel bar pockets intersected the shear key, as well as between pockets where only the shear key was present. Inspection of the removed cores and the core holes provided information on the distress which occurred along the joint. Figure 85 shows the distress observed in three of the core holes, while Figure 86 provides an illustration of the visible distress observed on top of the deck and within

68

the joint. Debonding of the grout from the UHPC flange tips was evident in many of the cores. Cracking/shearing of the grout near the northern point of the shear key diamond was also evident in many of the cores. Note that cracks shown in Figure 86 represent the distress visible to the naked eye; additional structural cracking visible only with the aid of an alcohol spray was observed between the line denoting the extents of the grout pockets and the legs of the girder halves. Identification of these cracks was made difficult by the irregular surface of the deck. These cracks tended to parallel the length of the girder between the load points then turn at a shallow angle toward the joint as they progressed beyond the load points. There were approximately three to five of these cracks on both the north and south sides of the joint.

The cracking observed on the south face of the south web and on the north face of the north web was similar to the cracking observed during Test T1J. These cracks emanated symmetrically from midspan toward the ends of the specimen. The cracking was more prevalent on the north side than on the south side. On the south face of the south girder six generally horizontal cracks were noted at 890 kN (200 kips) of applied load, and twelve were noted at 1330 kN (300 kips), all running symmetrically about midspan. The cracking at specific locations on the north face of the north web was mapped after the conclusion of the test. Figure 87 shows both cracks visible with the aid of an alcohol spray as well as cracks marked in red wax crayon. The cracks at this location in the web just above the diaphragm were longitudinal and closely spaced. Toward midspan, the longitudinal cracking on the north face of the north web became more dispersed and was interspersed with vertical cracks caused by primary flexure. This is shown in the crack map in Figure 88, which it must be noted was not fully completed to include all cracks being marked over their entire lengths.
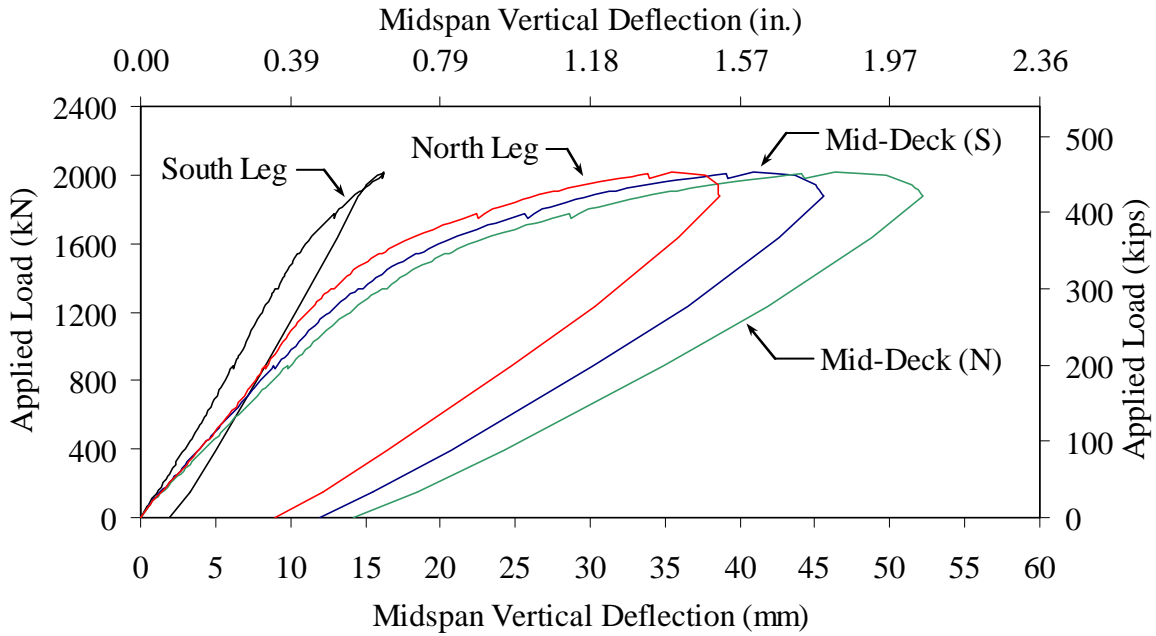
Figure 73. Graph. Load versus midspan deflection response from Test T2J.
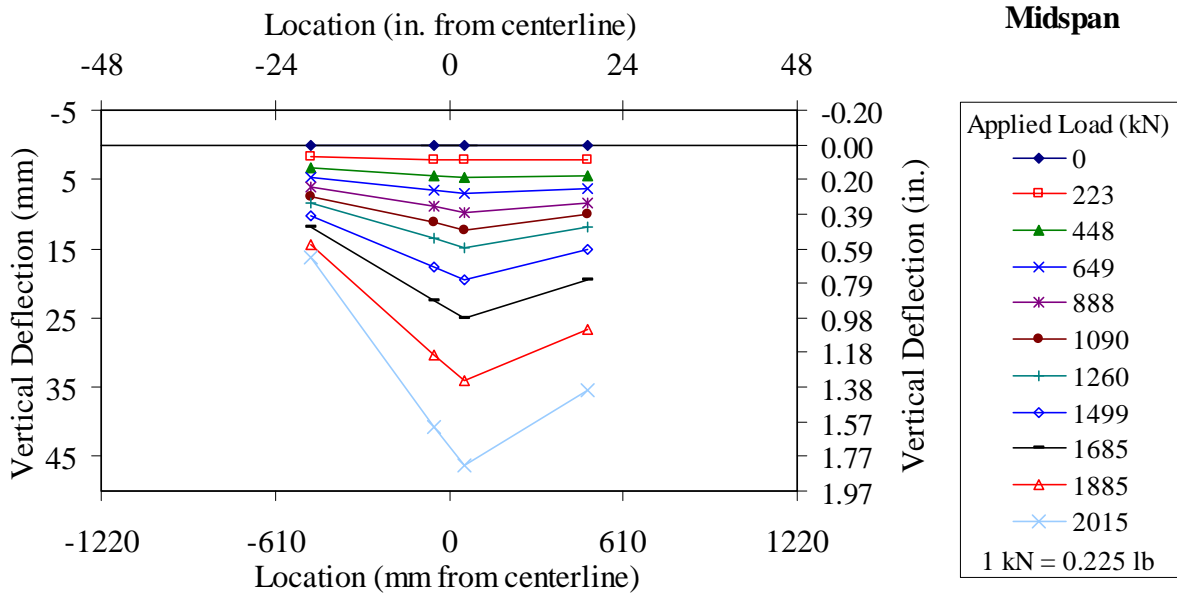
Figure 74. Graph. Load versus deflection response across T2J at midspan.
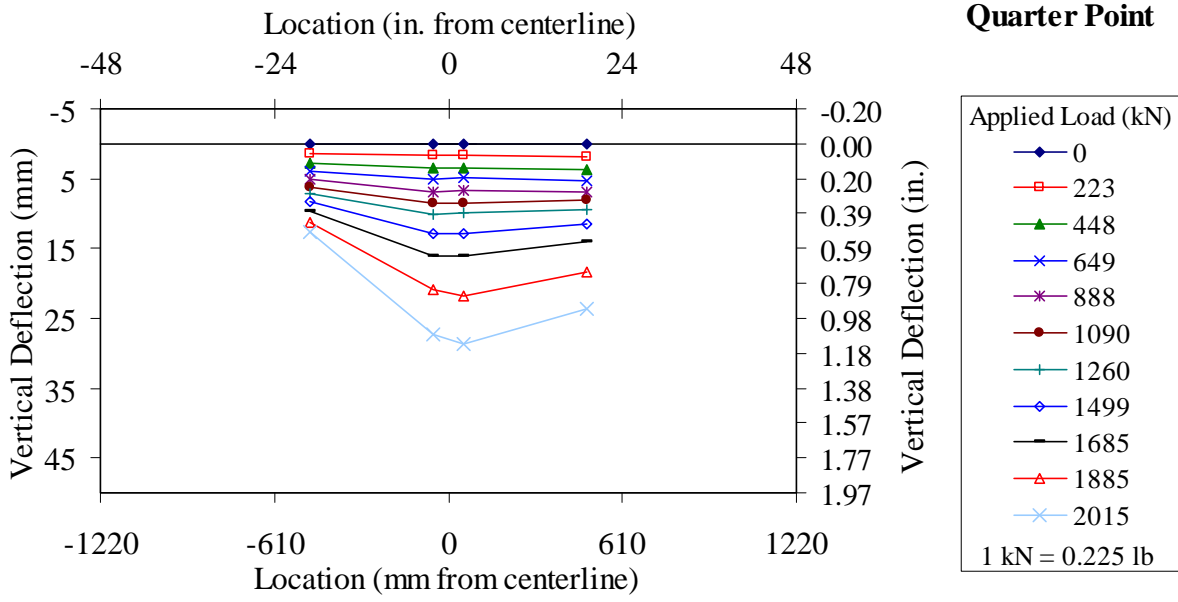
Figure 75. Graph. Load versus deflection response across T2J at quarter span.
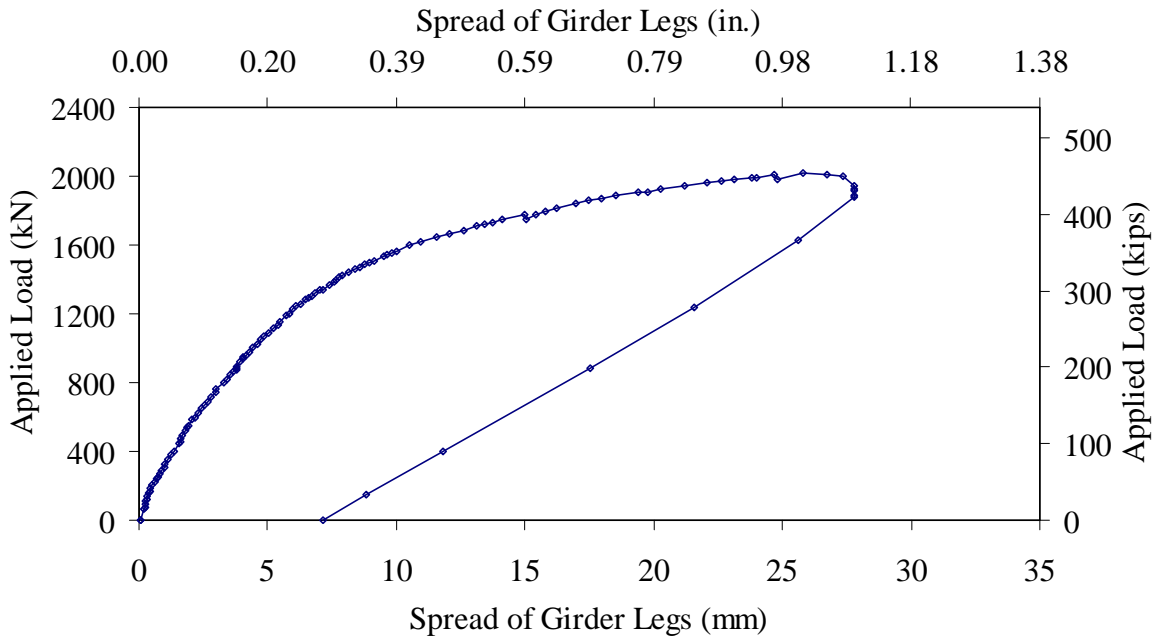
Figure 76. Graph. Spreading between bulbs at midspan of Test T2J.
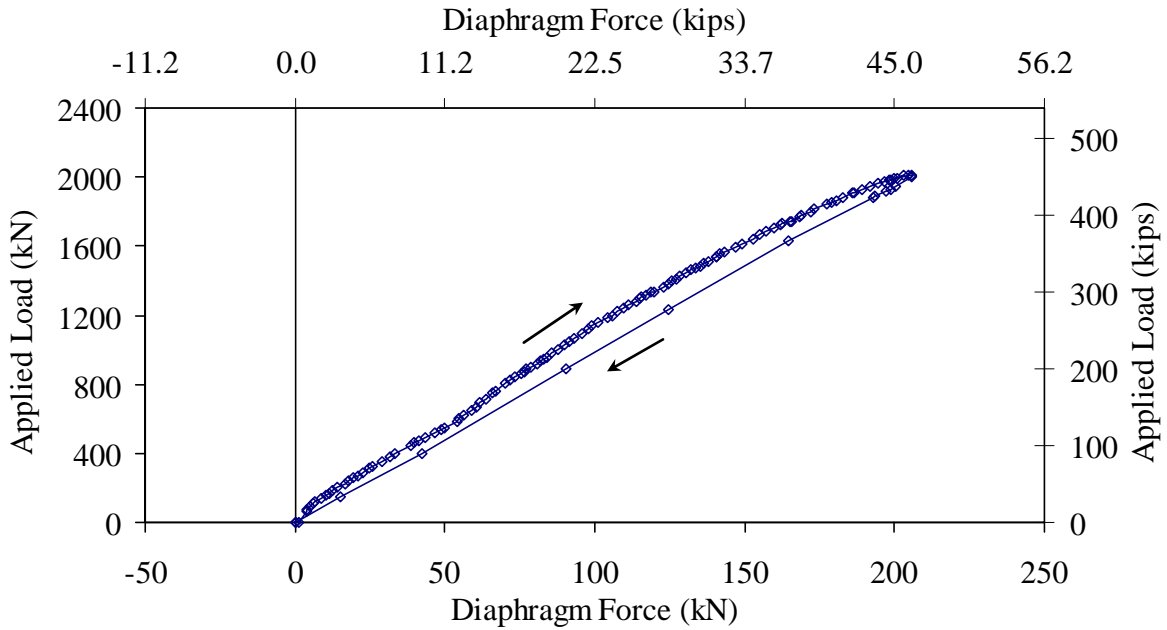
Figure 77. Graph. West Diaphragm force in Test T2J.
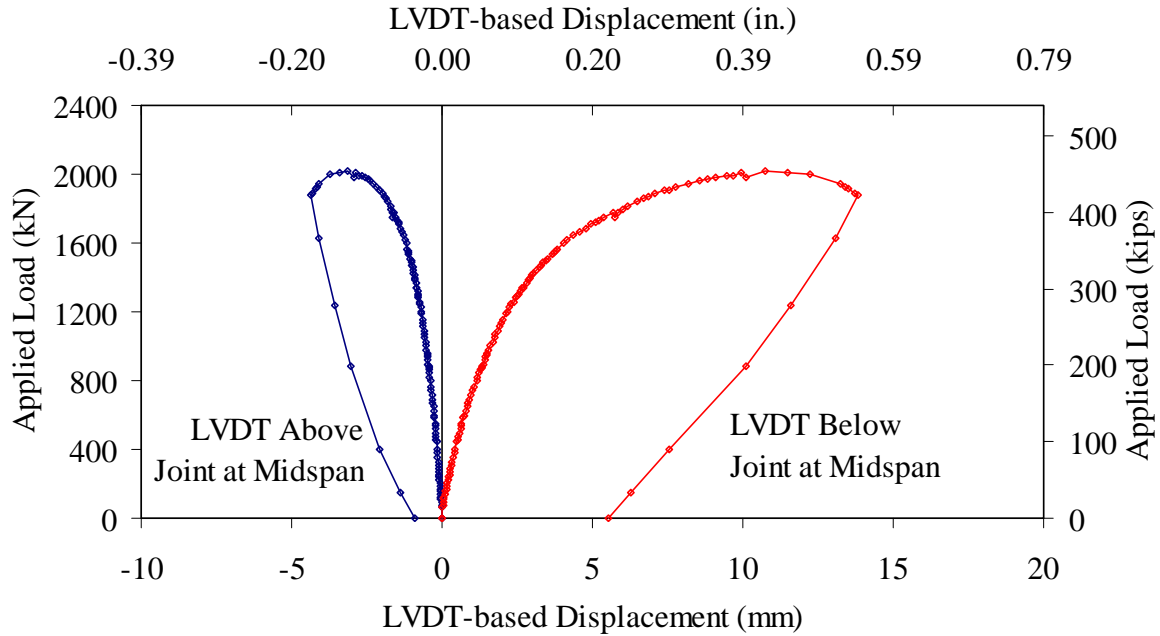
Figure 78. Graph. LVDT-based displacement across joint at midspan in Test T2J.

72
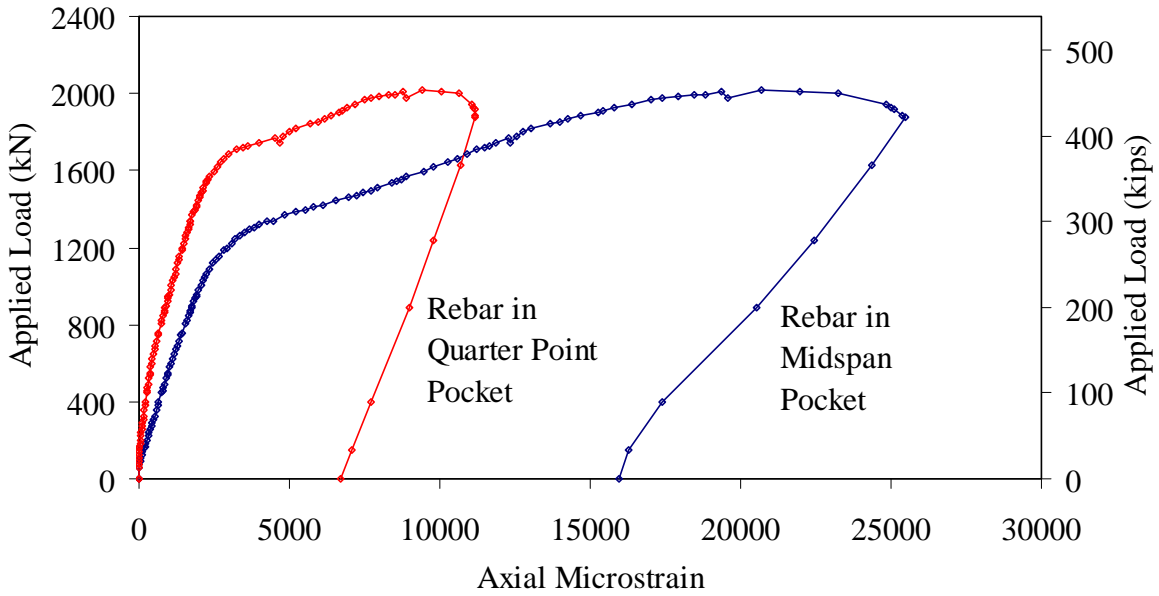
Figure 79. Graph. Axial strain in dowel rebars in Test T2J.
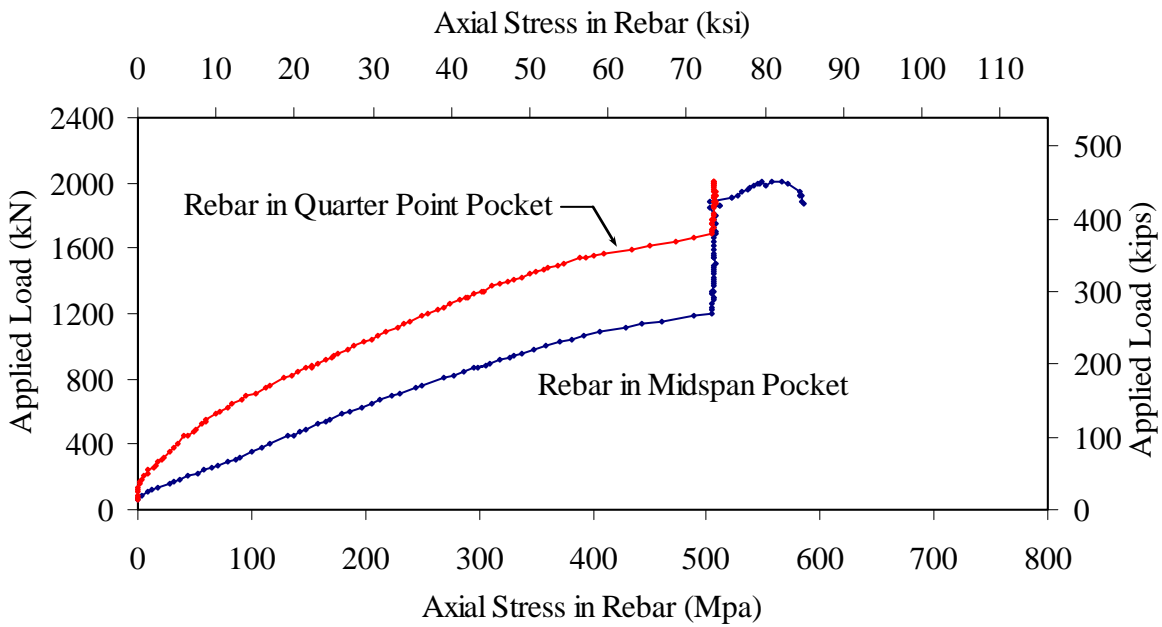
Figure 80. Graph. Axial stress in dowel rebars in Test T2J.
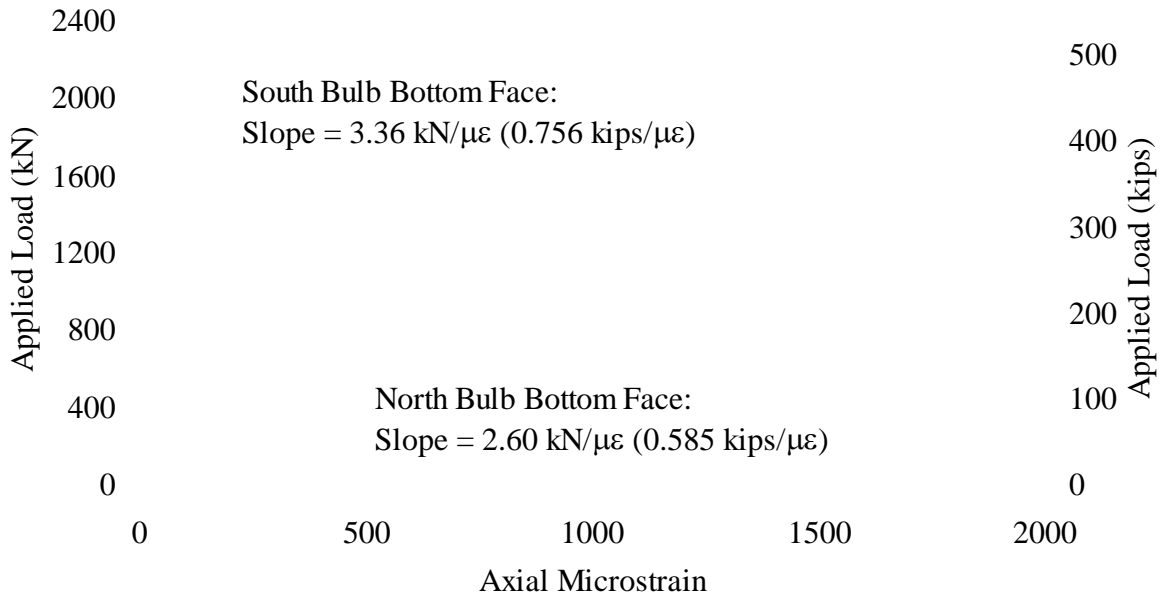
Figure 81. Graph. Bottom bulb tensile strains in Test T2J.
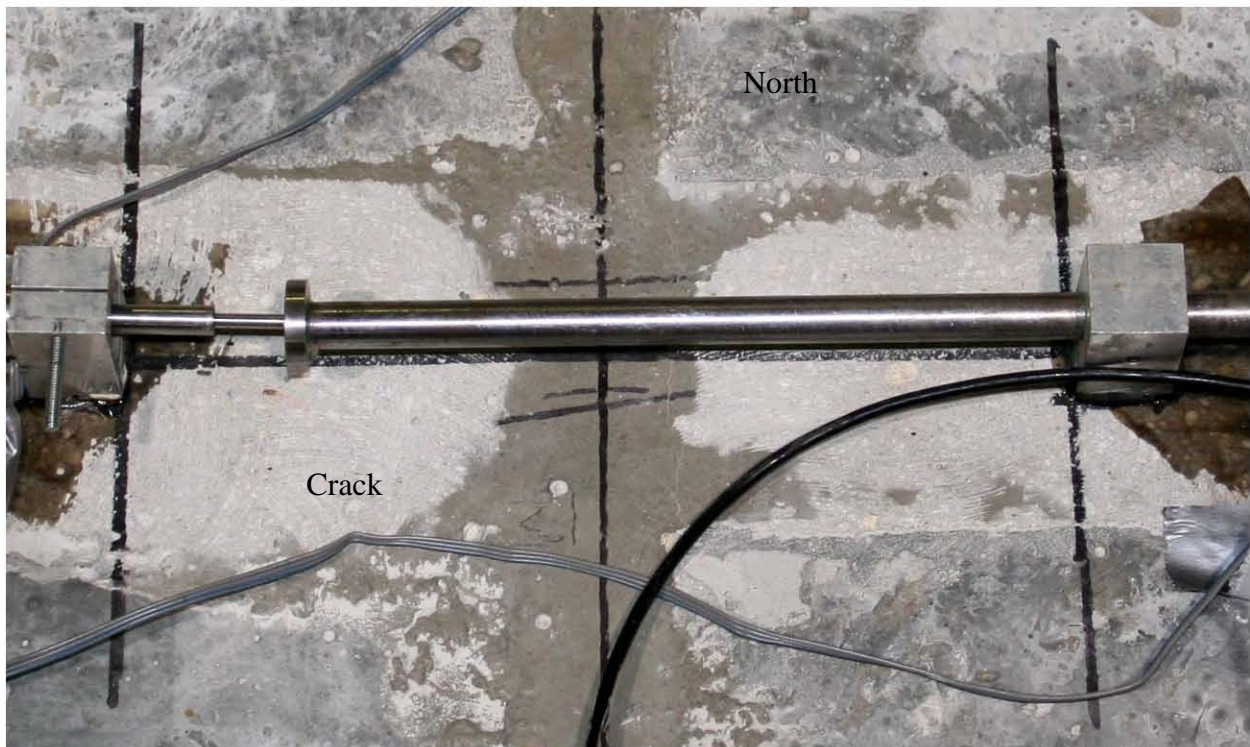
Figure 82. Photo. Crack in midspan group pocket at 1330 kN (300 kips) of applied load.

Figure 83. Photo. Top of deck at peak applied load during Test T2J.

UHPC Tensile Cracking

Crushing/Cracking

Crushing/Cracking

West Load Point

S
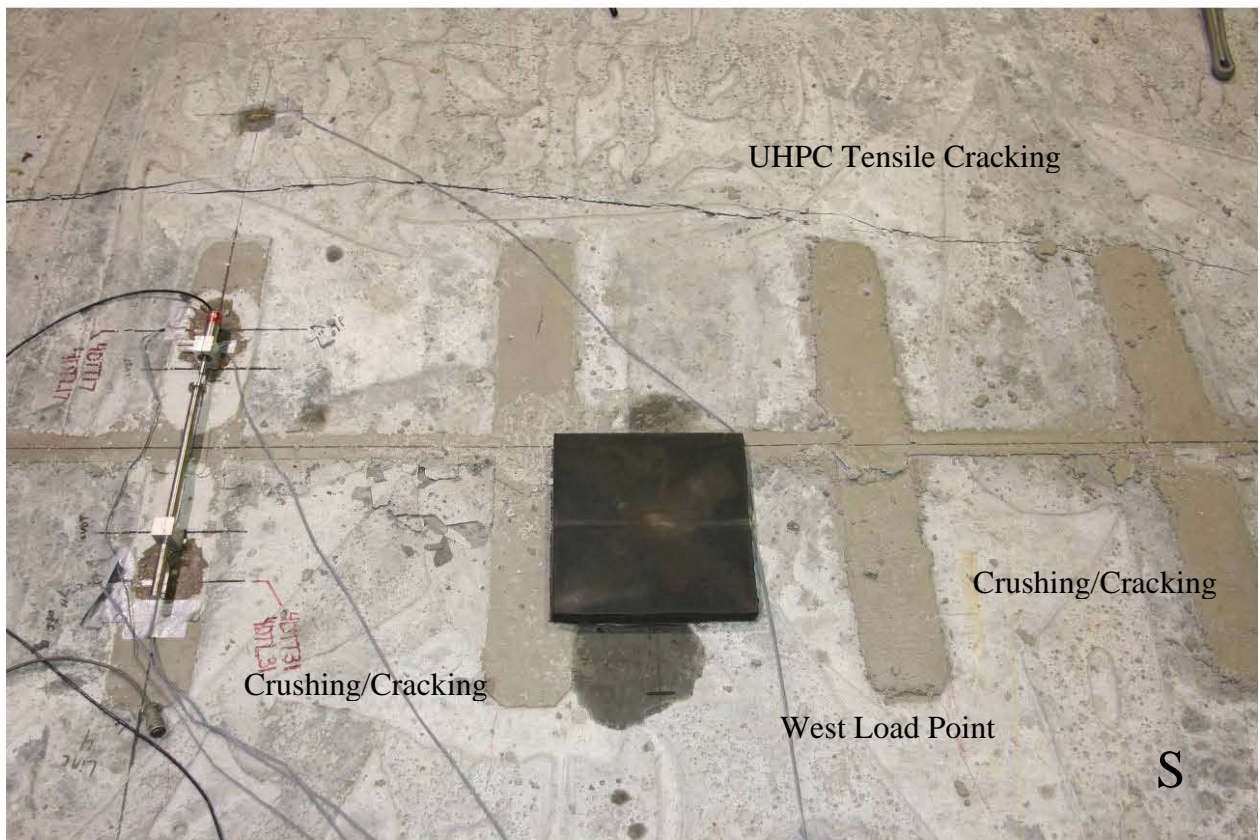
Figure 84. Photo. Distress visible on top of deck after Test T2J.

Grout Cracking
in Shear Key

Grout Debond

Grout Cracking
in Shear Key

Figure 85. Photo. Distress visible inside core holes after Test T2J.

Cores:

Top Surface of Deck

N
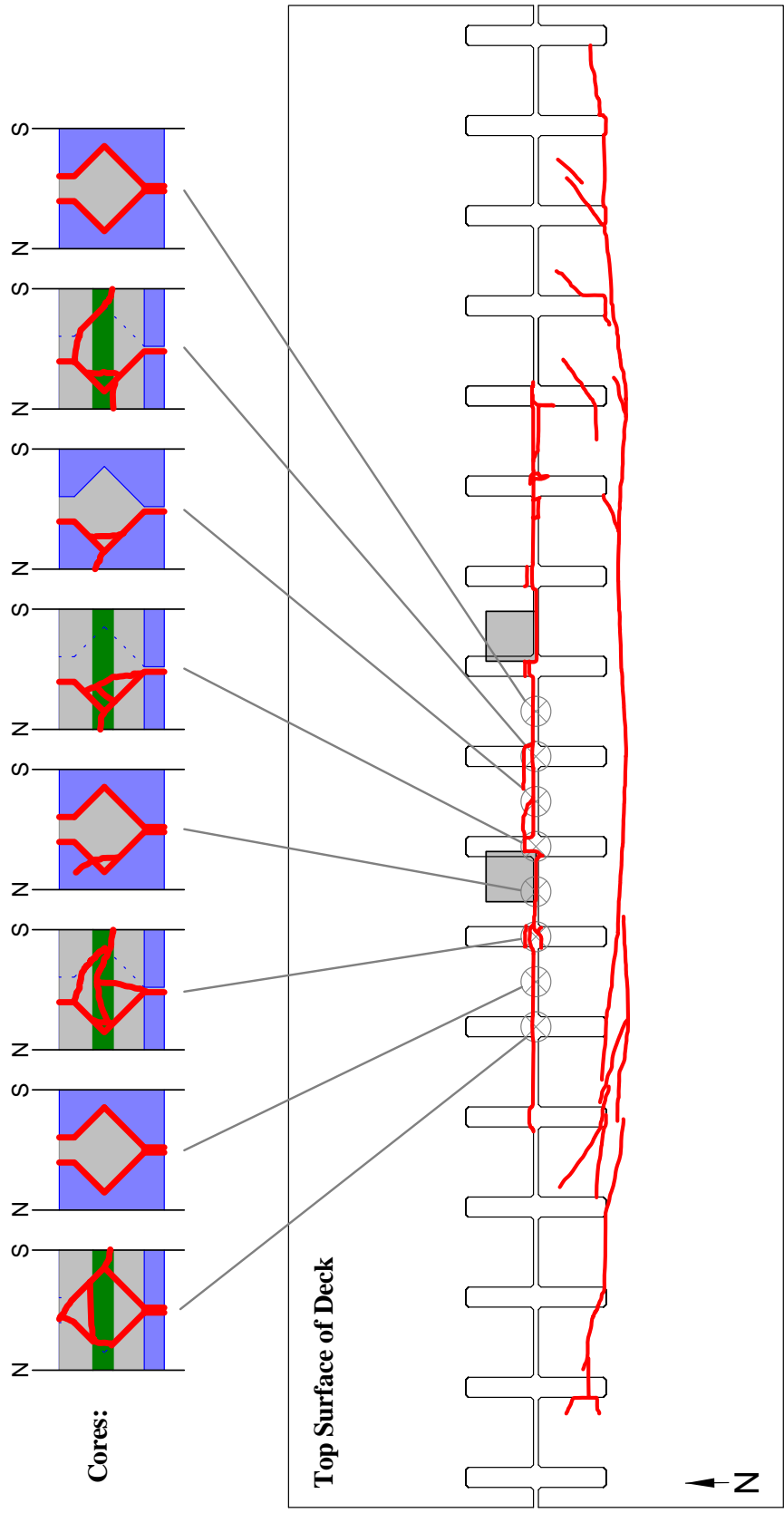
Figure 86. Illustration. Visible cracking in T2J deck and joint after conclusion of test.

Figure 87. Photo. Cracking on north face of north leg at east diaphragm after conclusion of Test T2J.
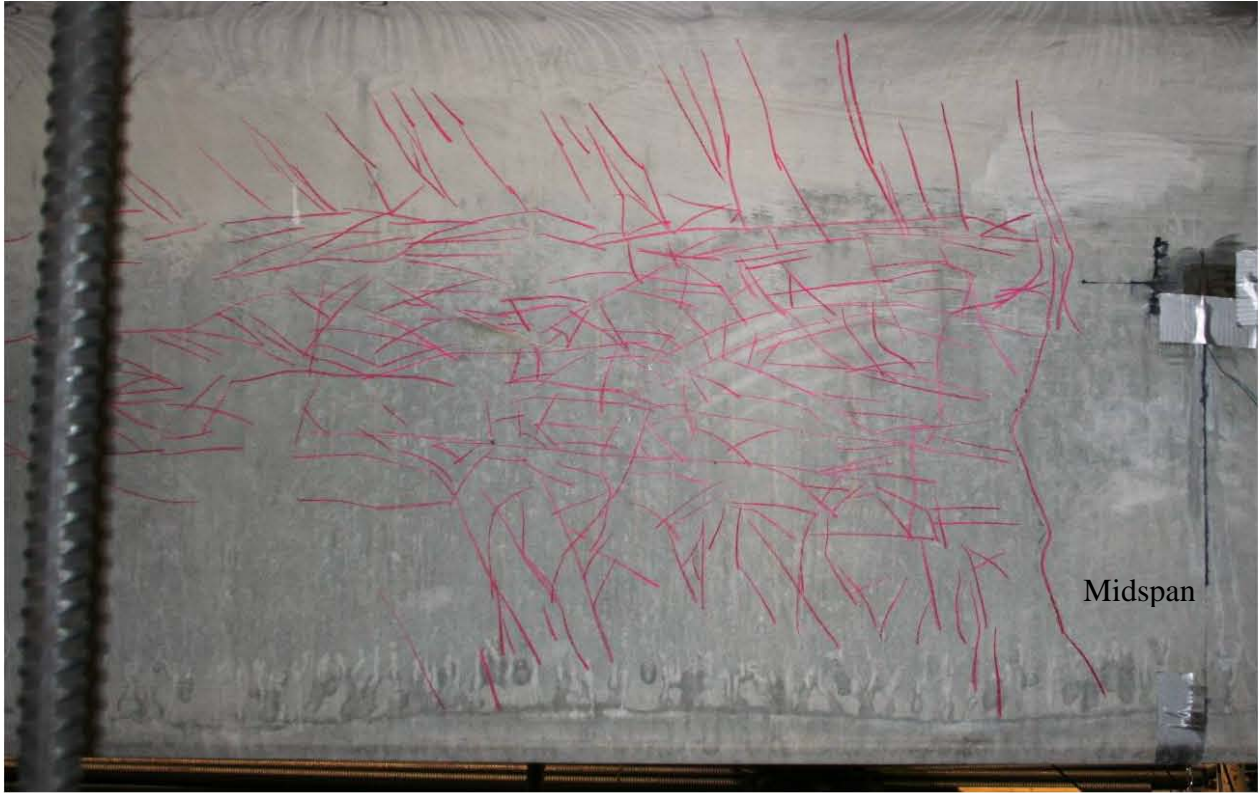
Midspan

Figure 88. Photo. Crack map of north face of north leg at midspan after conclusion of Test T2J.

CHAPTER 6.   DISCUSSION OF RESULTS

INTRODUCTION

This chapter presents an analysis and discussion of the results from the physical tests conducted in this research program. As with the test program as whole, this chapter focuses on the transverse flexural response of the 2nd generation UHPC pi-girder, the failure mechanisms observed, and the structural capacities that this girder is expected to possess.

TRANSVERSE FLEXURAL RESPONSE OF A 2nd GENERATION UHPC PI-GIRDER

As-Fabricated Girder Response

Tests T1D and T2D were completed on similar girders using similar loading setups. In both cases, simulated wheel loads were applied near midspan along the centerline of the deck. The only significant difference between the specimens was that Girder T1 contained #5 reinforcing steel in the deck, oriented transverse to the length of the bridge and spaced at 305 mm (12 inches).

Test T1D was completed first. Loads were increased until the overall peak applied load was 983 kN (221 kips). At this point the test was halted and the specimen unloaded due to concern for the integrity of the steel diaphragms. Test T2D was completed second and followed an identical loading procedure as Test T1D, except that this test was continued until failure which occurred after a peak load of 1510 kN (340 kips) had been applied. In this case, failure was defined as decreased girder resistance to an increase in applied vertical displacement at the load point. This failure was precipitated by failure of the steel diaphragms wherein the plate welded to the end of the steel tube pried away from the UHPC bulb coincidently with it tearing the weld connecting it to the steel tube.

Through the peak load applied in Test T1D, the results from these two tests are nearly identical. The similarity of results can be observed in Figure 89 which shows the vertical deflections captured from the middle of the deck at midspan, in Figure 90 which shows the vertical deflections captured from the north bulb, and in Figure 91 which shows the increase in relative distance between the inside faces of the girder bulbs. Similar behaviors were also observed in the all strain gage readings. Representative results are displayed in Figure 92 and Figure 93. Figure 92 shows the transverse strain readings captured on top of the middle of the deck at midspan. Figure 93 shows the transverse strain readings captured 356 mm (14 inch) south of the underside middle of the deck at the west diaphragm. As no significant differences in structural response were observed between T1D and T2D, it is anticipated that the mild steel reinforcement included in the deck of T1D provided minimal structural benefit up through the application of 983 kN (221 kips).
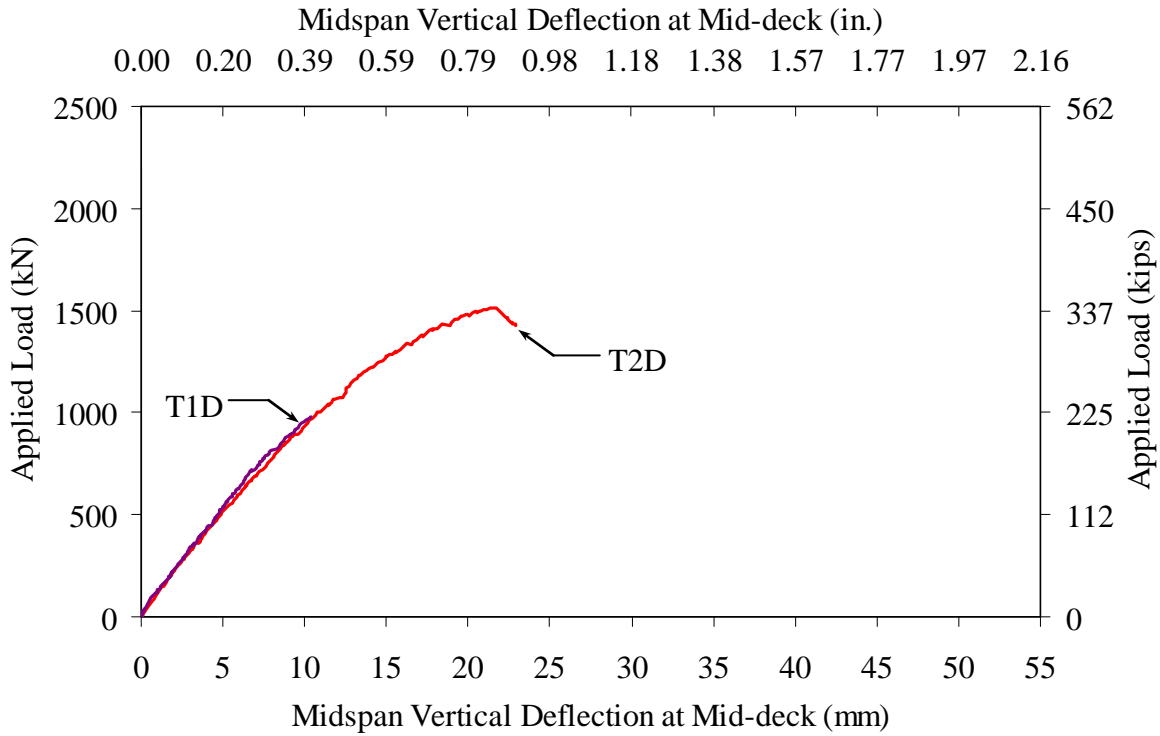
Figure 89. Graph. Midspan mid-deck vertical deflection results from Tests T1D and T2D.
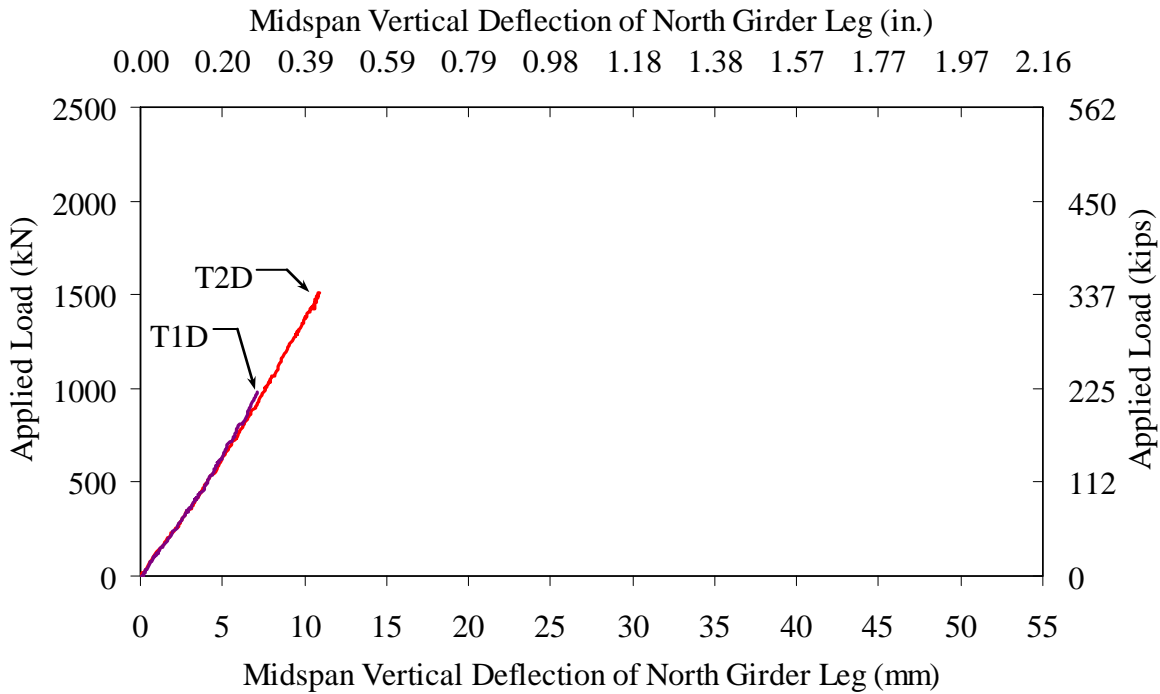

Figure 90. Graph. Midspan north leg vertical deflection results from Tests T1D and T2D.
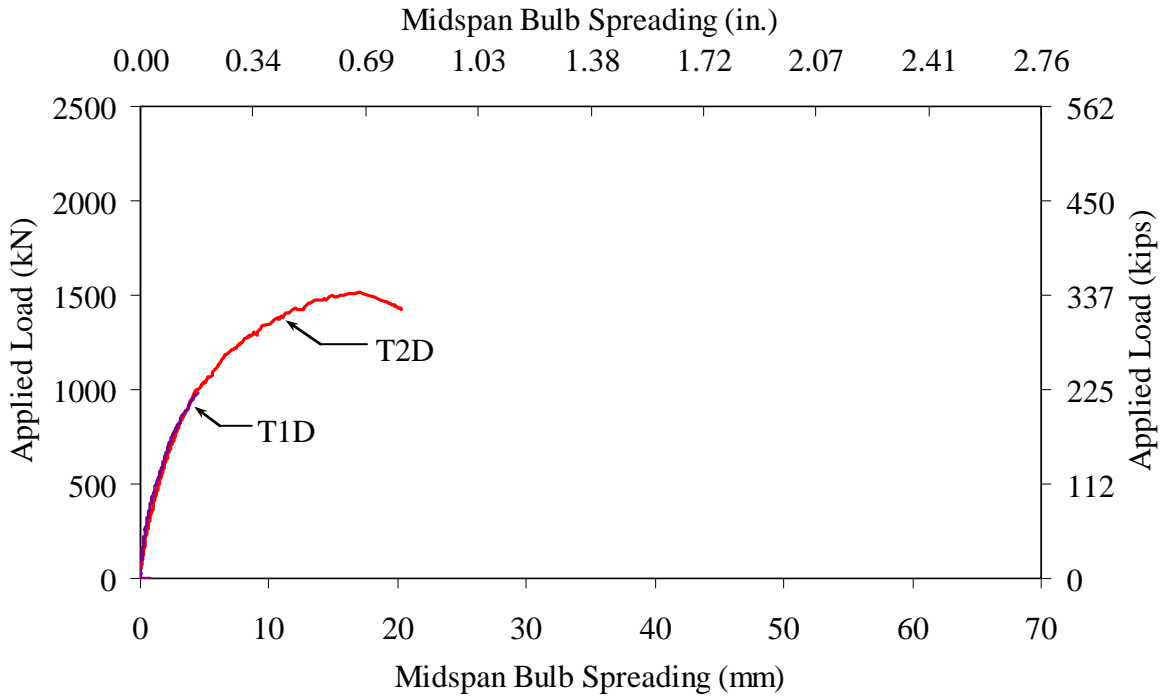
Figure 91. Graph. Midspan bulb spreading results from Tests T1D and T2D.
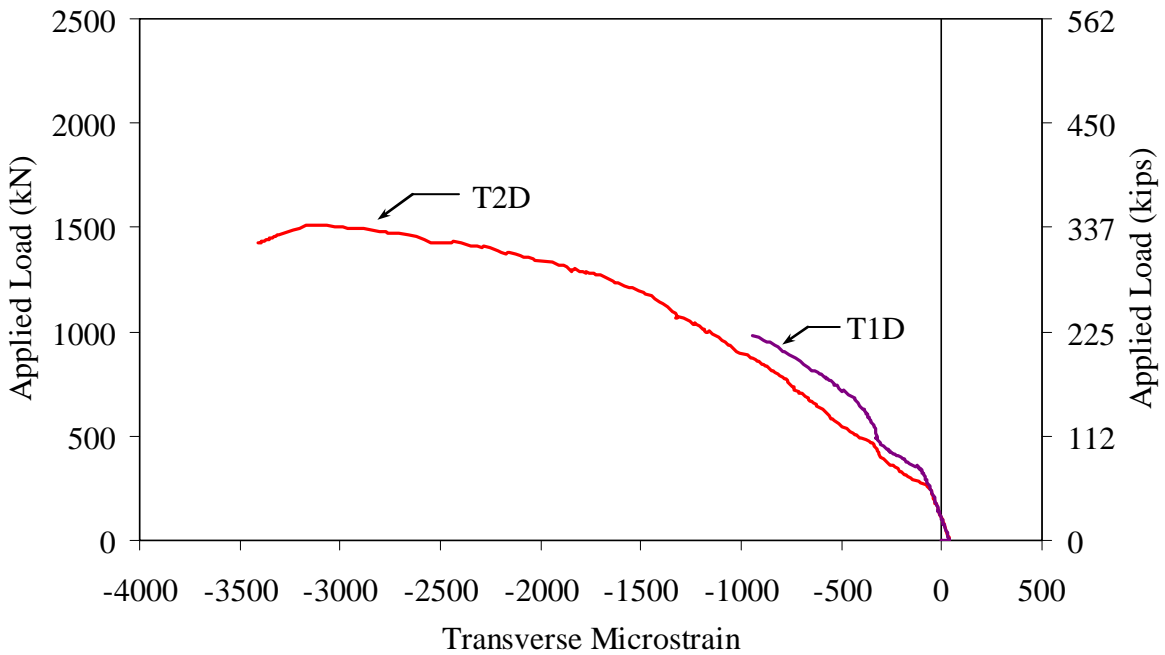
Figure 92. Graph. Transverse strain on top of deck at midspan and middeck from Tests T1D and T2D.
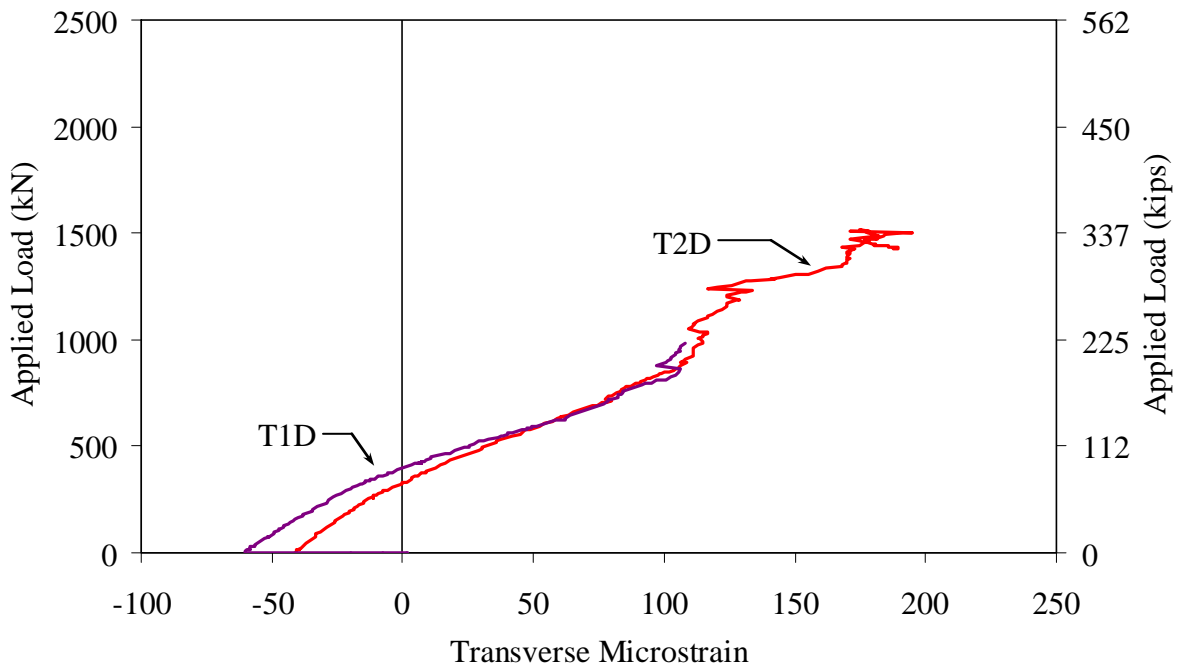
Figure 93. Graph. Transverse strain 356 mm (14 inch) south of middeck on underside at west diaphragm from Tests T1D and T2D.

Longitudinal Joint Response

Tests T1J and T2J were completed on similar girders using similar loading setups. In both cases, simulated wheel loads were applied near midspan just north of the centerline of the deck. The mild steel reinforcement contained in the overhanging top flanges of T1J was not anticipated to have any impact on the structural response of the member. The only significant difference between these two tests was the joint fill material used in the longitudinal joint connecting the girder halves. In Test T1J, UHPC was used as the joint fill material. In Test T2J, a magnesium phosphate structural grout was used.

Test T1J was completed first. Loads were increased until the overall peak applied load was 1880 kN (422 kips). At this point the test was halted and the specimen unloaded due to concern for the integrity of the steel diaphragms. Test T2J was completed second and followed an identical loading procedure as Test T1J, except that this test was continued until failure which occurred after a peak load of 2010 kN (453 kips) had been applied. In this case, failure was defined as decreased girder resistance to an increase in applied vertical displacement at the load point. The diaphragms remained intact through both of these tests. The failure of T2J was evidenced by a combined flexure and shear failure of the grouted joint combined with transverse flexural failures in the girder deck and web.

Overall, the responses of the two specimens up through the peak load applied in Test T1J were generally similar. For example, Figure 94 shows the vertical deflection of the north leg as recorded during the two tests. However, the local behavior of the longitudinal joint was

84

observed to differ between the two tests. This difference in behaviors is focused on two topics; namely, distribution of loads and joint capacity at failure.

The different capabilities of the T1J and T2J joints to distribute applied loads throughout the specimen is demonstrated in Figure 95 through Figure 101. Figure 95 presents a comparison between the vertical deflection observed at the north side of the joint at midspan in the two tests. Figure 96 presents a comparison between the relative spreading of the bulbs at midspan in the two tests. In both plots the responses indicates that there was a greater tendency for the midspan cross-section to deflect and deform in the T2J test. A similar tendency is shown in Figure 97 which focuses on the local deformation of the longitudinal joint at midspan. This plot demonstrates that the T2J joint underwent greater local rotation per unit of applied load as compared to the T1J joint. The greater deformation within the joint is also observed in Figure 98 which shows that the reinforcing bars within the joint at midspan and at the quarter span tended to show higher axial strains in the T2J test per unit of applied load. Figure 99 and Figure 100 show abrupt changes in transverse strains occurring in the T2J test, possibly due inelastic behaviors occurring in the joint. Figure 99 shows that the transverse strain observed on the underside of the deck just north of the joint was initially consistent between the two tests at both the midspan and at the quarter span locations. However, at applied loads of 89 kN (20 kips) and 178 kN (40 kips) the responses diverge at midspan and quarter span, respectively. The decrease in strain observed in the T2J tests may indicate strain relief caused by a loss of tensile capacity within the lower portion of the longitudinal joint. Similar behaviors are observed in Figure 100 which presents transverse strain results observed on the outside faces of the webs at midspan. In both the north and south webs, there is a distinct increase in the transverse strain observed per unit of applied load beginning at approximately 178 kN (40 kips) in Test T2J. Finally, Figure 101 presents longitudinal strain results from the top of the deck just north of the joint at both midspan and at quarter span. Greater strain per unit applied load was observed at midspan in Test T2J than in Test T1J, while the opposite was true at the quarter span location. This indicates that the T1J joint was more effective than the T2J joint at distributing the applied loads both transversely and longitudinally along the specimen's south leg.

Figure 102 presents results related to the comparative joint capacity at failure. Recall that Test T2J was taken to failure with significant distress observed within the grouted joint. This figure shows that the transverse strain observed at quarter span on top of deck 178 mm (7 inch) north of joint began increasing rapidly as the applied loads approached 1560 kN (350 kips) in Test T2J. This response is indicative of the initiation of joint failure near midspan and the resulting shift in load path for the distribution of applied loads.
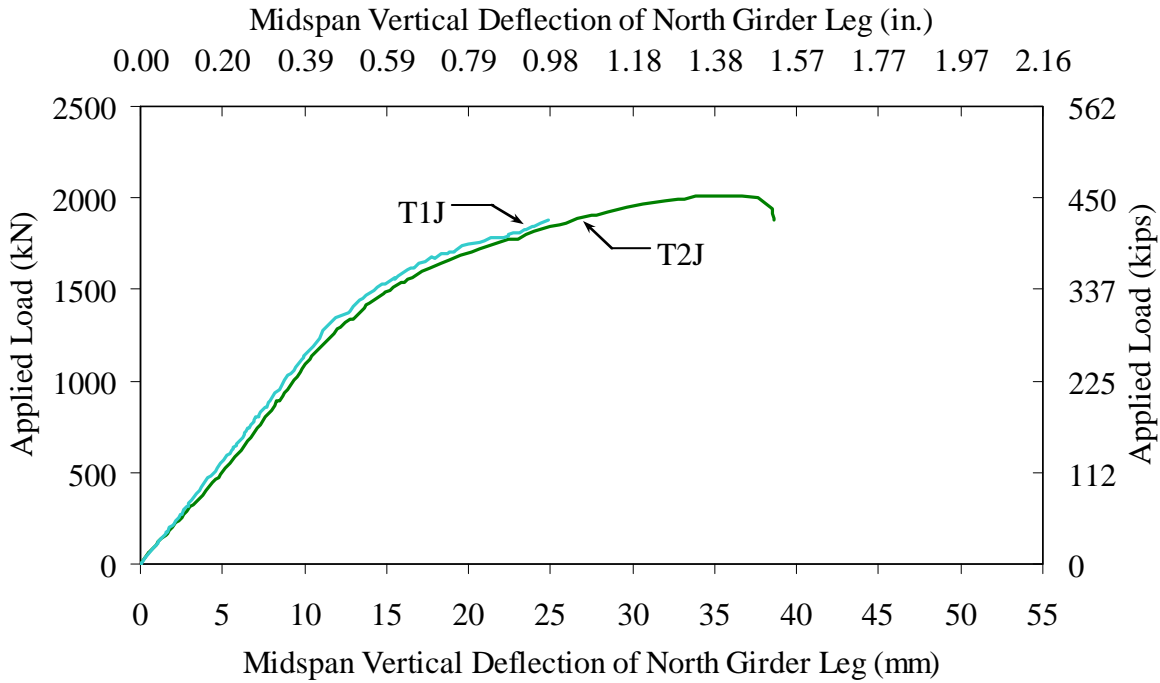
Figure 94. Graph. Midspan north leg vertical deflection results from Tests T1J and T2J.
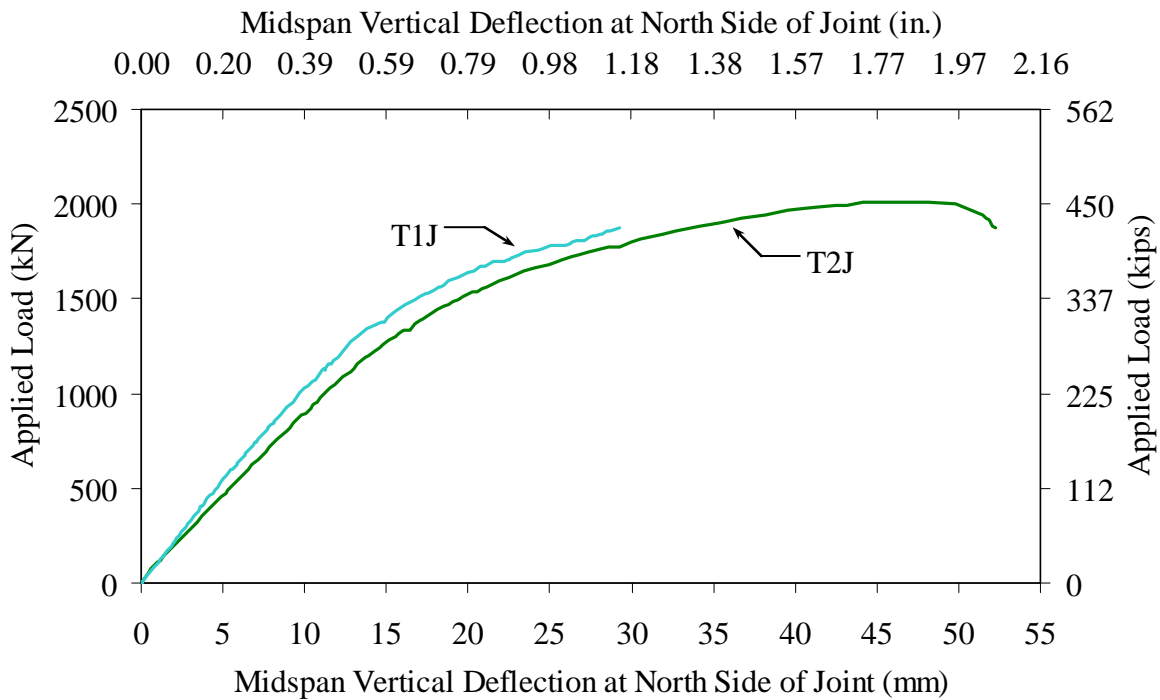
Figure 95. Graph. Midspan vertical deflection at north side of joint from Tests T1J and T2J.
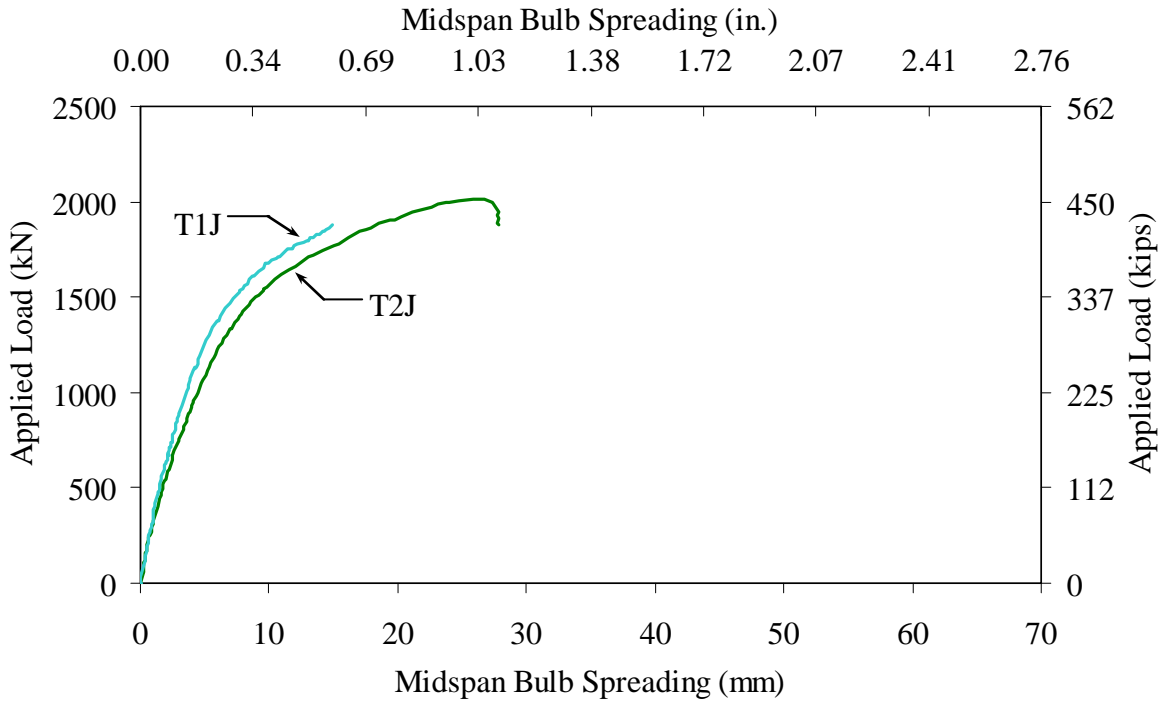
Figure 96. Graph. Midspan bulb spreading results from Tests T1J and T2J.
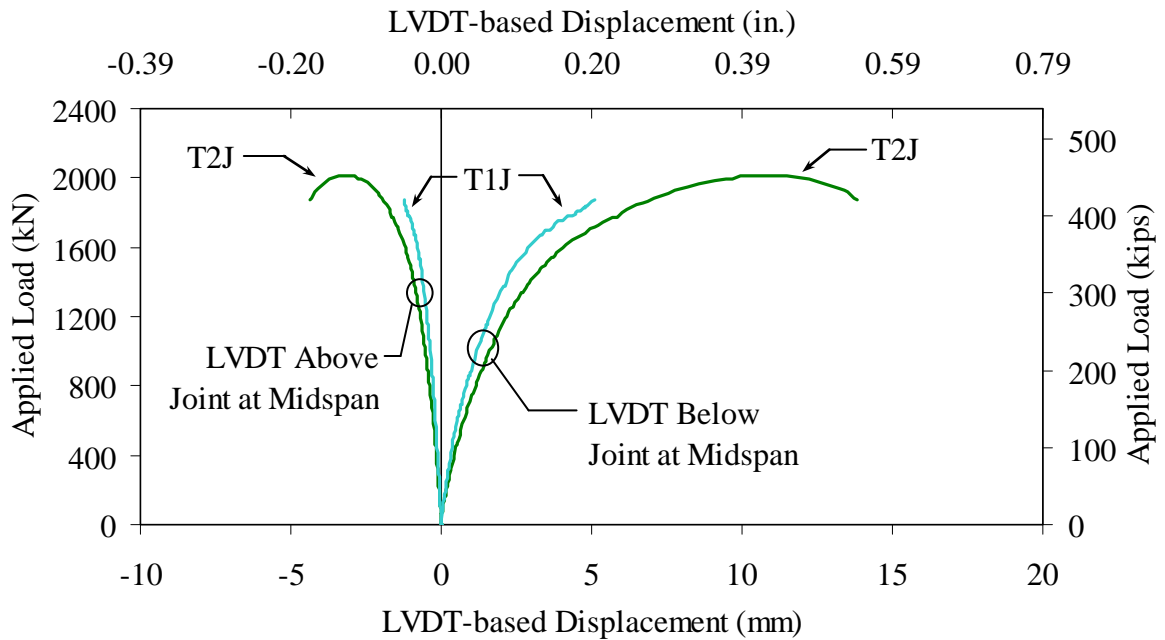
Figure 97. Graph. Transverse deformation of joint at midspan in Tests T1J and T2J.
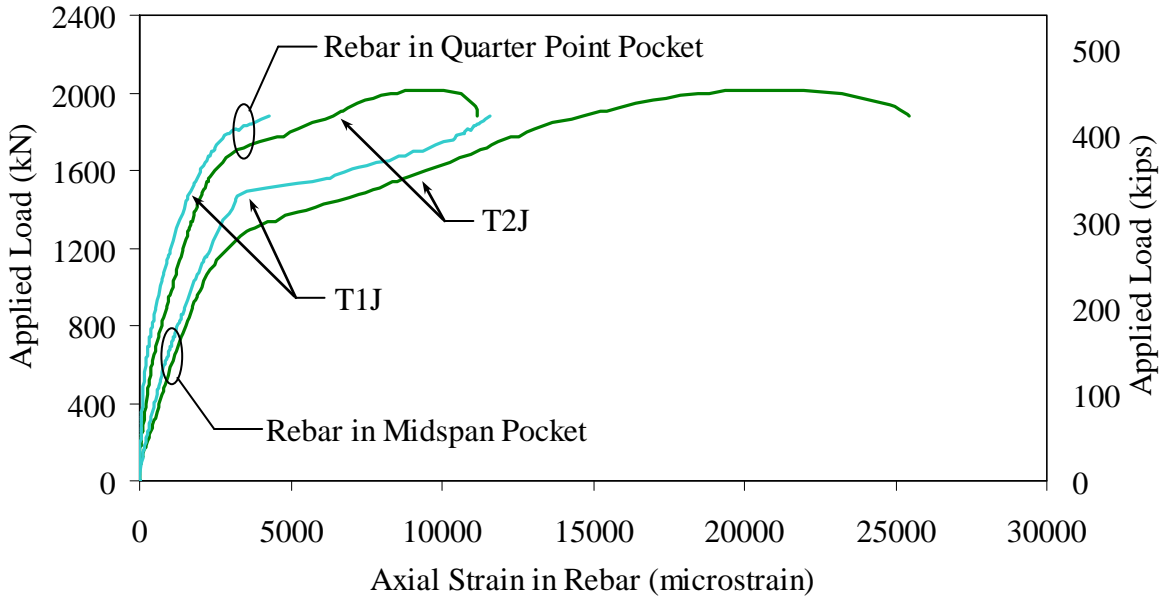
Figure 98. Graph. Axial strain in dowel reinforcing bars from Tests T1J and T2J.
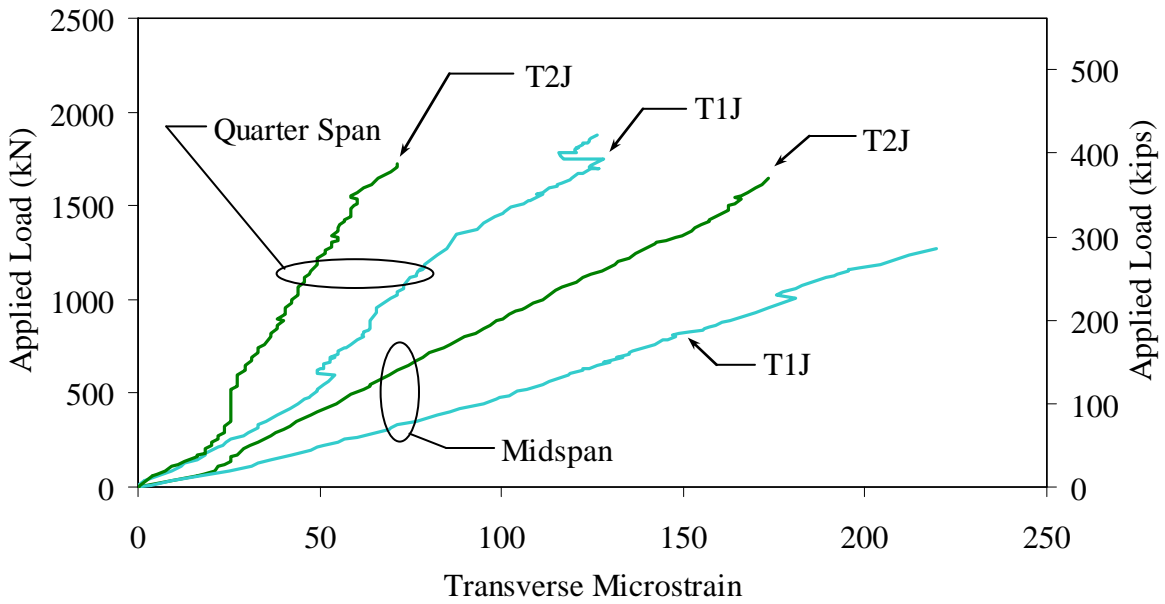
Figure 99. Graph. Transverse strain on underside of deck 178 mm (7 inch) north of joint from Tests T1J and T2J.
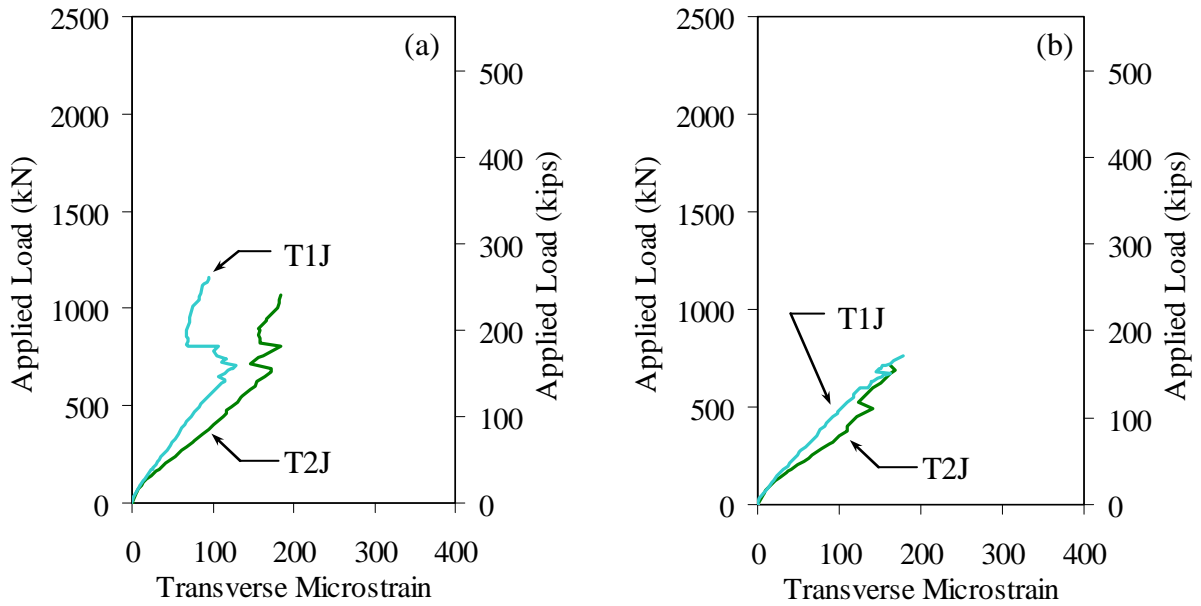
Figure 100. Graph. Transverse strain at midspan on (a) north side of north web and (b) south side of south web at 508 mm (20 inch) up from the bottom of the bulbs in Tests T1J and T2J.
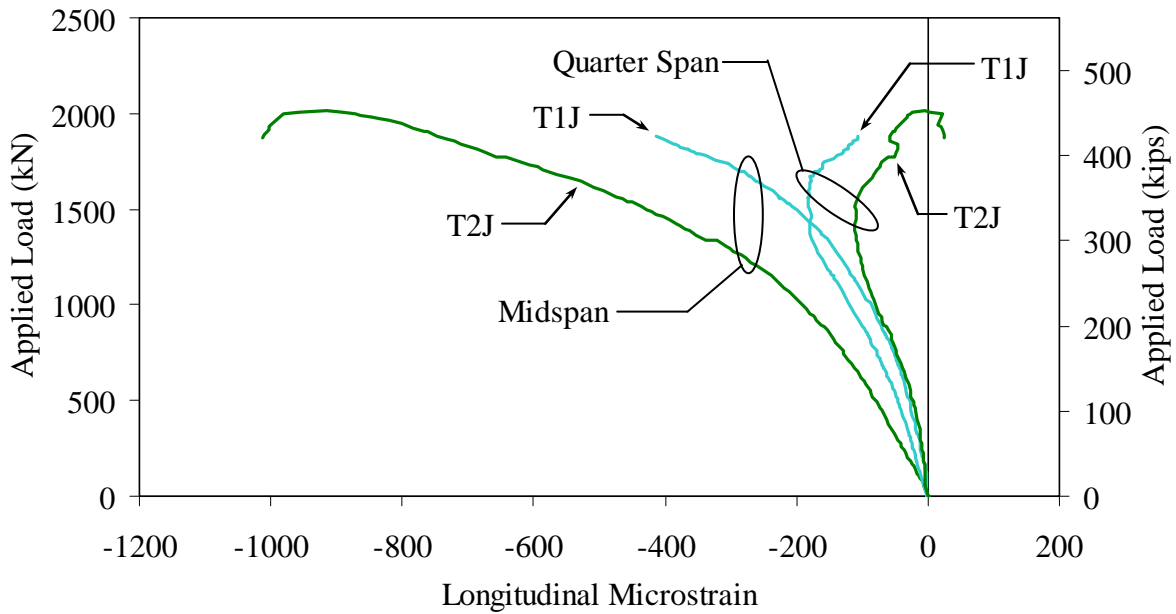
Figure 101. Graph. Longitudinal strain on top of deck 178 mm (7 inch) north of joint from Tests T1J and T2J.
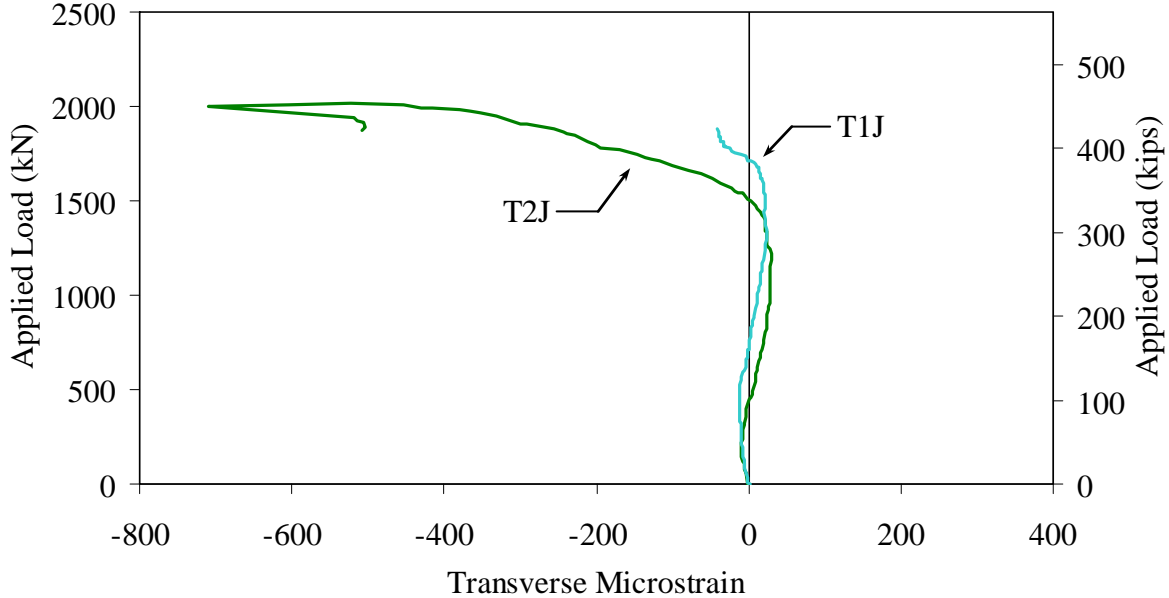
Figure 102. Graph. Transverse strain at quarter span on top of deck 178 mm (7 inch) north of joint from Tests T1J and T2J.

Overall Transverse Flexure Response

Tests T1D, T2D, T1J, and T2J were all designed to focus on the transverse flexural response of the 2nd generation UHPC pi-girder. The test setup was designed to focus the girder response heavily toward transverse flexure through the use of a relatively short span and through the application of loads midway between diaphragms and midway between girder legs. The test setup simulated the application of a pair of wheel loads from a pair of rear axles on a design truck, but allowed for the incremental increase of the applied loads up through failure of the specimen. In practice, this pair of wheels from the design truck, including the dynamic amplification factor, would weigh 95 kN (21.3 kips). Factoring this live load by 1.75 as specified in the Strength I load case of the AASHTO LRFD Bridge Design Specification[15] brings the value to 161 kN (37.3 kips). Recall that the first cracking observed on the underside of the deck in the tests of the girders as-fabricated occurred at approximately 222 kN (50 kips). The ultimate capacities demonstrated from the tests included 1510 kN (340 kips) for loads applied to the girder as fabricated, and 2010 kN (453 kips) for loads applied along the joint between two adjacent girders. Additionally, it must be recognized that the capacity of the girder cross section to these loading configurations would necessarily be larger in an as-constructed configuration due to adjacent girders providing additional continuity and resistance both in the deck and through the diaphragms. The testing completed in this program demonstrates that the transverse flexural resistance exceeds the specified demands.

The test setup and load application protocols implemented in these tests were very similar to tests P4-24T and P4-24D completed on the prototype UHPC pi-girder, thus allowing for direct comparison of results. Figure 103 presents the load versus deflection results from these six tests.

90

For tests P4-24T, P4-24D, T1D, and T2D, the reported deflection was obtained at the midspan, middeck location. For tests T1J and T2J, the reported deflection was obtained at midspan at the north edge of the longitudinal joint. The 2nd generation pi-girder response is significantly different than the prototype response. Focusing on tests T2D and T2J which were run through failure, it is evident that the 2nd generation pi-girder exhibits a stiffer, longer elastic response, and a stable inelastic response as the ultimate capacity is approached. Given that P4-24D included discrete structural members intended to assist in maintaining cross-sectional integrity, and that it failed through the formation of two negative and one positive moment hinges in the deck at a peak load of 406 kN (91 kips), it is clear that the modifications to the pi-girder cross section affected an enhanced response.

Further comparison of the results obtained from these six tests is presented in Figure 104. This figure shows the midspan bulb spreading results as related to applied load. The distinction here is between the five pi-girder tests which included some type of structural element connecting the bulbs together within the span, and the one test that did not. In terms of bulb spreading, the result from test P4-24D is very similar to the initial elastic results from the 2nd generation pi-girder tests and dramatically different than the result from P4-24T. The impact of including discrete structural members so as to maintain cross-sectional integrity along the span length is borne out in these results.

The combination of the results presented in Figure 103 and Figure 104 demonstrates that the modifications implemented in the development of the 2nd generation UHPC pi-girder significantly enhanced the structural response. The discrete diaphragms included at intermediate points along the span, as well and cross-sectional modifications to the shape of the pi-girder both contributed to a stiffer elastic response and a higher capacity. When combined with the results of test T2J which indicated that the longitudinal joint detail had greater transverse flexural capacity than the deck of the as-fabricated girder, these results in total indicate that the 2nd generation UHPC pi-girder exhibits acceptable transverse flexural behavior.
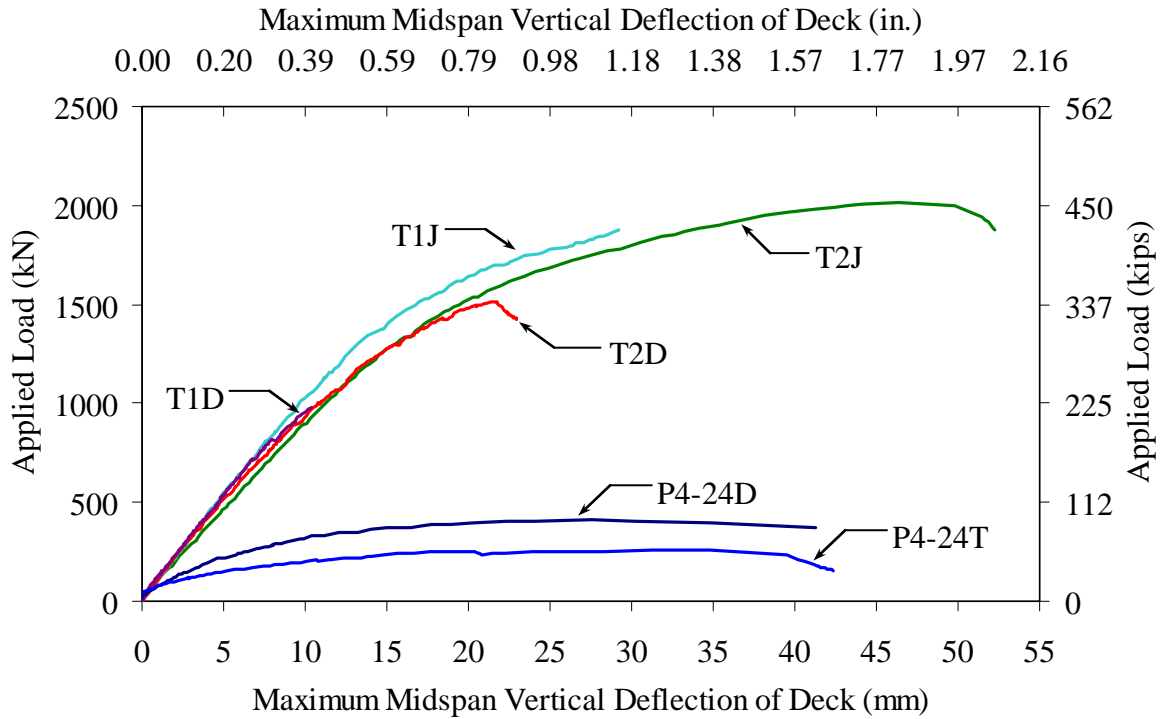
Figure 103. Graph. Deck midspan vertical deflection results from the six pi-girder transverse flexural response tests.
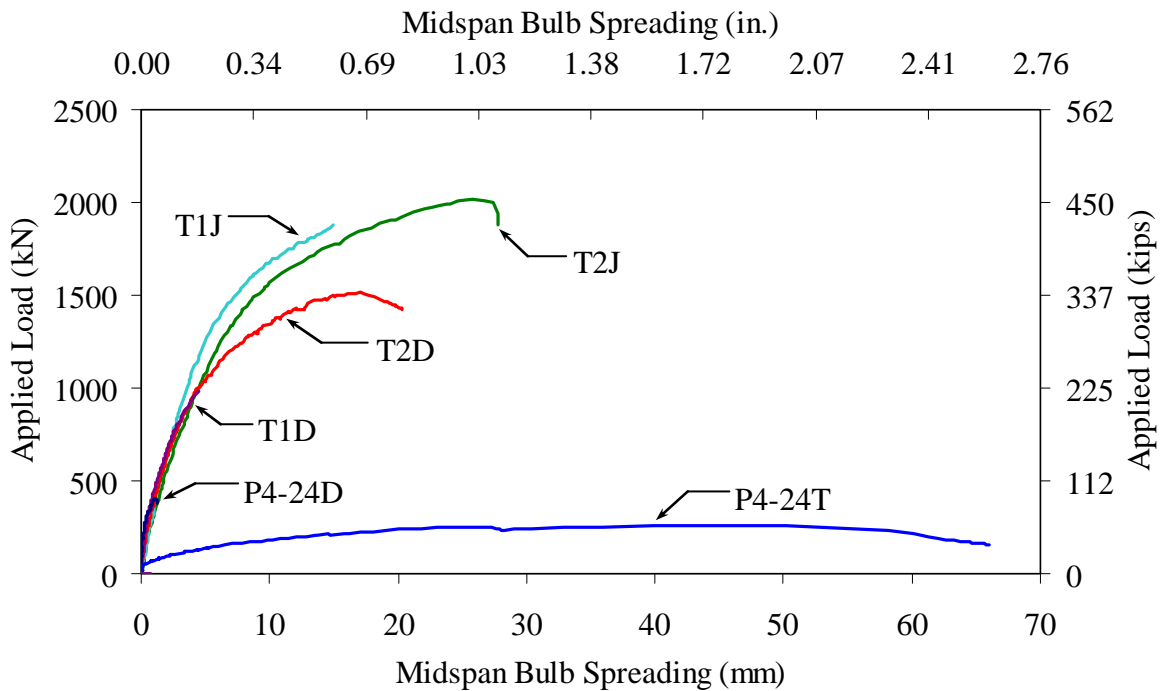

Figure 104. Graph. Deck midspan bulb spreading results from the six pi-girder transverse flexural response tests.

FAILURE MECHANISMS OBSERVED DURING TESTING OF THE 2nd GENERATION UHPC PI-GIRDER

The test setup and loading protocol implemented in this test program focused the test results toward the transverse flexural response of the pi-girder. Recall that these tests were very similar to tests P4-24T and P4-24T completed previously on the prototype pi-girder. Tests P4-24T, P4-24D, T2D, and T2J each were loaded through failure, with failure being defined as a decrease in resistance resulting from an increase in imposed displacement. In all cases, the specimens first exhibited an elastic response. After first cracking, which consistently occurred longitudinally on the underside of the deck near midspan, the specimens progressed through an inelastic stage which included the generation of additional parallel cracking and the further propagation of existing cracks. This stage concluded when the peak applied load was reached, which coincided with the formation of a transverse flexural mechanism in each specimen.

Figure 105 presents a conceptual illustration of the basic transverse flexural mechanisms which were observed in each of the four tests run through failure. Although there was multiple distributed parallel cracking in every test competed, as the peak load was reached local rotation of the cross section at critical crack locations always began to occur. In tests P4-24T and P4-24D, flexural hinging within the deck was sufficient to result in failure of the specimen. In test T2D, the hinging in the deck was combined with the tensile failure of the diaphragm to create a failure mechanism. Finally, in test T2J hinges formed in the UHPC deck, in the UHPC web, and in the mild-steel reinforced grouted joint to results in a mechanism and failure of the specimen. The local flexural hinging of the UHPC cross section consisted of rotation accumulating within specific cracks such that at fiber pullout occurred on the tensile face and the flexural depth of the member at the critical location decreased. The hinging in the grouted joint was akin to an underreinforced concrete section failing in flexure with the mild steel yielding and the concrete eventually crushing.
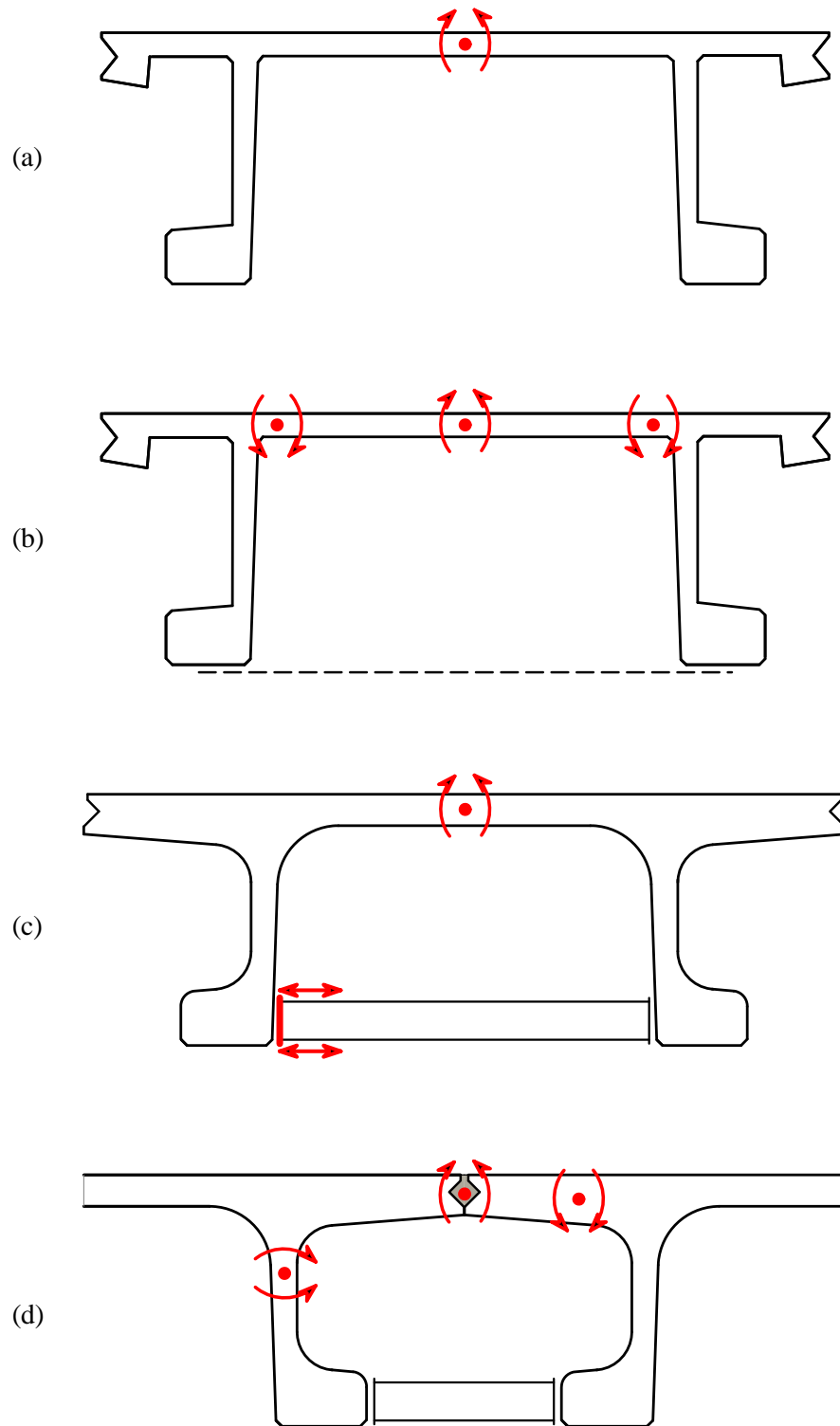
Figure 105. Illustration. Conceptual failure mechanisms observed in (a) Test P4-24T, (b) Test P4-24D, (c) Test T2D, and (d) Test T2J.

PRIMARY FLEXURE AND SHEAR RESPONSE OF A 2$^{\text{ND}}$ GENERATION PI-GIRDER

The test program reported herein focused specifically on the transverse flexural response of the 2$^{\text{nd}}$ generation UHPC pi-girder. Prior testing of the prototype UHPC pi-girder demonstrated that it possessed sufficient primary flexural and shear capacity to meet AASHTO LRFD Bridge Design Specification requirements. Given that the 2$^{\text{nd}}$ generation pi-girder possesses identical or increased cross-sectional dimensions throughout the cross section, it is expected to meet or exceed the performance limits set by the prototype section.

Predicted Primary Flexure and Shear Responses

In terms of primary flexural response, the 2$^{\text{nd}}$ generation pi-girder has a 19% larger moment of inertia, has the capacity to hold two additional strands in the bulbs, and has a thicker top flange. This new cross-sectional shape, with a full compliment of 32 15-mm (0.6-in.) prestressing strands in the bulbs, was analytically applied to the flexure tests completed on the prototype pi-girder. Using the strain compatibility analysis procedure described in reference (17), the stress-strain response of the UHPC in the prototype girder tests was determined. Then, the analysis was completed in reverse with the new cross section being applied and the predicted flexural response being determined. The predicted dead plus live load flexural cracking moment is 3,737 kN-m (33,080 kip-inches). The predicted dead plus live load flexural capacity is 6,690 kN-m (59,250 kip-inches). These values assume a tensile cracking strength of 10.3 MPa (1.5 ksi) and a fiber pullout strain of 0.007.

In terms of shear, the minimum thickness of an individual web has been increased by 45% from 56 mm (2.2 inch) to 81 mm (3.2 inch). Additionally, the transitions from the web to the bulbs and deck decrease the height over which the webs are at their minimum thickness. Following a similar concept to that discussed above, this new cross section shape was analytically applied to the shear tests completed on the prototype pi-girder. The tests on the prototype girder demonstrated that the UHPC crossing the critical failure crack in each shear test carried more than 13.8 MPa (2.0 ksi) of direct tension. The shear cracking and ultimate capacities can be estimated through the use of the design procedure detailed in reference (2) which is similar to the procedure presented in reference (16). In this procedure, relevant tensile stresses are applied to the cross section of the web at an assumed diagonal tensile failure angle. The predicted capacities are based on the 2$^{\text{nd}}$ generation pi-girder web height of 508 mm (20 inches), a total web width of 162 mm (6.4 inches) and a diagonal tensile failure angle of 41 degrees. Assuming a diagonal tensile cracking strength of 10.3 MPa (1.5 ksi), the predicted dead plus live load shear at shear cracking is 983 kN (221 kips). Assuming a diagonal tensile ultimate strength of 13.8 MPa (2.0 ksi), the predicated dead plus live load shear at shear failure is 1,310 kN (294 kips).

Primary Flexure and Shear Design

The predicted capacities detailed above provide an indication of the span ranges over which the 2$^{\text{nd}}$ generation pi-girder discussed within this report is applicable. The loading requirements for the flexural response of the girder were determined based on the provisions of the AASHTO LRFD Bridge Design Specifications[15]. For the determination of the applicable loads, each 2$^{\text{nd}}$ generation pi-girder was considered to be composed of two half-girders. This conservative

approximation was implemented so as to create a more severe loading case for the exterior half of the exterior girder. Figure 106 and Figure 107 show the loading configurations for the exterior and interior girder loadings, respectively. The distribution of live load per lane was completed according to the specification with the pi-girder being considered as a precast concrete double tee section with shear keys which is connected only enough to prevent relative vertical displacement at the interface. Given this superstructure, only the flexure on an interior girder case presents distributions factors different than that which are calculated via the Lever Rule.

The loads applied to the bridge included the HL-93 live load, the self weight of the pi-girder, a 122 kg/m^2 (25 lb/ft^2) wearing surface, and the Iowa Barrier Rail. The Iowa Barrier Rail was included as a bridge rail representative of common types frequently included on slab-on-stringer bridges. This barrier rail is 0.86-m (34-inches) tall and has a cross-sectional area of 0.265 m^2 (411 in^2). Note that half of the distributed load from the barrier rail was assumed to be carried by the exterior "girder", while the remainder was distributed among the interior "girders".

The Service III and Strength I limit states were considered. The demand results for the 21.3-m (70-ft) span length and for the 26.5-m (87-ft) span length are presented in Table 8 and Table 9 for the primary flexure and shear cases, respectively. For the flexural resistance calculation, a conservative resistance factor of 0.9 was implemented; in shear, the specified value of 0.9 was implemented.

A span of 26.5 m (87 feet) is the maximum span whose capacity is greater than the demand for both limit states in primary flexure and shear. The interior and exterior girder cases present very similar results in flexure, while the interior girder controls the shear analysis. The capacity is approximately 1% greater than the demand for Service III flexure, approximately 2% greater for Strength I shear, approximately 4% greater for Strength I flexure, and approximately 41% greater for Service III shear.

At a span of 26.5 m (87 feet), the recommended deflection limit in the Service III limit state is 33 mm (1.3 inches). The predicted live load deflection of an interior half-girder under the truck loading shown in Figure 107 is 23 mm (0.9 inches). Additionally, recognize that the true deflection would likely be lessened by load sharing and deflection compatibility with adjacent half-girders.
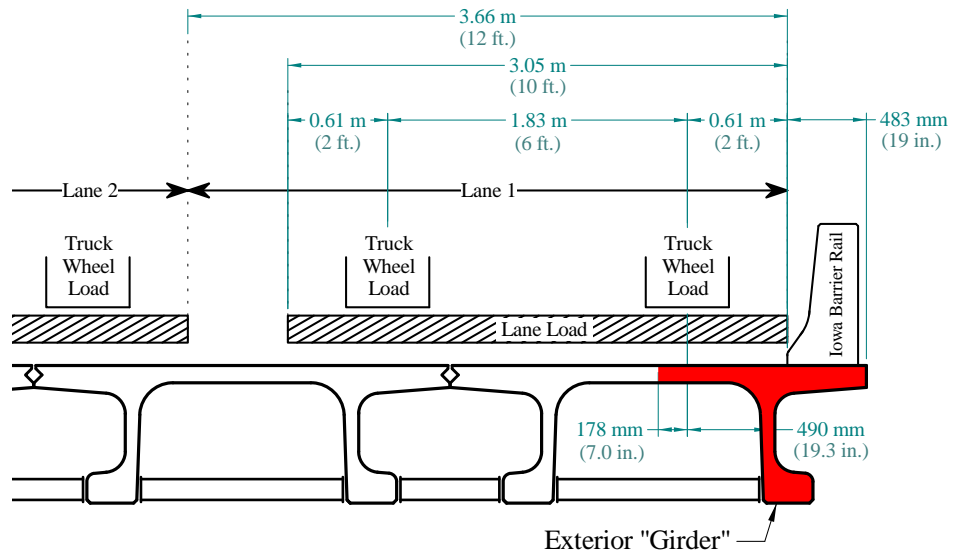
Figure 106. Illustration. Loading configuration for exterior "girder".
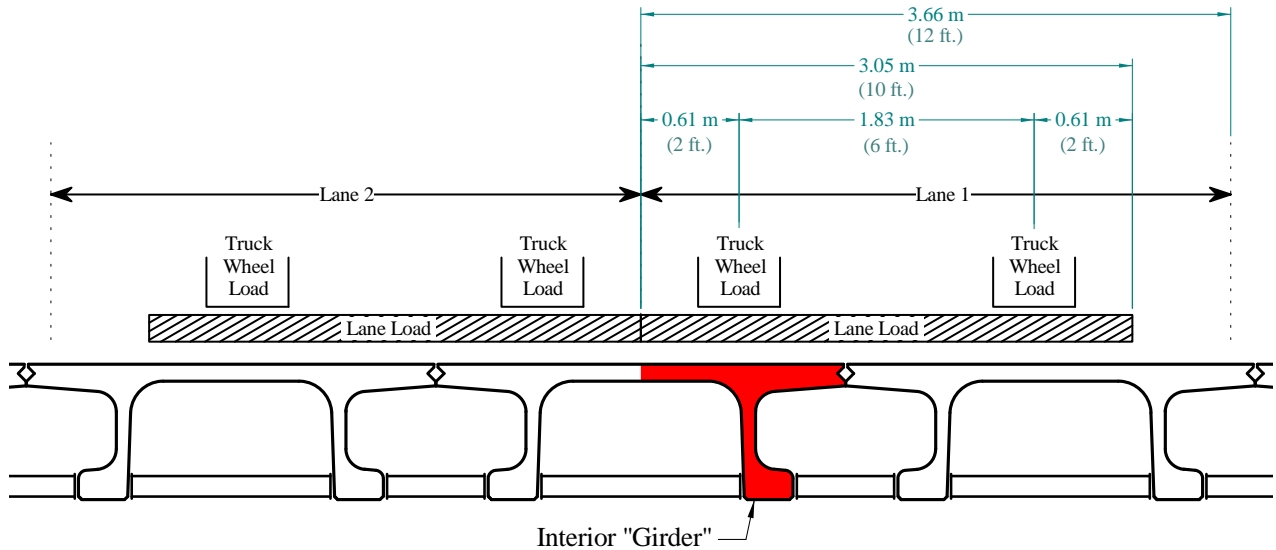
Figure 107. Illustration. Loading configuration for interior "girder".

Table 8. Flexural demand on 2nd generation pi-girder.

Span, m (ft)	Exterior "Girder", kN-m (kip-in.)		Interior "Girder", kN-m (kip-in.)	
	Service III	Strength I	Service III	Strength I
21.3 (70)	1,139 (10,080)	1,950 (17,260)	1,133 (10,032)	2,026 (17,930)
26.5 (87)	1,664 (14,730)	2,800 (24,780)	1,648 (14,590)	2,898 (25,650)

Note: In this table, "Girder" refers to ½ of a pi-girder as shown in Figure 106 and Figure 107.

97

Table 9. Shear demand on 2nd generation pi-girder.

Span, m (ft)	Exterior "Girder", kN (kip)		Interior "Girder", kN (kip)	
	Service III	Strength I	Service III	Strength I
21.3 (70)	226 (50.8)	391 (88.0)	277 (62.3)	519 (116.7)
26.8 (88)	262 (58.9)	444 (99.9)	314 (70.6)	578 (130.0)

Note: In this table, "Girder" refers to ½ of a pi-girder as shown in Figure 106 and Figure 107.

CHAPTER 7.   CONCLUSIONS

INTRODUCTION

This experimental investigation focused on the structural behavior of a newly developed highway bridge girder cross section, namely the pi-girder. This girder was developed and optimized specifically to exploit the advanced mechanical and durability properties of UHPC. The prototype version of the pi-girder was developed and tested through previous efforts within the present research program. A 2nd generation UHPC pi-girder was then developed, the fabrication and structural testing of which is discussed herein. The full-scale structural testing focused on the transverse flexural response of the girder to monotonic gravity loads. Conclusions resulting from this study are presented below. A brief discussion of ongoing and potential future research related to this topic is presented immediately thereafter.

CONCLUSIONS

The following conclusions are presented based on the research presented in this report.

1. The 2nd generation UHPC pi-girder exhibits sufficient transverse flexural capacity to resist the dead and live loads specified in the AASHTO LRFD Bridge Design Specification.

2. The predicted dead plus live load flexural capacity of the 2nd generation UHPC pi-girder is 6,690 kN-m (59,250 kip-inches). This capacity is achieved based on the flexural response observed in the testing of the prototype pi-girder and with the inclusion of a full complement of 32 15-mm (0.6-in.) prestressing strands in the bulbs.

3. The predicted dead plus live load shear capacity of the 2nd generation UHPC pi-girder is 1,310 kN (294 kips). This capacity is achieved based on the shear response observed in the testing of the prototype pi-girder and with an assumed diagonal tensile failure angle of 41 degrees and a diagonal tensile ultimate strength of 13.8 MPa (2.0 ksi).

4. The 2nd generation UHPC pi-girder meets the flexural and shear demands specified in the AASHTO LRFD Bridge Design Specifications up to a span length of 26.5 m (87 feet).

5. The grouted longitudinal joint investigated in this test program performed well, exhibiting an ultimate transverse flexural capacity greater than the capacity of the as-fabricated girder deck under a similar loading configuration. The ductility of the failure of this joint was similar to the ductility exhibited by the failure of the as-fabricated deck.

ONGOING AND FUTURE RESEARCH

The research presented herein has spurred the initiation of a series of follow-on research studies. These ongoing and future studies include:

1.   Develop a family of UHPC pi-girder cross sections applicable to a range of span lengths.

2. Develop finite element modeling techniques capable of predicting the structural performance of UHPC structural components. Utilize the full scale UHPC components test results presented in this and precursor reports as benchmarks for model development. Facilitate the further development of UHPC components through the use of these models.

3. Develop optimal connection details for UHPC decked-girder elements. This effort will primarily focus on the development of connections between adjacent girders and connections between girders and barrier rails.

REFERENCES

1. Graybeal, B.A., "Material Property Characterization of Ultra-High Performance Concrete," Federal Highway Administration, Report No. FHWA-HRT-06-103, August 2006, 186 pp.

2. Graybeal, B.A., "Structural Behavior of Ultra-High Performance Concrete Prestressed I-Girders," Federal Highway Administration, Report No. FHWA-HRT-06-115, August 2006, 104 pp.

3. Behloul, M., G. Causse, and D. Etienne, "Ductal® Footbridge in Seoul," First fib Congress, Osaka, Japan, October 2002, 11 pp.

4. Chuang, E., "Ductility Enhancement of High Performance Cementitious Composites and Structures," Massachusetts Institute of Technology, 2002, 319 pp.

5. Park, H., "Model-Based Optimization of Ultra High Performance Concrete Highway Bridge Girders," Massachusetts Institute of Technology, 2003, 139 pp.

6. Soh, M., "Model-Based Design of a Ultra High Performance Concrete Prototype Highway Bridge Girder," Massachusetts Institute of Technology, 2003, 64 pp.

7. Chuang, E., and F. Ulm, "Two-Phase Composite Model for High Performance Cementitious Composites," *Journal of Engineering Mechanics*, V. 128, No. 12, 2002, pp. 1314-1323.

8. AASHTO, *AASHTO LRFD Bridge Design Specifications, 2nd Edition*, American Association of State Highway and Transportation Officials, 2002.

9. Graybeal, B.A., "Structural Behavior of a Prototype Ultra-High Performance Concrete Pi-Girder," Federal Highway Administration, NTIS Accession No. PB2009-115495, 2009, 145 pp.

10. ASTM C39, "Standard Test Method for Compressive Strength of Cylindrical Concrete Specimens," American Society for Testing and Materials Standard Practice C39, Philadelphia, PA, 2001.

11. ASTM C469, "Standard Test Method for Static Modulus of Elasticity and Poisson's Ratio of Concrete in Compression," American Society for Testing and Materials Standard Practice C469, Philadelphia, PA, 2002.

12. Graybeal, B., "Practical Means for the Determination of the Tensile Behavior of Ultra-High Performance Concrete," *Journal of ASTM International*, V. 3, No. 8, December 2006, 9 pp.

13. ASTM C496, "Standard Test Method for Splitting Tensile Strength of Cylindrical Concrete Specimens," American Society for Testing and Materials Standard Practice C496, Philadelphia, PA, 2002.

14. ASTM A370, "Standard Test Methods and Definitions for Mechanical Testing of Steel Products," American Society for Testing and Materials Standard Practice A370, Philadelphia, PA, 1997.

15. AASHTO, *AASHTO LRFD Bridge Design Specifications, 4th Edition*, American Association of State Highway and Transportation Officials, 2007.

16. Association Française de Génie Civil, Interim Recommendations for Ultra High Performance Fibre-Reinforced Concretes, 2002.

17. Graybeal, B.A., "Flexural Performance of an Ultrahigh-Performance Concrete I-Girder," *ASCE Journal of Bridge Engineering*, V. 13, No. 6, November 2008, 602-610.